TAMPERE UNIVERSITY OF TECHNOLOGY

EEVA-MARIA KITTILÄ

IMPLEMENTATION AND EVALUATION OF WIND TURBINE CONTROL CONCEPTS

Master of Science Thesis

Examiner: Professor Matti Vilkko
Examiner and the topic approved in the Council Meeting of Automation, Mechanical and Materials Engineering Department on 11 January 2012.

ABSTRACT

TAMPERE UNIVERSITY OF TECHNOLOGY
Master's Degree Programme in Automation Technology
KITTILÄ, EEVA-MARIA: Implementation and Evaluation of Wind Turbine Control Concepts
Master of Science Thesis, 89 pages, 10 Appendix pages
August 2012
Major: Process Automation
Examiner: Professor Matti Vilkko
Keywords: Wind Turbine Control, Pitch Control, Individual Pitch Control, Wind Turbine Load Reduction, Wind Shear Compensation, Tower Shadow Compensation, FAST

Wind turbines used in the electricity production nowadays are extremely large systems. Due to the increased sizes of the wind turbines, varying loads affecting on the turbine have became more significant. These changing loads are mainly caused by the variations in the wind speed experienced by the turbine. Wind shear, describing the increase in the wind speed from bottom to upper in the height, can be regarded as the main reason to the changing loads of the blades and the top of the turbine. This loading can be alleviated significantly by individual pitch control, which means that the pitch angle of each blade is controlled individually; in a way that aerodynamic force is kept constant during a revolution. In the commercial wind turbines, collective pitch control is used to limit the output power of the turbine above the rated wind speeds and the turbines are already equipped with individual pitch actuators. This makes the implementation of individual pitch control rather simple. In addition to the wind shear, tower shadow, describing the decrease in the wind speed experienced by the blade when it is directly in front of the tower, has also some impact on the wind turbine loading.

The scope of this thesis is on the pitch control of the wind turbine blades. However, wind turbines and wind characteristics as well as the wind turbine control in general are discussed briefly at the beginning of this thesis. Simulations within this thesis are made for the NREL's 5 MW reference turbine by using the wind turbine simulation software FAST. Simulations can be divided into three different topics. First, performance of the collective pitch controller in the extreme wind conditions as well as the effect of wind shear on the wind turbine loading in the case of this controller are evaluated. Then, different individual pitch control schemes for the wind shear compensation are implemented and evaluated. Finally, the effect of tower shadow on the wind turbine loading is evaluated and different methods striving to compensate it are implemented.

The study indicates that the loads caused by wind shear can be decreased significantly by individual pitch control. All methods described within this thesis are able to alleviate the loading of the blades as well as the static component of the tilt and yaw moments at some rate. On the other hand, fluctuating components of the tilt and yaw moments are decreased only when the reduction of the 2*P* load component in the blade loads is also considered in the IPC algorithm. On the other hand, comprehensive reduction of the loading caused by tower shadow seems to be challenging. However, the effect of the tower shadow is also less significant than the effect of wind shear. This study has been made as a part of the larger project for the ABB Corporate Research Center in Germany.

TIIVISTELMÄ

TAMPEREEN TEKNILLINEN YLIOPISTO
Automaatiotekniikan koulutusohjelma
KITTILÄ, EEVA-MARIA: Tuuliturbiinin säätömenetelmät ja eri menetelmien arviointi
Diplomityö, 89 sivua, 10 liitesivua
Elokuu 2012
Pääaine: Prosessiautomaatio
Tarkastaja: Professori Matti Vilkko
Avainsanat: Tuuliturbiinin säätö, lapakulman säätö, yksittäinen lapakulman säätö, Tuuliturbiinin kuormitusten vähentäminen, Tuulen nopeuden vertikaalinen muutos, Tornin muodostama varjo, FAST

Sähköntuotantoon käytettävät tuuliturbiinit ovat nykyään erittäin suuria järjestelmiä. Turbiiniin vaikuttava tuulen nopeus ei jakaudu tasaisesti roottorin lapojen muodostaman pyyhkäisypinta-alan läpi, mistä aiheutuu huomattavia epäsymmetrisiä kuormitusmomentteja. Nämä kuormitusmomentit tulevat yhä merkittävämmiksi turbiinin koon kasvaessa ja täten niiden pienentäminen älykkäiden säätömenetelmien avulla on tärkeä osa tuuliturbiinin säätöjärjestelmää. Tuulen nopeuden vertikaalista muutosta, joka kuvaa tuulen nopeuden kasvua korkeuden kasvaessa, voidaan pitää merkittävimpänä syynä turbiiniin vaikuttavaan epäsymmetriseen kuormitukseen. Tätä kuormitusta voidaan vähentää merkittävästi yksittäisellä lapakulman säädöllä, eli säätämällä jokaisen lavan kallistuskulmaa yksitellen siten, että aerodynaaminen voima pysyy vakiona yhden kierroksen aikana. Suurin osa suurista tuuliturbiineista on nykyään muuttuvanopeuksisia turbiineja, joissa käytetään kollektiivista lapakulman säätöä tehon rajoittamiseen korkeammilla tuulen nopeuksilla. Näin ollen turbiinin lavoilla on jo valmiina yksittäiset kallistustoimilaitteensa, mikä tekee yksittäisen lapakulman säädön toteuttamisen suhteellisen yksinkertaiseksi. Tornin muodostama varjo lavan ollessa suoraan tornin edessä kasvattaa myös osaltaan epäsymmetrisiä kuormitusmomentteja..

Tämä diplomityö keskittyy tuuliturbiinin lapakulmien säätöön ja erilaisia menetelmiä kuormitusten vähentämiseksi toteutetaan ja arvioidaan työn puitteissa. Työn alussa käsitellään lyhyesti tuulen ja tuuliturbiinien ominaisuuksia sekä tuuliturbiinin säätöä yleisesti. Työn tutkimusosio voidaan jakaa kolmeen eri osa-alueeseen. Ensin käsitellään kollektiivista lapakulman säätöä, mistä jatketaan yksittäisen lapakulman säätöalgoritmien toteuttamisella sekä vertailulla. Lopuksi esitellään menetelmiä tornin muodostaman varjon aiheuttaman kuormituksen kompensoimiseksi.

Tämä tutkimus osoittaa, että tuulen nopeuden vertikaalisesta muutoksesta aiheutuvaa turbiinin kuormitusta voidaan pienentää huomattavasti yksittäisellä lapakulman säädöllä. Tornin muodostaman varjon aiheuttaman rasituksen pienentäminen vaikuttaa olevan haasteellisesta, mikä johtuu luultavammin äärimmäisen lyhyestä ajasta, jona kompensointi tulisi suorittaa. Tämä diplomityö on tehty osana laajempaa tutkimusprojektia ABB:n tutkimuskeskuksessa Ladenbugissa Saksassa.

PREFACE

This thesis was made in the ABB Corporate Research Center in Ladenburg, Germany. The work was done starting from January until the beginning of July 2012 as a part of the Blackfoot - Wind Turbine Pitch Control project. The scope of the project was to gain knowledge about the market potential of the wind turbine pitch controller system that could be developed and produced by ABB. The purpose of my thesis was to evaluate the purposes in which the pitch controller system could be used and how this could be implemented. I would like to thank my supervisor Dr.-Ing. Thomas Weickert for his guidance and support for this thesis. I am also very grateful for all my colleagues in the ABB Corporate Research Center for their advices and support for my thesis and stay in Germany.

Examiner for my thesis has been Professor Matti Vilkko from Tampere University of Technology and I would like to thank him for his advices and the examination of my work. Furthermore, I am very grateful to International Office of Tampere University of Technology as well as Tampereen Teknillinen Seura for their support for writing a thesis abroad. I would also like to thank German lecturers Norbert Jölich and Sibylle Kingelin from the Language Center of Tampere University of Technology for their encouragement for finishing my studies in Germany.

Finally, I want to thank Matti and my family for their support for this thesis and my studies as well as my stay in Germany. Without their love and understanding I would never have the courage to come and write my thesis in a foreign country.

Teuva, 31 July 2012

Eeva-Maria Kittilä

TABLE OF CONTENTS

TERMS AND DEFINITIONS

B	Tower shadow coefficient
C_P	Power coefficient
C_{Pmax}	Maximum power coefficient
q	Control gain for the feedforward IPC
q_{p1}	Control parameter for the minimization of the in-plane blade loading
q_{p2}	Control parameter for the minimization of the out of blade loading
G	Control gain for the feedforward tower shadow compensation controller
$I_{Drivetrain}$	Drivetrain inertia of the low-speed shaft
I_{Gen}	Generator inertia
I_{Rotor}	Rotor inertia
K_1	Wind shear gradient
K_I	Integral gain of the PI controller
K_P	Proportional gain of the PI controller
k	Gain correction factor for the gain scheduled feedforward IPC
M_1	Out of plane blade bending moment for the blade 1
M_2	Out of plane blade bending moment for the blade 2
M_3	Out of plane blade bending moment for the blade 3
M_d	Tilt Moment
M_q	Yaw Moment
M_{d2}	2*P* component of the tilt moment
M_{q2}	2*P* component of the yaw moment
M_{d4}	4*P* component of the tilt moment
M_{q4}	4*P* component of the yaw moment
M_{Shear}	Shear Moment
N_{Gear}	Gearbox ratio from the high-speed to low-speed shaft
P_{av}	Average power available from the wind
P	Mechanical power
P_0	Rated mechanical power
P_V	Power in the wind that passes through the rotor disk
R	Blade length

R_{tower}	Radius of the tower
R_{rotor}	Radius of the rotor
r	Radial distance from the rotor axis
T	Constant control response matrix for the higher harmonic controller
T_{Aero}	Aerodynamic torque of the low-speed shaft
T_{Gen}	Generator torque of the high-speed shaft
T_I	Integration time for the PI controller
u_d	Output signal of for the tilt moment controller
u_q	Output signal of for the yaw moment controller
u_{d2}	Output signal of for the 2*P* tilt moment controller
u_{q2}	Output signal of for the 2*P* yaw moment controller
u_{d4}	Output signal of for the 4*P* tilt moment controller
u_{q4}	Output signal of for the 4*P* yaw moment controller
u	Control signal amplitude for the higher harmonic controller
V	Wind peed
V_{bottom}	Wind speed at the bottom of the blade sweep area
V_{hub}	Hub-height wind speed
V_{min}	Cut-in wind speed
V_{max}	Cut-out wind speed
V_N	Rated wind speed
$V_{\Omega N}$	Wind speed at the rated rotor speed
V_{top}	Wind speed at the top of the blade sweep area
V_{tower}	Wind speed in the front of the tower
V_z	Wind speed at the certain height z
VSHR	Exponent of the power law wind shear profile
x	Longitudinal distance between a given point in the rotor plane and the tower centerline
y	Lateral distance between a given point in the rotor plane and the tower centerline
z	Certain height from the ground
z_{hub}	Hub-height
z	Sine and cosine components of the blade vibration at the certain frequency
$\mathbf{z_0}$	vibration amplitude for the nominal pitch angle defined by CPC at certain frequency

ρ	Air density
Ω	Rotor speed
Ω_0	Rated rotor speed
$\Delta\Omega$	Small perturbation of the rotor speed about the rated speed
$\Delta\dot{\Omega}$	Rotational acceleration of the rotor
λ	Tip-speed ratio
λ_0	Optimum tip-seed ratio
θ	Blade pitch angle
θ_1	Blade pitch angle for the blade 1
θ_2	Blade pitch angle for the blade 2
θ_3	Blade pitch angle for the blade 3
θ_{2p1}	Blade pitch angle demand for the blade 1 for the 2*P* load reduction
θ_{2p2}	Blade pitch angle demand for the blade 2 for the 2*P* load reduction
θ_{2p3}	Blade pitch angle demand for the blade 3 for the 2*P* load reduction
θ_{4p1}	Blade pitch angle demand for the blade 1 for the 4*P* load reduction
θ_{4p2}	Blade pitch angle demand for the blade 2 for the 4*P* load reduction
θ_{4p3}	Blade pitch angle demand for the blade 3 for the 4*P* load reduction
$\Delta\theta$	Small perturbation of the pitch angle from its operating point
θ_K	Blade pitch angle at which the pitch sensitivity has doubled from the value at rated wind speed
θ_P	Set-point for the blade pitch angle
$GK(\theta)$	Gain correction factor in the case of collective pitch controller
$\dot{\phi}$	Rotor speed error
ϕ	Azimuth angle of the rotor
ϕ_i	Azimuth angle position for the i:th blade
$\partial P/\partial\theta$	Pitch sensitivity
$\omega_{\phi n}$	Natural frequency
ς_ϕ	Damping ratio
σ	Phase correction factor

1*P*	Once per revolution frequency
2*P*	Twice per revolution frequency
3*P*	Three times per revolution frequency
Baseline IPC	Most well-known individual pitch control algorithm in the literature that is based on the d-q transformation and the utilization of the blade load sensors
CPC	Collective pitch controller
Cut-in wind speed	Minimum wind speed needed for the economical operation of the wind turbine
Cut-out wind speed	Wind speed at which the turbine has to be stopped in order to avoid damages
Downwind turbine	Wind turbine in which the rotor is located behind the tower
IPC	Individual pitch controller
IPC Blade Loads	Individual pitch controller equipped with the blade load sensors
ECD	Extreme coherent gust with direction change
EOG	Extreme operating gust
EWSV	Extreme vertical wind shear
EWSH	Extreme horizontal wind shear
Extended IPC	Individual pitch controller that combines the baseline IPC and the another algorithm for the 3*P* load reduction
FAST	NREL's wind turbine simulation software called Fatigue, Aerodynamics, Structures and Turbulence
Feedforward IPC	Individual pitch controller that uses the measurements of rotor position and the wind speed as measurement signals
FP	Fixed pitch
FS	Fixed speed
HHC	Higher harmonic control
Hub	Component of the wind turbine that links the blades to the conversion system
MBS	Multibody System
Nacelle	Covering enclosure for the components of the wind turbine
N*P*	*N* times per revolution frequency
NREL	National Renewable Energy Laboratory

Tilt Moment	Disturbing moment affecting on the top of the tower that tries to tilt the whole tower
Tip-speed ratio	The ratio between the rotational speed of the blade tip and the wind speed
Tower Shadow	When a blade of the turbine is passing by the tower, the airflow experienced by the blade is interrupted due to the tower
Turbulence	Stochastic short-term variations in the wind speed
Upwind turbine	Wind turbine in which the rotor is located in front of the tower
VP	Variable pitch
VS	Variable speed
WECS	Wind energy conversion system
Wind Shear	Increase in the wind speed from bottom to upper (vertical wind shear) or from right to left looking downwind (horizontal)
Yaw Control	Control of the direction of the turbine related to the direction of the wind
Yaw Moment	Disturbing moment affecting on the top of the tower that tries to yaw the tower

1 INTRODUCTION

Significance of the wind energy in power production has increased rapidly during the latest years. Increasing concern of nature, safety issues related to nuclear power and limited amount of fossil fuels have made the conventional energy sources less attractive. Wind energy does not cause any green house gas emissions and its amount is unlimited. Furthermore, new technologies and higher production scales have lead to the more efficient wind turbines, which has significantly lowered the costs of electricity produced by wind energy [1]. However, more efficient, high production scale wind turbines are also larger, which makes their components to be bulky and costly in order to be sustainable enough. Therefore, load reduction through intelligent control systems becomes more meaningful than the design of the components to withstand larger loads [2]. In addition, the energy capture can be maximized and the range of wind speeds for safe operation can be extended through a modern control of the wind turbines [3]. Furthermore, the quality of the produced power becomes increasingly important too when the amount of electricity produced by wind energy in the grid increases [4].

According to Bianchi et al. [1], the main purpose in wind turbine control is to minimize the cost of supplied energy. This purpose can be acquired by partial objectives which are maximization of energy capture, minimization of mechanical loads and as good power quality as possible. Most often, the control of conventionally used wind turbines relies on the two control systems: a generator-torque controller and a rotor-collective blade-pitch controller. The purpose of the generator-torque control is to maximize power conversion at the low wind speeds, i.e., below rated wind speed, and the collective blade-pitch controller regulates the generator speed at the wind speeds above the rated by affecting on the aerodynamic torque produced by the blades [5]. Wind energy conversion systems are used in the highly varying operating conditions, which has to be considered in their control. Aerodynamic characteristics of the turbine differ significantly from one wind speed to another and hence, linear control strategies do not work effectively through the whole range of different wind speeds. To be able to overcome this problem, gain scheduling techniques are typically used in the collective pitch control of the wind turbines. [1]. Furthermore, utilisation of the more sophisticated control techniques suitable for nonlinear systems in the wind turbines has been discussed in the papers too [6; 7].

The focus of this thesis is in the blade pitch control and especially in the load reduction by individual pitch control which is an important part of the wind turbine control nowadays. Because of the increasing turbine diameter, the asymmetric loads affecting on the turbine become more significant.

According to several researches [2; 3; 8; 9] these loads are caused by the wind speed variations across the rotor disc, and they can be reduced notably by *individual pitch control (IPC)*. Wind speed variations are mainly caused by the wind shear, which describes the increase in the wind from the bottom to the upper in the height. Furthermore, wind speed experienced by the turbine is also disturbed by the tower of the turbine. In other words, the blades of the turbine are experiencing decrease in the wind speed when they are directly in the front of the tower. This phenomenon is known as tower shadow and it is also affecting on the wind turbine loading [10]. The asymmetric loads produce disturbing tilt and yaw moments in the tower and they can be eliminated by controlling each pitch angle individually, in a way that aerodynamic force is kept constant during a revolution. Furthermore, the blades of the modern wind turbines are equipped with separate pitch motors, which enables the implementation of IPC without additional pitch motors [3].

The most well-known IPC method is based on the transformation from the rotating coordinate system to the static one through a d-q transformation borrowed from the electrical machine theory [2]. This method utilises the blade load measurements and hence, the blade load sensors are needed. However, a feedforward IPC scheme based on the measurement of the rotor position is also introduced in the literature [11]. Usually, conventional PI controllers are used in the individual pitch control because due to the transformation, the d- and q-axis signals can be treated separately and regarded as decoupled SISO system. However, modern control techniques suitable for multivariable systems have also been applied to the individual pitch control [2; 12]. In addition to the baseline IPC based on d-q transformation, further load reduction schemes have been introduced in the literature in order to attain more comprehensive load alleviation. Baseline IPC algorithm can be extended to aim at the reduction of the higher frequency load components [13; 14; 15] or higher harmonic control (HHC), more well-known in the helicopter control, can be applied to the wind turbine control instead [3].

Different control schemes are implemented in Matlab/Simulink for the 5-MW reference wind turbine created by National Renewable Energy Laboratory (NREL) [5] and their performances are evaluated within this thesis. Second chapter introduces the characteristics of the wind and wind turbines briefly. Chapter three focuses on the wind turbine control in general. Short introductions to the generator torque control as well as the nacelle yaw control are given and the theory behind the collective blade pitch control is discussed more detail. Chapter four begins with deriving the collective pitch controller for the 5-MW reference turbine and continues with the simulation results concerning the performance of this controller during the extreme wind scenarios. Furthermore, effect of wind shear on the wind turbine loading when the collective pitch control is used is evaluated through the simulations at the end of the chapter four. Chapters five and six are dealing with the different individual pitch control schemes for the alleviation of the loading due to the wind shear which were identified through the simulations in the chapter four. Chapter seven describes the effect of tower shadow in the wind turbine loading and different control algorithms are introduced in order to compensate this effect.

Different methods for the alleviation of the loading caused by wind shear described in chapters five and six as well as the different methods for tower shadow compensation discussed in the chapter seven are compared in the chapter eight. The purpose of the chapter nine is to draw conclusions from the simulation results and to give a reader some recommendations concerning the utilisation of the methods discussed in this thesis as well as give examples for the further research within the field of wind turbine load reduction.

2 WIND TURBINE AND WIND CHARACTERISTICS

Wind Turbines are relatively complicated systems with several subsystems affecting each other. Electrical, mechanical and aerodynamic characteristics have to all be considered when dealing with the control of wind turbines. In addition, stochastic characteristics of the wind have a major impact on the operation of the whole wind energy conversion system. Wind turbines and their main components as well as modeling of the turbines are briefly introduced in this chapter. Furthermore, the features of the wind and how they affect on the turbine are discussed.

2.1 Wind Turbines

Based on the orientation of the rotor axis, wind turbines are typically divided into vertical-axis and horizontal-axis wind turbines. Vertical-axis wind turbines are not normally used in commercial purposes because of the reduced energy capture and maintenance difficulties. Thus, nearly all wind turbines connected to the grid are horizontal-axis two-bladed or three-bladed wind turbines. [1]. Furthermore, the turbines can be divided into upwind and downwind turbines based on the location of the rotor concerning the tower. The rotor is located behind the tower in a downwind turbine and in front of the tower in an upwind turbine, respectively. [16]. Three-bladed horizontal-axis upwind turbines are most common nowadays, and for this reason only they are treated in this thesis.

2.1.1 Main Components

According to Nelson [17], the main components of the wind turbine are typically rotor, consisting of the blades and the hub, gearbox, conversion system and tower. Horizontal axis wind turbine and its main components are illustrated in the figure 2.1.

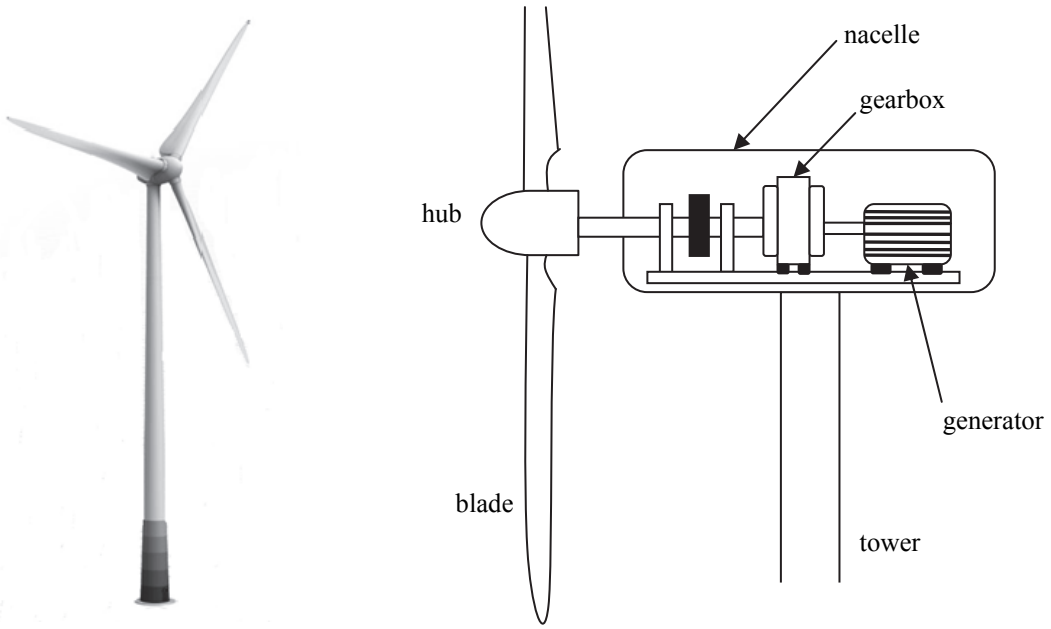

Figure 2.1. *Horizontal-axis wind turbine and its main components [1; 18]*

Three-dimensional wind field is converted into centralized forces on the blades and the hub is needed to link the blades to the conversion system. In addition, the pitch servos, that are used to pitch the blades, are located inside the hub. [1]. The output of the rotor, i.e. rotational kinetic energy, is converted into the electrical energy in a generator. [17]. A gearbox is used in order to increase the rotor speed to suitable range for the generator. However, there are also gearless generator solutions available nowadays [19]. When dealing with the variable-speed wind turbines, the electronic converter is also needed in order to create an interface between the AC grid and the stator or rotor windings. [1]. The nacelle creates a covering enclosure for the components of a turbine [17].

2.1.2 Modeling of a Wind Turbine

According to Bianchi et al. [1], a model of entire wind energy conversion system can be divided into interconnected subsystems, which are aerodynamic subsystem, mechanical subsystem, electrical subsystem and actuator subsystem. The aerodynamic subsystem illustrates the transformation of the wind speed into forces affecting on the blades producing the rotational movement. The mechanical subsystem includes the drive-train and the support structure. The drive-train is needed to transfer the aerodynamic torque affecting on the blades to the generator shaft. The rotor, the transmission and the mechanical parts of the generator are included in the drive-train. The tower and foundations are the parts of the support structure.

The electrical subsystem, in turn, encompasses the conversion of mechanical power at the generator shaft into electricity. The actuator subsystem describes the behavior of the pitch servos. [1]. The dominant dynamics of the wind energy conversion systems are related to the mechanical subsystem and thus the horizontal-axis wind turbine can be treated as a complex mechanical subsystem that consists of several interacting components. The interaction of the drive-train, the tower and the foundations leads to the high-order nonlinear models because the structures are fixed to a reference frame which is rotating with respect to the other. Furthermore, the forces affecting to these structures are mostly derived from a three-dimensional wind field which increases the complexity even more. [1].

High-order nonlinear models are usually not suitable for control purposes. High-order models are complicated and most controller design techniques cannot be used with nonlinear systems. In according to Bianchi et al. [1], control-oriented models of the wind energy conversion systems are hence usually derived based on Multibody System (MBS) approach. The mechanical structure of the turbine is arranged into rigid bodies connected by flexible joints and the amount of these joints determines the degrees of freedom of the system, and hence, the order of the model. Based on this technique, models with reduced order and deep physical insight can be gained. Because the scope of this thesis is in the wind turbine pitch control, the modeling issues are not dealt with more deeply. More detailed information about the wind turbine modeling can be found for example in [1; 20].

2.2 Wind Characteristics

Even though the wind has many advantages as an energy source, there is also one significant challenge related to it. Wind is highly variable and furthermore, these variations occur both with the time and with the geographical location. According to Bossanyi et al [21], the amount of available energy in the wind varies as the cube of the wind speed. For this reason, the variations in the wind are directly related to the amount of available wind energy. Furthermore, geographical variations have significant impact on the amount of available wind energy. The areas on the mountains are more windy than flat areas and the wind speed is higher offshore than onshore, for example.

Temporal variations can be divided into different time-scales. Long term variations mean that amount of wind can be different from year to another which complicates the analyzing of the profitability of a wind farm in a construction phase, for example. Daily variations in the wind, in turn, have a great impact on the operation of a wind farm when integrating significant amount of wind power into electricity grid. Variations in wind on minutes or seconds are the most relevant from the control point of view of an individual turbine. These short-time variations in the wind are known as turbulence. [21]. According to Bianchi et al., [1] turbulence includes the fluctuations in wind speed on a time-scale from seconds to minutes. Turbulence has a minor effect on the annual energy capture but its influence on aerodynamic loads and power quality is significant.

2.3 Wind Speed Experienced by the Turbine

Wind speed distribution through the area swept by the blades is not uniform and it may vary significantly both in its mean and turbulent components. For this reason, a blade element will encounter different wind speeds while it rotates. If it is assumed that the wind speed is frozen, i.e. the wind speed is constant at each point during a revolution, the wind speed affecting on a blade element is a periodical signal with fundamental frequency 1*P* (once per a revolution). This variation in wind speed is known as rotational sampling which creates cyclic fluctuations on the aerodynamic and rotational torques. Furthermore, N*P* frequencies of these fluctuations are reflected down the drive-train and the structure of the turbine causing fatigue stress to the components and reducing the quality of the produced power. [1].

According to Bianchi et al. [1], the wind speed affecting on the turbine at a defined point can be divided into quasi-steady mean speed and the turbulence. Thus, the mean wind speed can be thought to be constant during a revolution. The changing component of the wind can further be divided into deterministic and stochastic components. Deterministic component is mainly caused by wind shear and tower shadow and the stochastic component is derived from the temporal and spatial distribution of the wind turbulence. [1]

2.3.1 Wind Shear

According to Haarnoja [3], wind shear is the main cause of fatigue stress that reduces the lifetime of a wind turbine. Wind shear occurs because the wind is not divided equally on the rotor sweep area, but the wind speed increases from the bottom to upper. Wind shear can be divided into horizontal and vertical wind shear and both of them can be either positive or negative. Positive vertical wind shear describes the increase in wind speed with height above ground, whereas positive horizontal wind shear means that wind speed increases to left when looking downwind. [22]. Overhead view of the horizontal wind shear and cross-section view of the vertical wind shear are illustrated in the figure 2.2.

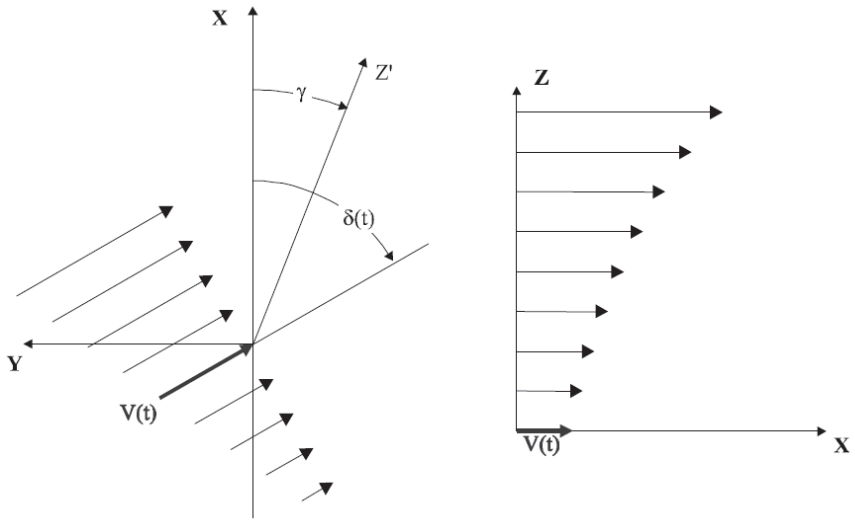

Figure 2.2. *Horizontal (on left) and vertical wind shear (on right). [22]*

Wind shear causes cyclic torque fluctuations in each blade which are nearly sinusoidal with fundamental frequency 1*P* (once per revolution) [1]. In the case of a three-bladed rotor, the load components are 120° out of phase between the three blades and thus, only the harmonics at 3*P*, 6*P*, etc. will be experienced by the hub and the rest of the structure while 1*P* and other harmonics tend to cancel out [2].

2.3.2 Tower Shadow

When a blade of the turbine is passing by the tower, the airflow experienced by the blade is interrupted and the mechanical torque experiences a small dip. This dip is transferred to the generator, which causes a small dip in the output power of the wind turbine. [23]. The decrease in the wind speed due to the presence of the tower is illustrated in the figure 2.3.

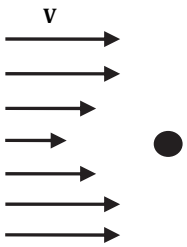

Figure 2.3. *Wind speed profile due to tower shadow effect partly from [24]*

These torque dips are most significant when a turbine has blades downwind of the tower and thus, the most wind turbines nowadays have upwind rotors [16]. Furthermore, tower shadow has an effect on the loading of the blades and the fixed parts of the turbine structure. The effect of tower shadow is sometimes called 3*P* effect because each of the blades is directly in front of the tower once per revolution and hence, the whole turbine structure will experience the phenomenon three times per revolution. [10]. In addition to tower, buildings or other wind turbines, for example, can cause similar shadow effect leading to power drops and increased loading.

3 BASIC CONTROL OF A WIND TURBINE

Control has a crucial role in the modern wind energy conversion systems (WECS). By proper control the turbine capacity can be utilized more effectively and the aerodynamic and mechanical loads reducing the life time of the WECS can be alleviated. Furthermore, as the size of the turbines and the amount of the WECS increase, more and more power to the grid is produced through wind energy. This increases the concern of power quality produced by wind energy, which increases importance of the active control too. However, active control has a direct effect on the cost of power. Therefore, effective and reliable controllers are needed in order to gain an optimum compromise between different control objectives. [1].

Wind turbines can be programmed to operate at different operation modes, i.e., the turbine can be actuated by different ways. Because of the varying operation conditions of the wind turbines, the modes of operation are usually combined in order to gain the most satisfying performance through the whole operation area. [1]. Most common combination of the operation modes nowadays is the variable-speed variable-pitch operation, which is achieved by combining the generator torque control and the collective pitch control of the rotor blades. Furthermore, nacelle yaw control is used in order to guarantee the optimum direction of the turbine related to the wind direction.

This chapter begins with the definitions of control objectives. Then, different operation modes of the wind turbines are introduced. Finally, the different parts of the baseline control system of the variable-speed variable-pitch wind turbine are described.

3.1 Control Objectives

A purpose of the operation of a wind turbine is to produce as much power from the wind energy as possible with the minimum costs. In addition, safe operation of the turbine has to be ensured and the demands of the power quality and acoustic emission standards have to be met. Minimization of the energy costs can be gained by finding a balanced compromise between partial control objectives, which are maximization of energy capture, minimization of mechanical loads and as good power quality as possible. [1].

3.1.1 Maximization of Energy Capture

Generation capacity of a wind turbine is usually defined as a curve on the generated power – wind speed plane [1]. This so-called ideal power curve for a typical wind turbine is represented in the figure 3.1.

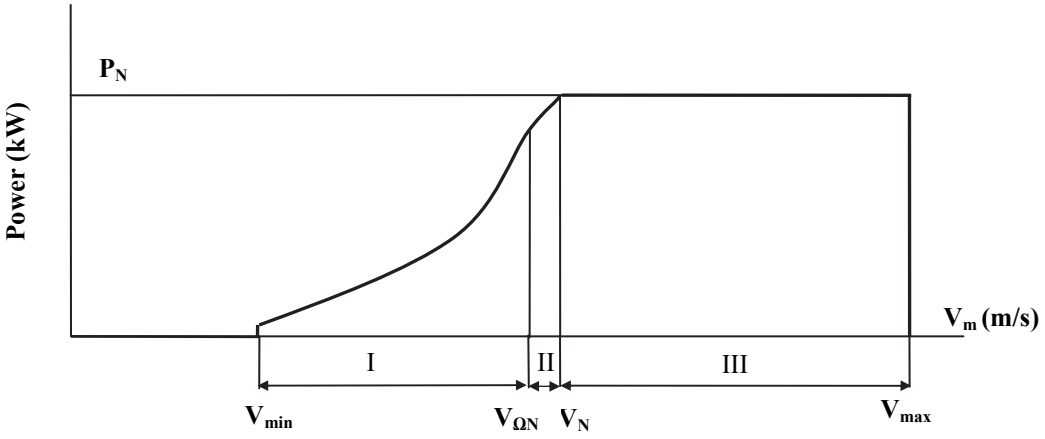

Figure 3.1. *Ideal power curve for the typical wind turbine [1]*

At wind speeds below cut-in wind speed (V_{min}) the turbine remains stopped, because the wind speed is not high enough for the economical operation of the wind turbine. On the other hand, if the wind speed is higher than the cut-out (V_{max}) wind speed, the turbine will be stopped in order to guarantee the safe operation of the turbine. Above the rated wind speed V_N, the ideal power curve remains constant at rated power. According to Bianchi et al. [1], it is not profitable to design the turbine to extract all the available energy up to cut-out wind speed, because it would only increase the energy costs per kW.

The ideal power curve can be divided into three different regions with different generation objectives. In the region I, when the wind speed is below V_N, the generation objective is to capture all the available power. The available power is thus lower than the rated power and can be defined as

$$P_{av} = C_{Pmax}P_v = \frac{1}{2}\rho\pi R_{rotor}^2 C_{Pmax}V^3, \tag{3.1}$$

where P_v is the power in the wind and C_{Pmax} is the maximum power coefficient and furthermore, R_{rotor} is the radius of the rotor, V is the wind speed and ρ is the air density. In the region III, where the wind speed is higher than the rated wind speed, the generation objective is to limit the generation power below the rated power. So, the turbine is operating with the efficiency lower than C_{Pmax}. In the control region II, which is actually the transition between the regions I and III, the rotor speed is limited in order to decrease noise emissions and centrifugal forces. [1].

3.1.2 Minimization of Mechanical Loads

Mechanical loads affecting on the components decrease the useful lifetime of the wind turbine. For this reason, they increase the cost of produced energy and their minimization should be considered in the economical operation of a wind turbine in addition to the maximization of energy capture. Bianchi et al. [1], present that these mechanical loads can be divided into static and dynamic loads. Static loads are caused by the quasi-steady mean wind speed affecting on the turbine. However, dynamic loads, induced by uneven distribution of the wind speed over the blades, are more significant from the control point of view. These disturbing moments affecting on the turbine causing, for example, in-plane and out of plane movements of the rotor blades or bending of the tower, are illustrated in the figure 3.2.

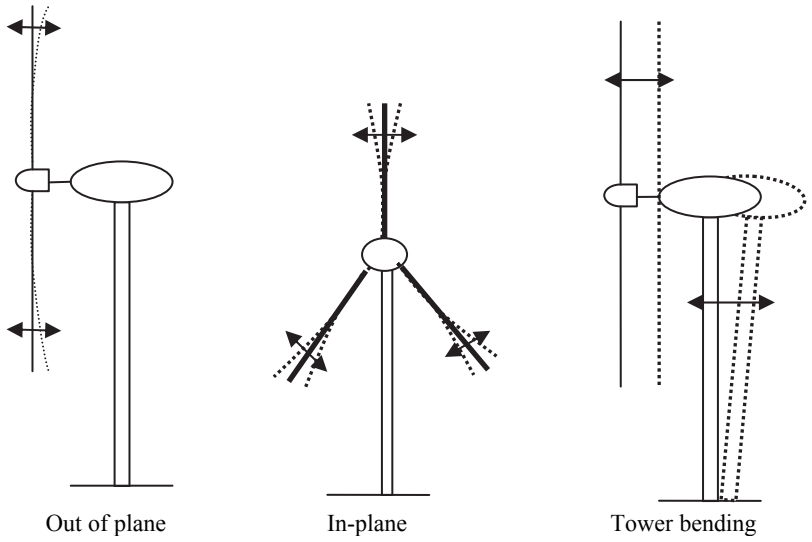

Figure 3.2. *Oscillatory movements of a wind turbine [1]*

Vibration modes described above should be considered in the design of the turbine and the controller because unsuitable rotational sampling or control strategy can excite some of these vibration modes. This reduces the lifetime of the components and in the worst case, may lead to the fatigue breakdown of the entire turbine. [1]

3.1.3 Power Quality

Electricity produced by wind turbines is typically considered as poor quality power. Because of the significant variations in the amount of produced power by WECS, other energy suppliers are always needed in order to remain the defined voltage and frequency level in the grid. However, while the wind turbines are becoming larger and the amount of them increases, the significance of the wind power as an energy source becomes more remarkable. Therefore, the quality of power produced by WECS becomes more critical issue and has to be considered in the control of the WECS.

Fluctuations in the output power of the wind turbines are caused by the stochastic and deterministic variations in the wind experienced by the turbine. Deterministic or periodic variations are more significant and the largest periodical effect on the quality of the output power is tower shadow effect. [25]. As mentioned in the chapter two, tower shadow contributes to the 3*P* effect, which leads to the drops in the output power at 3*P* frequency. Furthermore, 3*P* effect together with the stochastic variations in the wind due to gusts and turbulence results in flicker emissions in the grid. According to Anaya-Lara et al. [4], flicker problem is less significant in the case of variable-speed wind turbines, which are the most common nowadays, than in the case of fixed speed turbines because variations in wind speed are not directly translated into fluctuations in the output power. However, another issue affecting on the power quality has to be considered with variable speed turbines, namely the harmonic distortion. Variable speed turbines contain power electronic converters which produce high-frequency harmonic currents.

Different methods for power quality improvement in the case of wind turbines have been introduced in the literature. Hu et al. [26] introduce flicker mitigation method based on the damping of 3*P* power oscillations by active power control, whereas Bin et al. [27] use the individual pitch control for flicker reduction. Furthermore, Amin et al. [28] introduce a method using an uncontrolled rectifier-digitally controlled inverter for power quality improvement. However, methods aiming at improvements in output power are not discussed further in the scope of this thesis.

3.2 Operation Modes of a Wind Turbine

Wind turbines can be programmed to operate in various ways. Fixed-speed, variable-speed, fixed-pitch and variable-pitch are the modes of operation that are typically used. Fixed-speed fixed-pitch (FS-FP) operation has been the most common during some decades but it has become less attractive in commercial wind turbines nowadays. In the FS-FP mode, the asynchronous machine is connected directly to the grid and thus, the generator speed is locked to the power line frequency. [1]. This scheme is simple and low-cost but the performance is poor because the conversion efficiency is low and no active control can be done in order to gain load alleviation or power quality improvement. The limitation of power above rated wind speeds is gained by passive stall, which results in a decrease in aerodynamic torque and power. [1; 4]. In fixed-speed variable-pitch (FS-VP) mode of operation, power limitation above rated wind speeds is attained by controlling the pitch angle of the blades. This can be done by pitch-to-feather or by pitch-to-stall method. The blades are feathered as wind speed rises in the former method and the pitch angle is reduced as wind speed rises in the latter method respectively. So, the difference between pitch-to-feather and pitch-to-stall methods lies in the direction in which the pitch angle is adjusted as wind speed arises. [1]

Variable-speed operation increases the energy capture at low wind speeds and it also enables dynamic load alleviation and power quality enhancement. Variable-speed fixed pitch (VS-FP) mode can be implemented either by passive or assisted stall regulation. Variable-pitch operation, in turn, enables an efficient power regulation at higher wind speeds. In addition, by varying the pitch angle, transient loads can be alleviated which is an important benefit compared to the fixed-pitch operation mode. [1]. Therefore, variable-speed variable-pitch (VS-VP) wind turbines are the most common turbine configurations in the conventional use nowadays.

3.3 Control System

Control of power-production operation in variable-speed variable pitch wind turbines is based on two basic control systems: generator torque control and collective pitch control of the rotor blades. Furthermore, the active nacelle yaw control is used in MW turbines in order to guarantee the ideal direction of the turbine related to the direction of wind. Generator-torque control is used to maximize the power capture below the rated wind speed and the purpose of the collective blade pitch control is to limit the rotor speed at the wind speeds above rated [5]. These two controllers are usually controlled separately. Power curve for the 5 MW wind turbine is expressed in the figure 3.3 and it can be divided into three different operation regions with different control objectives.

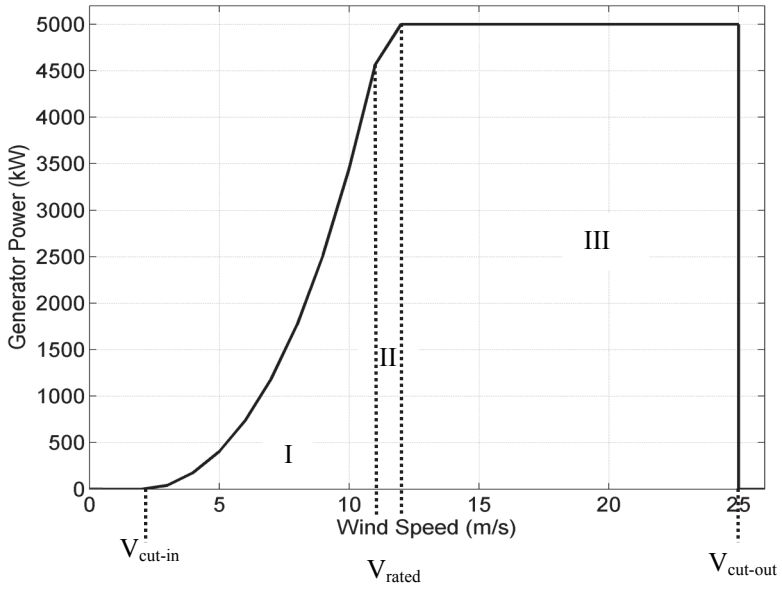

Figure 3.3. *Power curve for the 5-MW reference turbine*

In the region I, the wind speed and thus generator torque are below rated and the blade pitch angle is held constant. Generation purpose in this region is to maximize the energy capture. In region III, i.e. above rated wind speed, available power exceeds rated power and the rotor speed and thus generator torque are limited by varying the collective blade pitch angle. When the generator torque is kept constant, the aerodynamic power can be affected by regulating the turbine speed by the control of the blade pitch angle. Region II is a transition between the optimal power curve in region I and the constant power line in region III. Furthermore, below cut-in wind speed, the turbine remains stopped because the available wind energy is too low for efficient power production. Above cut-out wind speed, for turn, the turbine is shut down in order to avoid damages. [1; 5].

3.3.1 Generator-torque Controller

Below rated wind speed, control of a wind turbine is based on the control of the generator torque and the purpose is to maximize the energy capture. The turbine is operated at variable speed and the pitch angle is kept constant in order to capture as much energy as possible. Available power can be defined as the power in the wind which passes through the rotor disk multiplied by the maximum power coefficient C_{Pmax} according to (3.1). For convenience, the equation is repeated here:

$$P_{av} = C_{Pmax}P_v = \frac{1}{2}\rho\pi R_{rotor}^2 C_{Pmax}V^3, \tag{3.1}$$

Maximum efficiency is gained at particular pitch angle θ_0 and tip speed ratio λ_0. Tip speed ratio is defined as the ratio between the rotational speed of the blade tip and the wind speed. Thus, both of them should be kept constant at these values in order to maximize the energy capture below rated power. This means that the rotor speed Ω_{r0} must change proportionally to the wind speed:

$$\Omega_{r0} = \frac{\lambda_0 V}{R_{rotor}}. \tag{3.2}$$

In this operation region, the generator torque T_{r0} that gives the optimal tip speed ratio λ_0 is gained as a function of rotor speed:

$$T_{r0} = c \cdot \Omega_{r0}, \tag{3.3}$$

Where the gain c is

$$c = \frac{1}{2}\rho\pi R_{rotor}^5 \frac{C_{Pmax}}{\lambda_0^3}. \tag{3.4}$$

The turbine can be controlled to operate in different operating points by controlling the generator torque and thus gain the maximum energy capture even though the wind speed is changing. The control of the generator torque is handled by a suitable control of the electronic converters related to the generator. [1; 29]. Because the scope of this thesis is in the pitch control, generator torque control is not dealt with more detail. Further information about generator-torque control can be found for example from [4; 30].

3.3.2 Collective Blade Pitch Controller

Collective blade pitch control (CPC) becomes active in the operation region III, where the wind speed is equal or greater than the rated wind speed. Generator torque is kept constant at its rated value and the aerodynamic power is limited by controlling the blade pitch angle in order to regulate turbine speed at its rated value. Collective pitch control means that a common angle request is sent for all of the three blades of the turbine. CPC uses generator speed as a measurement signal and a PI controller is typically used in the collective pitch control of a wind turbine [31]. A simple free-body diagram for the drivetrain of the wind turbine is shown in the figure 4.1.

Figure 3.4. *Free-body diagram for the drivetrain of the turbine*

According to Butterfield et al. [5], from the free-body diagram, the equation of motion for the wind turbine can be expressed as

$$T_{Aero} - N_{Gear}T_{Gen} = (I_{Rotor} + N_{Gear}^2 I_{Gen})\frac{d}{dt}(\Omega_0 + \Delta\Omega) = I_{Drivetrain}\Delta\dot{\Omega}, \qquad (3.5)$$

Where T_{Aero} is the aerodynamic torque of the low speed shaft, T_{Gen} is the generator torque of the high-speed shaft, N_{Gear} is the gearbox ratio from high-speed to low-speed, $I_{Drivetrain}$ is the inertia of the complete drivetrain as experienced on the low-speed side, I_{Rotor} is the rotor inertia, I_{Gen} is the generator inertia, Ω_0 is the rated rotor speed, $\Delta\Omega$ is the small perturbation of the rotor speed about the rated speed and $\Delta\dot{\Omega}$ is the rotational acceleration of the rotor. [5].

In the control region III, in which the collective pitch control is active, the generator-torque controller holds the generator power constant and thus, the generator torque is inversely proportional to the generator speed:

$$T_{Gen}(N_{Gear}\Omega) = \frac{P_0}{N_{Gear}\Omega} \tag{3.6}$$

Where P_0 is the rated mechanical power and Ω is the rotor speed. The aerodynamic torque can be calculated at the same manner, assuming that the torque variations with rotor speed are negligible:

$$T_{Aero}(\theta) = \frac{P(\theta, \Omega_0)}{\Omega_0}, \tag{3.7}$$

where P is the mechanical power and θ is the collective blade pitch angle. [5]. By linearization it can be derived from (3.6) and (3.7)

$$T_{Gen} \approx \frac{P_0}{NR_0} - \frac{P_0}{N_{Gear}\Omega_0^2}\Delta\Omega \tag{3.8}$$

and

$$T_{Aero} \approx \frac{P(\theta^*, \Omega_0)}{\Omega_0} + \frac{1}{\Omega_0}\left(\frac{\partial P}{\partial \theta}\right)\Big|_{\theta=\theta^*}, \tag{3.9}$$

where $\Delta\theta$ is a small perturbation of the collective blade-pitch angle about its operating point θ^*. When the PI control is used, $\Delta\theta$ can be derived from the perturbations of the rotor speed

$$\Delta\theta = K_P N_{Gear}\Delta\Omega + K_I \int_0^t N_{Gear}\Delta\Omega dt, \tag{3.10}$$

where K_P is the proportional and K_I the integral gain of the collective blade-pitch controller. By defining the rotor speed error $\Delta\Omega = \dot{\phi}$ and combining the equations introduced above the equation of motion for the rotor speed error can be expressed as

$$\underbrace{I_{Drivetrain}}_{M_\phi}\ddot{\phi} + \underbrace{\left(\frac{1}{\Omega_0}\left(-\frac{\partial P}{\partial \theta}\Big|_{\theta=\theta^*}\right)N_{Gear}K_P - \frac{P_0}{\Omega_0^2}\right)}_{C_\phi}\dot{\phi} + \underbrace{\left(\frac{1}{\Omega_0}\left(-\frac{\partial P}{\partial \theta}\Big|_{\theta=\theta^*}\right)N_{Gear}K_I\right)}_{K_\phi}\phi = 0 \tag{3.11}$$

Properties of this second order system can be expressed by natural frequency

$$\omega_{\phi n} = \sqrt{\frac{K_\phi}{M_\phi}} \tag{3.12}$$

and damping ratio

$$\varsigma_\phi = \frac{C_\phi}{2\sqrt{K_\phi M_\phi}} = \frac{C_\phi}{2M_\phi \omega_{\phi n}}. \tag{3.13}$$

Now, according to Butterfield et al., [5] the proportional gain K_P and integral gain K_I can be solved from (3.11), when fixing the values of $\omega_{\phi n}$ and ς_ϕ and neglecting the small negative damping term $-\frac{P_0}{\Omega_0^2}$:

$$K_P = \frac{2I_{Drivetrain}\Omega_0 \varsigma_\phi \omega_{\phi n}}{N_{gear}\left(-\frac{\partial P}{\partial \theta}\right)} \tag{3.14}$$

and

$$K_I = \frac{I_{Drivetrain}\Omega_0 \omega_{\phi n}^2}{N_{gear}\left(-\frac{\partial P}{\partial \theta}\right)} \tag{3.15}$$

Unfortunately the PI controller derived above cannot be used in its simplest form. The problem is the pitch sensitivity $\partial P/\partial \theta$ which is a nonlinear term that depends on the wind speed, rotor speed and blade-pitch angle. [5].

To be able to overcome this problem, gain scheduling techniques are typically used in the case of collective pitch control. Gain scheduling has been extensively used in industry and the controllers based on this technique can be found in many applications. Basic gain scheduling is based on the linearization of nonlinear or time-varying system around a selected group of operation points. Then, a linear controller is designed for each of these linear time-invariant systems and the gain-scheduled controller is chosen from the group of linear controllers depending on the current operation point. Despite of the popularity and the good performance of the gain-scheduled controllers, there are also some challenges concerning them. Stability, robustness and performance properties of the gain-scheduling controlled system cannot be defined from the feedback properties of the group of linear time-invariant systems. [1]. However, the technique is widely used in industrial applications and good results based on the method have been gained also in the collective pitch control of the wind turbine blades.

3.3.3 Yaw Controller

According to Bossanyi et al. [21], the nacelle of the wind turbine is typically free to yaw and thus, the turbine will naturally be pointing into the wind. However, the direction of the turbine is not exactly optimal into the wind and some active control of the nacelle angle may be needed in order to maximize the energy capture. In addition, it is presented in the researches [32; 33], that the loads affecting on the yaw mechanism become so significant when the turbines become larger, that the active yaw control is needed to mitigate these loads.

Nowadays, most wind turbines are equipped with a wind vane on the top of the turbine in order to get information about the speed and the direction of the wind. The purpose of the yaw control is to minimize the error between wind and nacelle directions because the power output of a wind turbine is proportional to the cosine value of this yaw error. Hence, the maximum efficiency is gained with a zero error angle. It is worth of noting, that the constant fluctuations in the wind cause continuous small yaw movements which cause fatigue stress for the mechanical components of the turbine. [33] Therefore, the yaw vane signal has to be averaged heavily before it is taken as an input to the controller [21]. The nacelle is operated to follow the shortest path into the wind and thus, yawing to a certain direction may cause the twisting of the cables. For this reason, the yaw controller system needs to be equipped with the algorithm that prevents this cable twist. [32]. Because the main focus in this thesis will be in the blade pitch control, yaw control is not dealt further in the thesis. More detailed information about wind turbine yaw control can be found for example in [32; 33].

4 COLLECTIVE PITCH CONTROL

As discussed in the chapter 3.3, the collective blade pitch control (CPC) becomes active in control region III, where the wind speed is equal or greater than the rated wind speed. The generator torque is kept constant at its rated value and the aerodynamic power is limited by controlling the blade pitch angle in order to regulate the turbine speed at its rated value. CPC uses generator speed as a measurement and conventional PI control strategies combined with the gain scheduling techniques are typically used. [29].

Within this thesis, performance of the collective pitch controller for the 5-MW reference turbine developed by National Renewable Energy Laboratory (NREL) [5] in the presence of extreme wind scenarios based on the standard IEC-61400-1 [34] was evaluated. Furthermore, the effects of the extreme wind scenarios and the normal wind shear on the wind turbine loading were investigated. Simulations were made by using NREL's wind turbine simulation software called Fatigue, Aerodynamics, Structures and Turbulence (FAST) [35; 36]. This chapter begins with introducing the 5-MW reference turbine and the CPC scheme for this controller. The chapter continues with the simulation results. First, extreme wind scenarios and the performance of the CPC in the presence of them are introduced. Then, the loads affecting on the wind turbine during its operation are discussed together with the corresponding simulation results. Finally, the effect of wind shear on the wind turbine loading is discussed more detail.

4.1 Simulation Environment

All simulations within this thesis are made by using the 5-MW reference wind turbine developed by National Renewable Energy Laboratory (NREL) [5]. This turbine is a horizontal-axis, three-bladed upwind turbine which is the most common turbine structure of the large-scale wind turbines nowadays. The turbine model is described in details in [5], but some basic parameters are shown in the table 4.1.

Table 4.1. *Basic parameters for the Reference Wind Turbine Model [5]*

Rating	5 MW
Rotor Orientation, Configuration	Upwind, 3 Blades
Control	Variable Speed, Variable Pitch
Drivetrain	High speed, Multiple-Stage Gearbox
Rotor, Hub Diameter	126 m, 3 m
Hub Height	90 m
Cut-In, Rated, Cut-Out Wind Speed	3 m/s, 11.4 m/s, 25 m/s
Cut-In, Rated Rotor Speed	6.9 rpm, 12.1 rpm
Rated Tip Speed	80 m/s
Overhang, Shaft Tilt, Precone	5 m, 5°, 2.5°
Rotor Mass	110,000 kg
Nacelle Mass	240,000 kg
Tower Mass	347,460 kg
Coordinate Location of Overall CM	(-0.2 m, 0.0 m, 64 m)

Simulations were made by using NREL's wind turbine simulation software called Fatigue, Aerodynamics, Structures and Turbulence [35; 36]. FAST is an open-source software and written in Fortran. FAST models the wind turbine as a combination of rigid and flexible bodies. Aerodynamic forces along the blades are generated from the AeroDyn subroutine package, which is also an open-source software library developed by Windward Engineering [37].

All three basic control methods described in the chapter three are available in FAST: pitch control of the blades, generator-torque control and nacelle yaw control. Utilization of these controllers needs only some appropriate input parameters to be added but the user can also implement more sophisticated control methods in a Simulink model with which FAST can be interfaced to. [35]. In this thesis, collective pitch control simulations were made by using the simple generator-torque control available in FAST and the collective pitch controller was implemented and ran by Simulink. Parameters needed in the simple generator-torque control were gained from the report of Butterfield et al. [5]. Furthermore, simple high speed shaft brake model available in FAST was used. No yaw control was used based on the recommendations in other reports. According to Butterfield et al. [5], the nacelle-yaw control system can be neglected in this kind of simulations because of its slow enough response that does not generally contribute to large extreme loads.

4.2 Gain Scheduled CPC for the 5-MW Reference Turbine

To overcome the problems caused by the nonlinearity of the pitch sensitivity $\partial P/\partial\theta$ mentioned previously in chapter 3.3, controller gains of the collective pitch controller are normally varied as a function of the pitch angle. To be able to schedule the gains of the PI controller, the pitch sensitivity from a linearized and uncontrolled system has to be measured. [3]. Linearization analysis has to be made at different wind speeds; at rated rotor speed and at the corresponding blade-pitch angles that produce the rated mechanical power. With the linearization procedure built in the FAST the pitch angle can be varied gently around the stable operating point θ^* and the resulting variation in the rotor power can be measured. Then, the same actions are repeated for other wind speeds. [5]. Linearization results derived in [5], are shown in the table 4.2.

Table 4.2. *Sensitivity of Aerodynamic Power to Blade Pitch Angle [5]*

Wind Speed (m/s)	**Rotor Speed (rpm)**	**Pitch Angle θ^* (deg)**	**$\partial P/\partial\theta$ (watt/rad)**
11.4 (Rated)	12.1	0.00	-28.24E+6
12.0	12.1	3.83	-43.73E+6
13.0	12.1	6.60	-51.66 E+6
14.0	12.1	8.70	-58.44 E+6
15.0	12.1	10.45	-64.44 E+6
16.0	12.1	12.06	-70.46 E+6
17.0	12.1	13.54	-76.53 E+6
18.0	12.1	14.92	-83.94 E+6
19.0	12.1	16.23	-90.67 E+6
20.0	12.1	17.47	-94.71 E+6
21.0	12.1	18.70	-99.04 E+6
22.0	12.1	19.94	-105.90 E+6
23.0	12.1	21.18	-114.30 E+6
24.0	12.1	22.35	-120.20 E+6
25.0	12.1	23.47	-125.30 E+6

It can be seen in the table above that the pitch sensitivity varies considerably over the control region III (above rated wind speed). Pitch sensitivity over the pitch angle is plotted in the figure 4.2 which shows that the sensitivity, however, varies almost linearly with blade-pitch angle. [5].

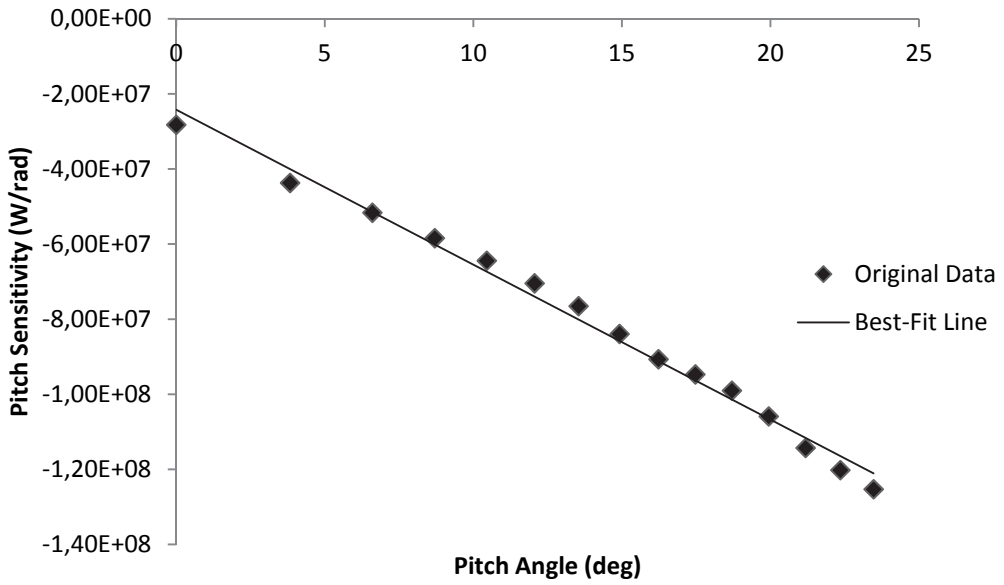

Figure 4.1. *Pitch sensitivity, original data and best-fit line [3; 5]*

So, according to Butterfield et. al. [5], the pitch sensitivity can now be expressed as

$$\frac{\partial P}{\partial \theta} = \left[\frac{\frac{\partial P}{\partial \theta}(\theta = 0)}{\theta_K}\right]\theta + \left[\frac{\partial P}{\partial \theta}\right](\theta = 0) \tag{4.1a}$$

or

$$\frac{1}{\frac{\partial P}{\partial \theta}} = \frac{1}{\frac{\partial P}{\partial \theta}(\theta = 0)\left(1 + \frac{\theta}{\theta_K}\right)}, \tag{4.1b}$$

Where $\frac{\partial P}{\partial \theta}(\theta = 0)$ is the pitch sensitivity at rated wind speed and $\theta_K$is the blade pitch angle at which the pitch sensitivity has doubled from the value at rated wind speed:

$$\frac{\partial P}{\partial \theta}(\theta = \theta_K) = 2\frac{\partial P}{\partial \theta}(\theta = 0). \tag{4.2}$$

Now, when the pitch sensitivity is known, proportional and integral gains can be derived based on the equations (3.14) and (3.15) which are repeated here for convenience:

$$K_P = \frac{2I_{Drivetrain}\Omega_0\varsigma_\phi\omega_{\phi n}}{N_{gear}\left(-\frac{\partial P}{\partial \theta}\right)} \tag{3.14}$$

$$K_I = \frac{I_{Drivetrain}\Omega_0\omega_{\phi n}^2}{N_{gear}\left(-\frac{\partial P}{\partial \theta}\right)} \tag{3.15}$$

Taking the (4.1b) into account too, one gets

$$K_P = \frac{2I_{Drivetrain}\Omega_0\varsigma_\phi\omega_{\phi n}}{N_{gear}\left[-\frac{\partial P}{\partial \theta}(\theta = 0)\right]}GK(\theta) \tag{4.3}$$

$$K_I = \frac{I_{Drivetrain}\Omega_0\omega_{\phi n}^2}{N_{gear}\left[-\frac{\partial P}{\partial \theta}(\theta = 0)\right]}GK(\theta), \tag{4.4}$$

where $GK(\theta)$, in according to Hansen et al., [36] is the dimensionless gain-correction factor depending on the pitch angle:

$$GK(\theta) = \frac{1}{1 + \frac{\theta}{\theta_K}}. \tag{4.5}$$

Based on the recommendations in the literature [36], values of $\omega_{\phi n} = 0.6\ rad/s$ and $\varsigma_\phi = 0.6\ to\ 0.7$ should lead to the desired response characteristics of the collective pitch controller. Finally, all parameters in (4.3) and (4.4) are known and the controller gains K_P and K_I can be defined.

Based on the equations above, collective pitch controller shown in the figure 4.3 at the next page is gained. Measurement signal of the generator speed has to be filtered in order to filter out the high-frequency components from the signal. Based on the recommendations in the report of Butterfield et al. [5], a simple first order low-pass filter can be used to filter the measurement signal because no additional value is gained with more sophisticated filter. The corner frequency of the filter was set to be 0.25 Hz, which is roughly one-quarter of the blade's first edgewise natural frequency [5].

Wind speed measurement is used as a feedforward signal in order to create so called operating pitch angle, i.e. θ in (4.16). This operating pitch angle is derived by using a simple lookup table that defines pitch angles at different wind speeds based on the table 4.1. In addition, the wind speed measurement is low-pass filtered too in order to model the dynamics of the wind speed measurement. Wind speed measurements in the real wind turbines are typically based on the average value of the time period from five to ten minutes. Therefore, the corner frequency of the wind speed filter was set to the value of 1/300 Hz, which describes the wind speed measurement based on the average value of five minutes.

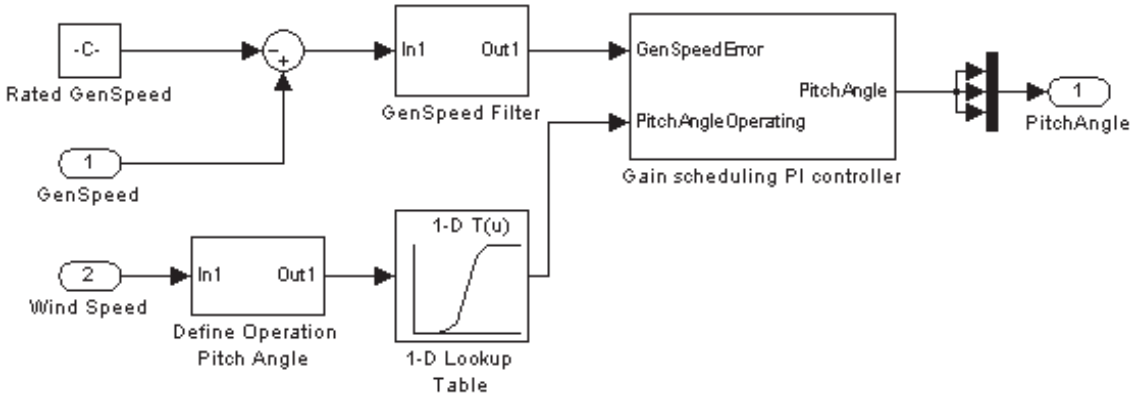

Figure 4.2. *Collective Pitch Controller used in the simulations*

Simulink model of the gain scheduling PI controller is shown in the figure 4.4. Pitch angle demand is created by adding small perturbation term created by PI controller to the operating pitch angle that is based on the feedforward wind speed measurement. Operating pitch angle is also used in the gain scheduling in order to derive the gain correction factor $GK(\theta)$ which is needed in (4.14) and (4.15). Anti wind-up connection is used in order to avoid eventual problems caused by the saturation of the pitch actuators. Based on the recommendations in [5], pitch angle demand is limited between 0 and 90 degrees and the pitch-rate limit is set to be 8°/s. By this way, the dynamics of the pitch actuators can be considered at some extent.

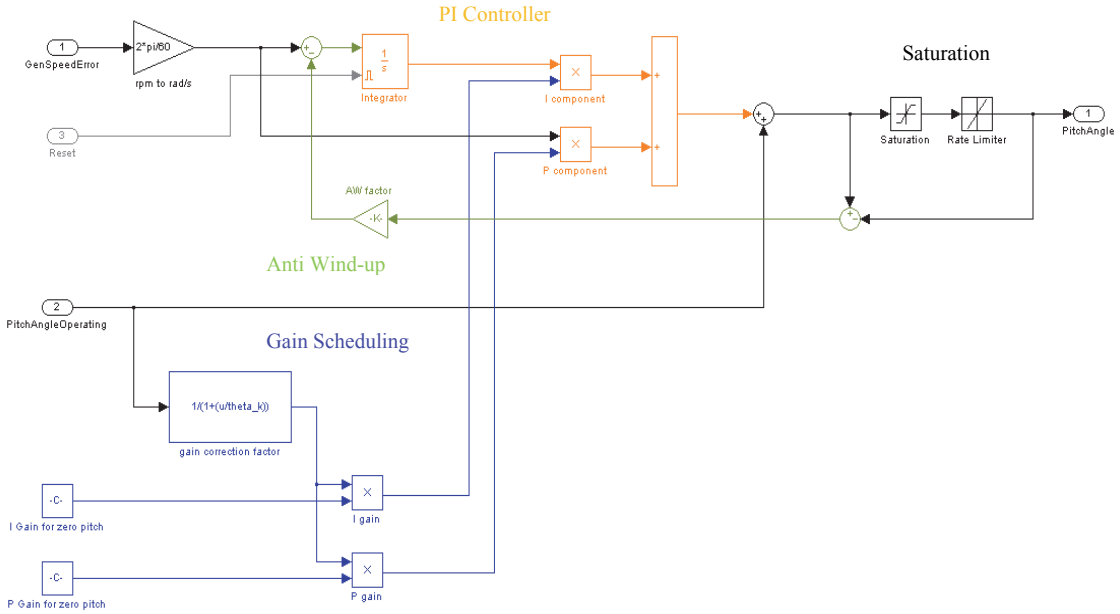

Figure 4.3 *Gain scheduling PI controller of the collective pitch control system*

Simulink model of the collective pitch controller was already available within the project in which this thesis is related. So, only the evaluation of the performance of the controller was done within this thesis.

4.3 Performance of the CPC during the Extreme Wind Scenarios

Performance of the collective pitch controller described in the previous chapter was evaluated in the presence of extreme wind scenarios defined in the standard IEC-61400-1 [34]. In other words, the purpose of the simulations was to investigate how the controller succeeds to limit the output power of the turbine above rated wind speeds and how it reacts to the extreme wind scenarios. In addition, the effects of extreme wind scenarios and the normal wind shear on the wind turbine loading were evaluated too. Before going to the simulation results in detail, the extreme wind scenarios and their characteristics are introduced briefly.

4.3.1 Extreme Wind Scenarios

According to the standard IEC-61400-1 [34], wind turbines must to be designed to withstand the normal frequently occurring wind conditions and the extreme wind conditions which are divided, based on the recurrence period, into 1-year or 50-year conditions. The standard defines two normal wind conditions and six different extreme wind scenarios. The normal wind profile *(NWP)* is used to define the average wind speed and the average vertical wind shear across the rotor swept area. Another normal wind profile based on IEC-61400-1 is the normal turbulence model *(NTM)* which is used to describe the normal short-term variations in the wind speed.

Extreme wind conditions in IEC-61400-1 [34], include extreme wind shear events and peak wind speeds caused by storms and rapid changes in the speed and the direction of the wind. In the extreme wind speed model *(EWM)*, either the extreme wind speed with a recurrence period of 50 years or 1 year can be used. A longitudinal standard deviation is added into the normal wind profile model in the extreme turbulence model (ETM) to model the extreme turbulence in the wind. Furthermore, extreme operating gust *(EOG)* defines a rapid short-time increase in the wind speed and extreme direction change *(EDC)* describes the extreme changes in the direction of the wind. Extreme coherent gust with direction change *(ECD)* combines a gust speed and direction change occurring simultaneously. Finally, there are the extreme wind shear *(EWS)* scenarios which can be divided into vertical and horizontal wind shear scenarios.

Based on the guidelines in [38], only *normal wind profile, extreme operating gust* and *extreme wind shear* scenarios were used in the simulations. Other scenarios are not that critical from the blade pitch control point of view. For example, during the extreme wind speed, the turbine is shut down and no pitch control is then needed either.

On the other hand, *extreme coherent gust with direction change* was meant to be used in the simulations. However, it was pointed out that the direction change in this scenario, causing nacelle yaw error, leads to the significant oscillations in the rotor speed. Rotor speed with and without nacelle yaw control, after the extreme coherent gust with direction change, is represented in the figure 4.5. Hence, in order to get comparable simulation results in the presence of ECD, active nacelle yaw control is needed. However, nacelle yaw control is not dealt within this thesis and therefore the ECD wind scenario was not used in the simulations. Consequently, three extreme wind scenarios were simulated; EOG as well as vertical and horizontal wind shear scenarios EWSV and EWSH, respectively.

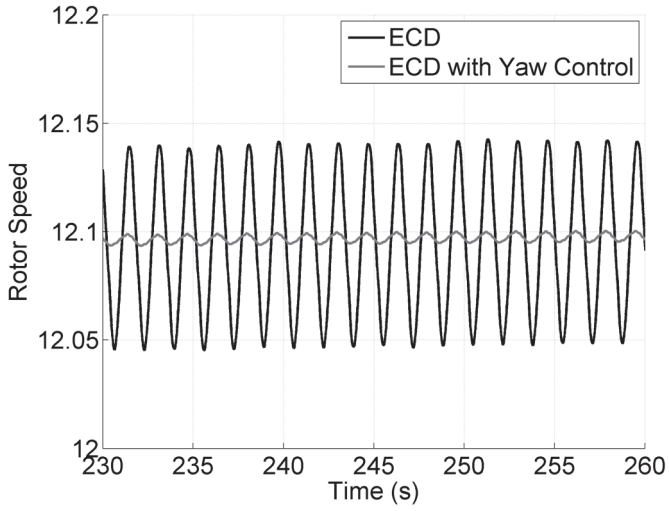

Figure 4.4. *Rotor Speed after the extreme coherent gust with direction change*

Wind files based on the standard and compatible with the simulation tools used are available. The most interesting of them were chosen based on the typical wind range in the power production where the collective pitch control is active. So, because the rated wind speed for the reference 5-MW wind turbine model is 11.4 m/s [5], wind speed has to be greater than this in order to activate the CPC.

In the EOG wind scenario used, a transient gust wind speed is added to the normal wind profile with the wind speed of 15 m/s at the time of 100 seconds. After the gust, wind speed returns to average value of 15 m/s, as it was before the guest. In the extreme wind shear scenarios, wind speed is 13 m/s. A transient vertical wind shear is added to the normal wind profile in EWSV and a transient horizontal wind shear in EWSH. In both cases, the extreme wind shear is applied on the time of 100 seconds. Wind speed profiles in the case of EOG and EWSV are illustrated in the figures A.1 and A.2 in the appendix A, respectively. The shape of EWSH profile is similar to the profile of EWSV. The only difference is that instead of linear vertical shear, linear horizontal shear is present.

4.3.2 Performance of the Controller

As mentioned earlier, the extreme wind conditions are applied into the system at the time of 100 seconds in every wind scenario simulated. The responses of the system are shown in the figure 4.6, the pitch angle of the blade one is shown on the top and the rotor speed on the bottom of the figure. It should be noted, that the pitch angle is thus the same for the blades two and three, and therefore only one of them is illustrated here. One can see that basically the collective pitch controller is operating fine in the presence of extreme wind conditions. Changes in the rotor speed can be seen when the extreme wind conditions are applied to the system. In the consequence, the collective pitch controller responses to these changes by changing the pitch angle. At the normal wind conditions, in other words, before and after the extreme wind conditions, the collective pitch controller is able to remain the rated rotor speed (12.1 rpm). However, especially in the case of EOG, there are significant fluctuations in the rotor speed when the gust speed is present which the collective pitch controller cannot eliminate. Therefore, some kind of predictive wind measurements would be valuable in order to adapt the operation of the controller for the variations in the wind speed. The effect of extreme wind shear conditions are much less significant and only slight changes can be seen in the blade pitch angle and the rotor speed.

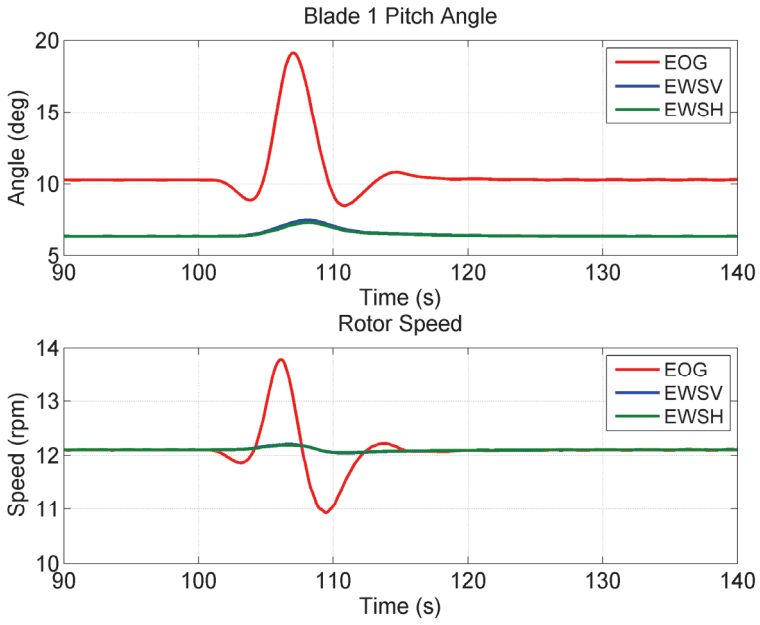

Figure 4.5. *Blade 1 Pitch Angle and Rotor Speed*

Fluctuations in the rotor speed result in the fluctuations in the generator power too. These fluctuations are illustrated in the figure 4.7. At the presence of extreme operating gust in EOG scenario, the produced power drops significantly and it takes approximately 20 seconds before the power is settled down after the gust. A drop in the generator power can be seen in the case of both extreme wind shear scenarios too, but the drop is notably smaller compared to the EOG scenario.

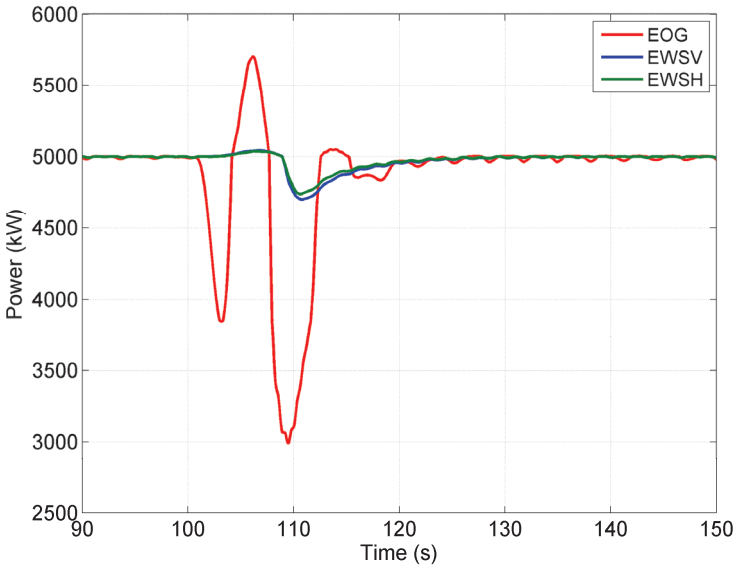

Figure 4.6. *Generator power in extreme wind conditions*

It is worth of noting, that the simple generator-torque control available in FAST was used in the simulations. So, the operation of the generator-torque controller is not probably the most optimal in the presence of a sudden gust in the wind speed which might influence on the behavior of rotor speed and hence, the generation power too. So, by more sophisticated generator-torque control, the drop in generator power could probably be decreased.

As described in the chapter 4.1, wind speed measurement in the simulations is low-pass filtered in order to simulate the wind speed measurement in a real wind turbine. Typically, the devices measuring the wind speed in the turbine are located on the nacelle behind the rotor and hence, only a very turbulent wind speed can be measured. Therefore, the measurement data has to be averaged over several minutes to be able to use this measurement data for the control purposes. Within this thesis however, the effect of ideal wind speed measurement in the presence of extreme operating gust was also simulated by running the simulation without filtering the wind speed. Differences in rotor speed and generator power between normal wind speed measurement of 5 minutes average and ideal case are illustrated in the figure 4.8.

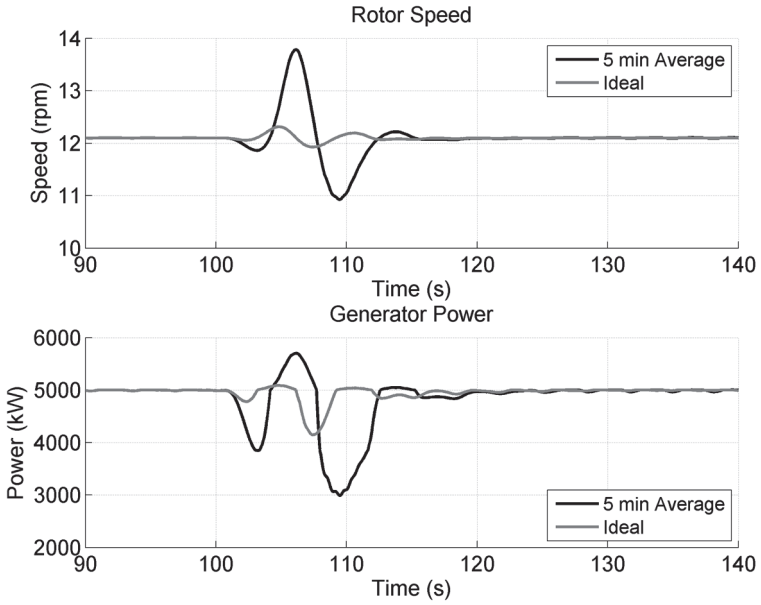

Figure 4.7. *Differences in rotor speed and generator power between different wind speed measurements in the presence of EOG.*

It can be seen, that the changes in the rotor speed and the generator power could be decreased significantly if the wind speed could be measured faster. This point contributes to the utilization of modern measurement techniques, for example LIDAR (light detection and ranging), in the wind turbine control purposes. Measurement speed of the commercial LIDAR measurement products is typically 1 second [39] and thus, it might be possible to decrease the effect of sudden gust speed significantly by using them in the wind turbines.

4.4 Wind Turbine Loading

In addition to the behavior of the rotor speed, there are also other interesting variables that should be considered when defining the performance of the collective pitch controller. During the operation of a wind turbine, there are different loads affecting on the blades and other parts of the turbine. The most significant loads are cyclic in-plane and out of plane moments affecting on the blades, as well as the tilt and yaw moments affecting on the top of the tower. Out of plane moments of the three blades can be represented as two non-rotating moments affecting on the top of the tower, i.e., as tilt and yaw moments. These disturbing blade and tower top moments are illustrated in the figure 4.9.

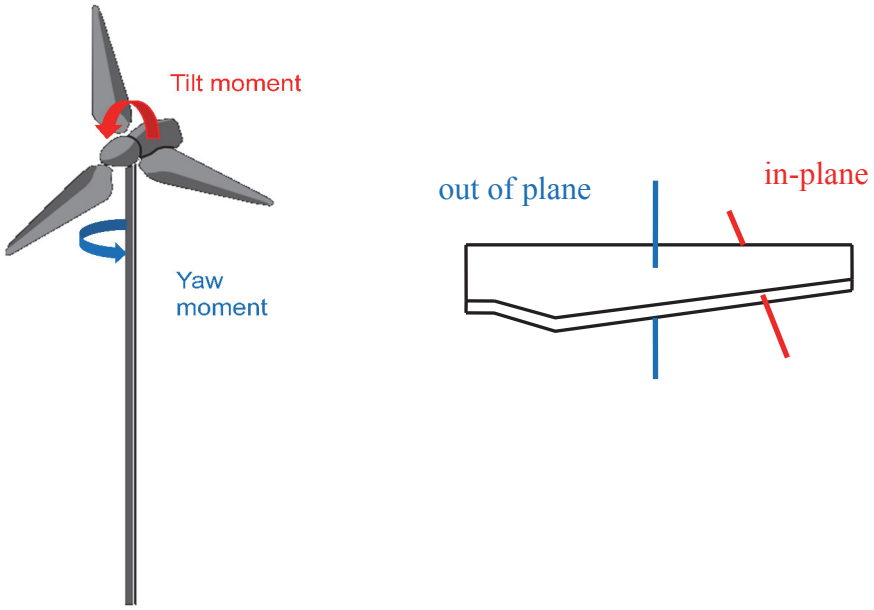

Figure 4.8. *Disturbing moments affecting on the turbine*

Main cause of the tilt and yaw moment is the effect of wind shear, in other words the uneven distribution of the wind speed through the rotor swept area [3]. Most significant oscillations in the blade loads occur at the fundamental frequency of 1*P*, in other words at the rotor frequency, whereas the loading of the hub and other fixed parts of the turbine is caused by the 3*P* frequency components and its harmonics. The cancellation of the fundamental component from the tilt and yaw moments is due to the averaging effect of the three blades. [1].

4.4.1 Wind Turbine Loading in the presence of Extreme Wind Scenarios

Extreme wind scenarios affect on the wind turbine loading too. Figure 4.10 shows the effect of the extreme wind scenarios on the out of plane and in-plane blade moments for the blade one. The effect of extreme wind scenarios can be seen in the out of plane blade moments in each case and the influence of extreme operating gust is the most remarkable. However, the in-plane moment remains nearly unchangeable in the case of EOG and EWSV. Only the horizontal wind shear affects on the in-plane loading by decreasing it slightly.

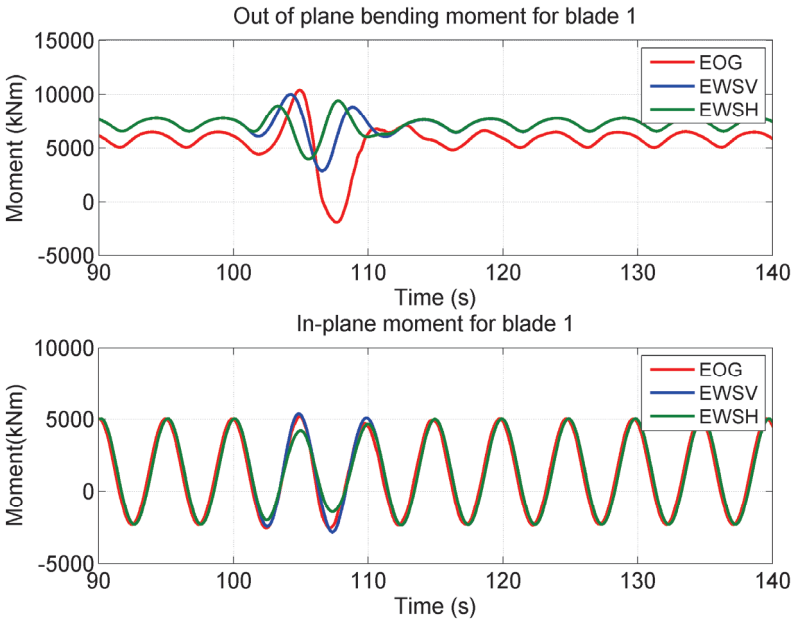

Figure 4.9. *Blade 1 In-plane and out of plane moments in the presence of extreme wind scenarios*

Disturbing tilt and yaw moments affecting on the top of the tower in the presence of extreme wind scenarios are illustrated in the figure 4.11. Changes in the tilt and yaw moments are most significant in the case of both extreme wind shear scenarios. When the extreme vertical wind shear is applied to the system, significant peak can be seen in the tilt moment. On the other hand, the extreme horizontal wind shear has the greatest impact on the yaw moment. This is quite obvious when the definitions of horizontal and vertical wind shear (see figure 2.2) as well as tilt and yaw moments (see figure 4.9) are considered.

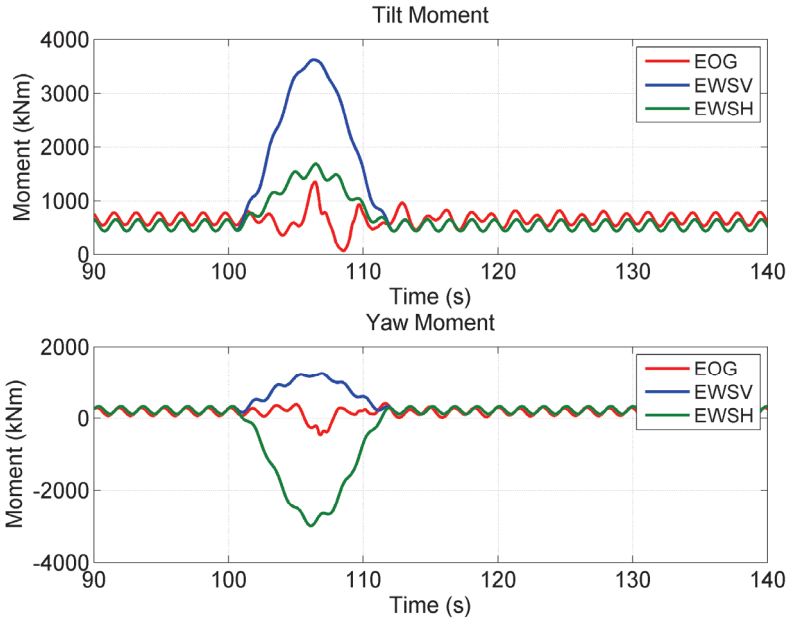

Figure 4.10. *Tilt and Yaw Moments in the presence of extreme wind scenarios*

As a conclusion, it can be said the extreme wind shear, both vertical and horizontal, has a major impact on the tower top loading whereas the sudden gust causes significant fluctuations in the out of plane blade moment.

4.4.2 Effect of Wind Shear on the Wind Turbine Loading

In addition to the simulations concerning the performance of the collective pitch controller in the extreme wind conditions, some simulations were made in normal wind conditions to analyze the effect of wind shear more precisely. It should be noted that normally when dealing with the wind shear vertical wind shear is meant (see the figure 2.2 on the right). As discussed earlier in this thesis, the wind shear can be regarded as the main cause of fatigue stress of the turbine. A typical way to simulate wind shear is to use a concept of vertical power law shear. According to [22], the vertical power law shear, *VSHR*, is the exponent of a power law shear profile and it is used to define the wind speed V_z at any height z.

$$V_z = V_{hub}(z/z_{hub})^{VSHR}, \tag{4.6}$$

where z_{hub} is the hub-height and V_{hub} is the hub-height wind speed.

Firstly, the operation of the system was simulated in the ideal case, where the wind speed is constant and no wind shear is affecting on the turbine. In other words, the exponent in (4.6) was set to zero. Secondly, the vertical power law shear of 0.14 was added to the system. This wind shear can be treated as a normal vertical wind shear, which can be assumed to be present in the normal operation conditions of a wind turbine [40]. Simulations were made with two different wind speeds; 13 m/s and 23.7 m/s in order to see how the system is operating near the rated wind speed (11.4 m/s) and near the cut-out wind speed (25 m/s). Out of plane blade root bending moment and in-plane blade moment for the blade 1 at the wind speed of 13 m/s are illustrated in the figure 4.12. Corresponding figure at the wind speed of 23.7 m/s is expressed in the figure A.3 in the appendix A. So, when the wind shear is added to the system, the amplitude of the out of plane root bending moment more than doubles itself, compared to the situation where no wind shear is present. In addition to the increase in amplitude, there is also phase shift between the steady and the wind shear conditions, which is greater at the lower than the higher wind speed. Sinusoidal out of plane blade moment in the case where no wind shear is present is due to the gravitational forces acting on the pre-coned blades. It is also worth of noting, that the in-plane blade moments are nearly equal in both cases. Therefore, it can be seen that the normal vertical wind shear do not contribute to the in-plane blade loading but it has a significant impact on the out of plane loading.

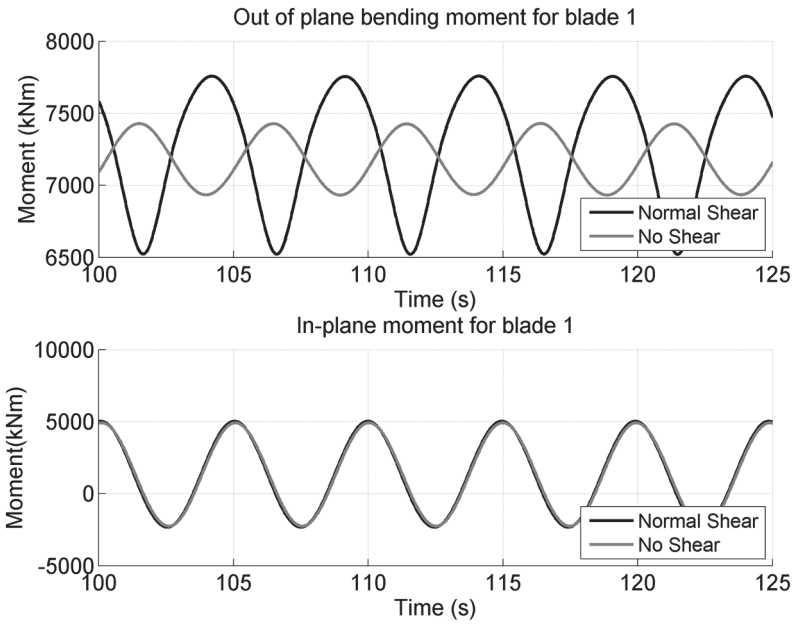

Figure 4.11. *Out of plane and in-plane moments of the blade 1 at the wind speed of 13 m/s.*

Cyclic blade moments are nearly sinusoidal at the frequency of 1*P*. According to Haarnoja [3], the amplitude of 1*P* frequency in the out of plane blade bending moment is the main cause for the disturbing moments affecting on the top of the tower. These disturbing moments, tilt moment on the top and yaw moment on the bottom are shown in the figure 4.13 at the wind speed of 13 m/s. Corresponding figure at the wind speed of 23.7 m/s is expressed in the figure A.4 in the appendix A.

The effect of wind shear on these moments can be clearly seen in the figures. When no wind shear is present, there are nearly no fluctuations in the tilt and yaw moments, but when the wind shear is added to the system, a pulsating component can be clearly seen in both moments. The frequency of the fluctuations is approximately 3*P*, which is due to the rotating motion of the three-bladed rotor [3].

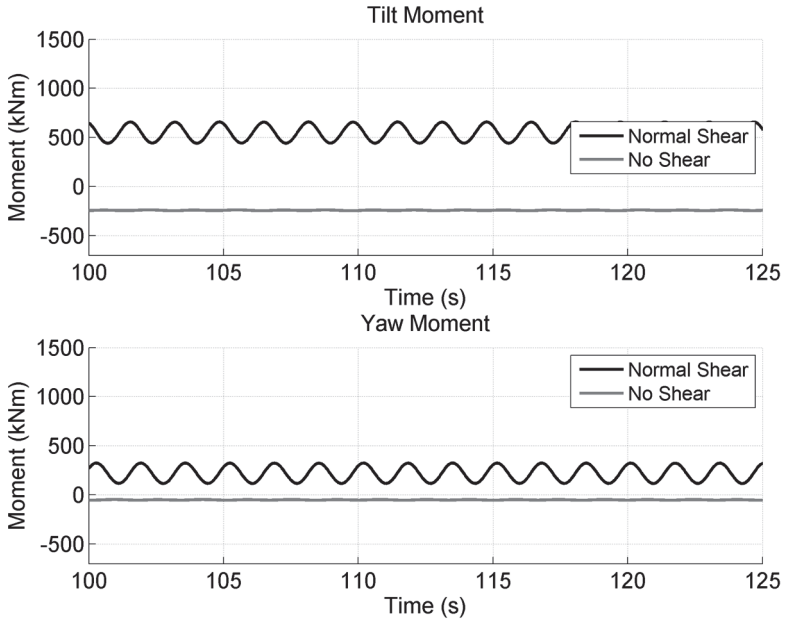

Figure 4.12. *Effect of the wind shear on the tilt and yaw moments affecting on the top of the tower at the wind speed of 13 m/s*

According to Haarnoja [3], the static component of the tilt moment can be dominated by the gravity at low wind speeds which causes a moment into opposite direction. This phenomenon can be seen clearly in the plots without wind shear; at the wind speed of 13 m/s, there is a constant negative tilt moment, but at the wind speed of 23.7 m/s the tilt moment is almost zero. It is mentioned in the report of Haarnoja [3], that the cause of the static yaw moment is not that obvious. Actually, the behavior of the yaw moment is quite opposite; at the lower wind speed the yaw moment is near zero but it becomes greater into the negative direction when the wind speed increases. In addition, the static component in the yaw moment is greater without the wind shear than in the presence of normal wind shear.

The disturbing moments, illustrated in the figures above, can be regarded as the main cause to the fatigue stress of the wind turbine components. So, by mitigating these loads, the useful life-time of the turbine could be increased and thus, the costs of produced energy could be decreased. As already mentioned in the chapter one, these loads could be alleviated significantly by *individual pitch control*, which is the topic of the next chapter.

5 LOAD REDUCTION BY INDIVIDUAL PITCH CONTROL

Due to the increased sizes of the wind turbines, the loads affecting on them have become more significant and the reduction of them is thus an important control objective in today's large-scale wind turbines. As mentioned in the previous chapter, a well-known method for load reduction in the wind turbines is the individual pitch control, in which pitch angle of each of the three blades is controlled individually in such a way, that the aerodynamic force is kept constant during a revolution. Therefore, the net axial force can be shifted to the centre of the hub and the disturbing tilt and yaw moments can be eliminated. [3]. According to Bossanyi [2], the possibility to use the individual pitch control for the load reduction has been known for years but the utilization of it in commercial wind turbines has become meaningful just during the latest years. The individual pitch actuators are typically used in the today's large-scale wind turbines anyway, which makes the implementation of the individual pitch control rather simple. [2].

Usually the individual pitch control is based on the load sensors measuring the blade loads. These blade load measurements are available in FAST and hence, the control algorithm based on load sensors is implemented and evaluated in this chapter. However, the load sensors reliable enough for this purpose can be quite expensive which increases the component costs of the wind turbine and thus, increases the costs of produced energy too. For this reason, another IPC concept that needs only the measurement of the rotor position, which is already available in the most wind turbines, is implemented too.

This chapter begins with the baseline IPC that is based on the measurements of the blade loads. First, the theory and the implementation of the controller in Simulink are described and then, the performance of the controller is evaluated in normal wind conditions as well as in the presence of extreme wind scenarios. Furthermore, sensitivity issues related to this IPC are briefly discussed. The chapter continues with the implementation and evaluation of the feedforward individual pitch controller.

5.1 IPC Algorithms based on Blade Load Sensors

Most IPC schemes introduced in the papers are based on the measurement of the blade loads. According to Bossanyi [2], the load sensors reliable enough for the control purposes have now become available which enables the commissioning of the IPC algorithms. There are several researches, for example from Bossanyi [2], Camblong et al. [12], or Niemann et al. [41] dealing with more sophisticated control methods, such as LQ, LQG and H_∞ methods based on the blade load measurements.

However, it is often mentioned in the reports [2; 3] that good results can be gained by conventional PI-controllers too. In addition, basic PI-control strategies are usually preferred in the real-life applications which contributes to their utilization within this thesis too.

5.1.1 Control System Properties

According to Bossanyi [2], the d-q axis representation borrowed from the three-phase electrical machine theory has proved to be successful also in the individual pitch control of the three-bladed wind turbine. According to this d-q axis approach, three blade root load signals are transformed into a mean value and variations about direct and quadrature axes. Described in the report of Haarnoja [3], these d-q load signals describe now the tilt and yaw moments in the static rotor coordinate system and are defined by:

$$\begin{bmatrix} M_d \\ M_q \end{bmatrix} = \frac{2}{3} \begin{bmatrix} \cos\phi & \cos\left(\phi + \frac{2\pi}{3}\right) & \cos\left(\phi + \frac{4\pi}{3}\right) \\ \sin\phi & \sin\left(\phi + \frac{2\pi}{3}\right) & \sin\left(\phi + \frac{4\pi}{3}\right) \end{bmatrix} \begin{bmatrix} M_1 \\ M_2 \\ M_3 \end{bmatrix}, \tag{5.1}$$

where M_d and M_q are the tilt and yaw moments, ϕ the azimuth angle, i.e. the rotor position, and M_1, M_2 and M_3 are the out of plane root bending moments of a three-bladed rotor in the rotating coordinate system, respectively. By this way, the moments can be treated as two decoupled SISO systems and conventional PI-controllers can be applied separately to the d- and q-axes. Before the control signals can be fed to the pitch actuators, inverse d-q transformation is needed to convert the signals back to the rotating coordinate system:

$$\begin{bmatrix} \theta_1 \\ \theta_2 \\ \theta_3 \end{bmatrix} = \begin{bmatrix} \cos\phi & \sin\phi \\ \cos\left(\phi + \frac{2\pi}{3}\right) & \sin\left(\phi + \frac{2\pi}{3}\right) \\ \cos\left(\phi + \frac{4\pi}{3}\right) & \sin\left(\phi + \frac{4\pi}{3}\right) \end{bmatrix} \begin{bmatrix} u_d \\ u_q \end{bmatrix}, \tag{5.2}$$

where θ_1, θ_2 and θ_3 are the pitch angle demands for the blades one, two and three, respectively and u_d and u_q are the controller output signals which can be interpreted as virtual pitch angles in the d-q coordinate system. Pitch angle demands received from the inverse transformation are then summed up with the collective pitch angle demand from the CPC and fed to the pitch motors. The Simulink model of the controller based on equations above is shown in the figure 5.1.

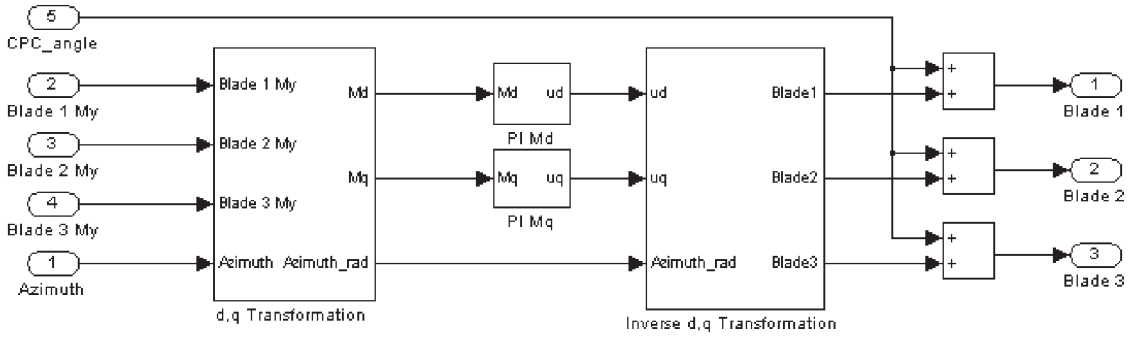

Figure 5.1. *Individual pitch controller based on the blade load sensors*

According to Haarnoja [3] and Barone et al. [8], only an integral controller is needed to drive the average tilt and yaw moments to zero, but the effect of adding a proportional term to the controller was also investigated through the simulations. Figure 5.2 shows the responses of the tilt and yaw moments when the wind speed increases from 12 m/s to 14 m/s at the time of 100 seconds. The controller becomes slightly faster when the small proportional term is added but however, the differences between PI and only I controller are rather small.

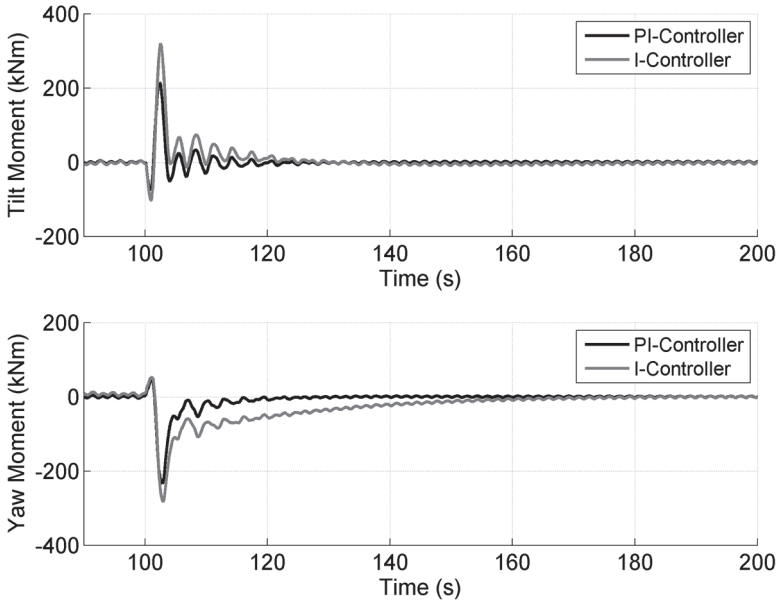

Figure 5.2. *Comparison of the PI and I controller*

However, the PI controller was used in the simulations within this thesis, and the control parameters for the controller were chosen to be $K_P = 8e^{-6}$ and $T_I = 2$. Parameters for K_P and T_I were found through experimental simulations by testing different parameters and their effect on the performance of the controller. Several other parameter combinations were tested too but none of them improved the performance of the controller. Theoretical background behind the parameters was not considered to be extremely important because the controller is only used for the disturbance compensation instead of the overall control of the system.

5.1.2 Load reduction

Performance of the individual pitch controller was simulated at the wind speeds of 13 m/s and 23.7 m/s at the presence of the normal vertical power law wind shear of 0.14. Figure 5.3 shows how the individual pitch controller is performing compared to the collective one in the terms of the out of plane root bending moment for the blade 1 and the tilt and yaw moments. Corresponding figure at the wind speed of 23.7 m/s is represented in the figure A.5 in the appendix A. As discussed previously in this thesis, wind shear is not contributing to the in-plane loading of the blades. In addition, it is mentioned in [11] that very little reduction can be achieved by periodically variable pitching in the in-plane loading. For this reason, only the blade load reduction in the out of plane direction will be discussed further in this thesis.

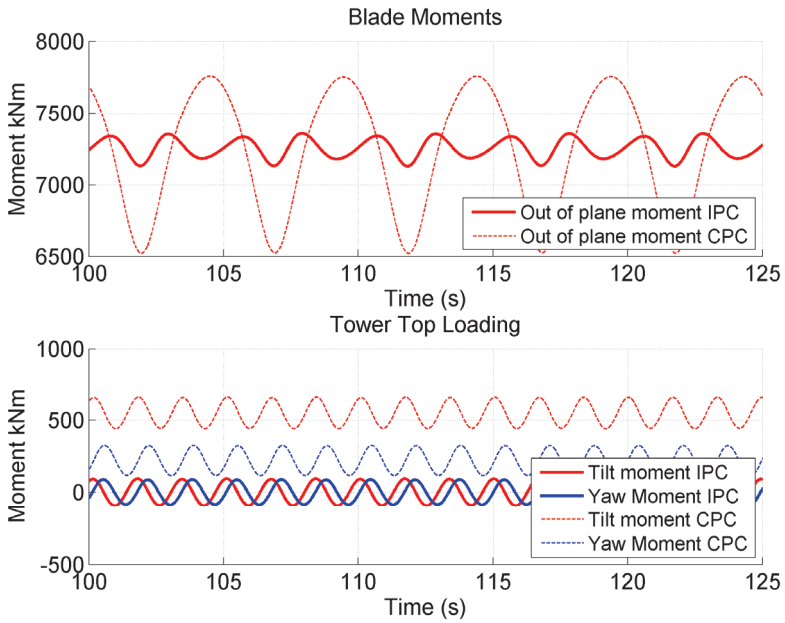

Figure 5.3. *Comparison of the CPC and IPC at the wind speed of 13 m/s*

It can be seen in the figure 5.3 that the controller is operating well in the purpose it was implemented for. The amplitude of the 1*P* oscillations in the out of plane blade root bending moment is decreased significantly and the disturbing tower top tilt and yaw moments are now zero on average at the both wind speeds. However, the oscillations of the tilt and yaw moments remain the same even though the moments are now oscillating around zero.

Oscillations in the tilt and yaw moments are illustrated more carefully in the figure 5.4. The frequency of the oscillations in the tilt and yaw moments is approximately 3*P*, in other words, three times the rotational frequency of the rotor. Furthermore, it can be seen that the tilt moment has its maximum value around the rotor azimuth angle of 0 ° whereas the yaw moment has its maximum around the azimuth angle of 90 °. Maximum values for the tilt and yaw moments are then repeated after the 120 ° for the blade two and again after 240 ° degrees for the blade three, which coincides with the definition of the tilt and yaw moments in (5.1).

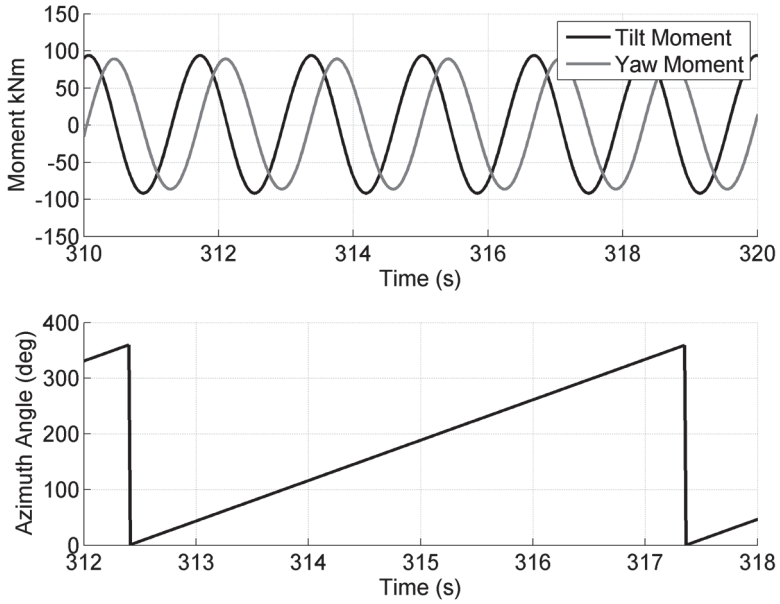

Figure 5.4. *Oscillations in the tilt and yaw moments as the azimuth angle changes*

So, it seems that no load reduction is attained in 3*P* loading with this IPC algorithm which is due to the utilisation of the transformation from one coordinate system to another. In other words, if the control error is zero the d-q axis controllers produce constant outputs which are transformed to the sinusoidal blade pitch angles at the rotor frequency 1*P*. According to Larsen et al. [42], the 3*P* loads can be changed by a non-sinusoidal approach, for example, by higher-order harmonic control. This method allows actual independent control of the three pitch angles because they are not coupled as is the case due to the coordinate transformation in the IPC described above [3]. On the other hand, there are also reports concerning the methods focusing on the 3*P* load reduction by sinusoidal approach which add another term at multiply rotor frequency to the blade pitch angle [13; 14]. So, it is clear that more sophisticated control algorithm is needed in order to influence in 3*P* load components of the tilt and yaw moments.

Differences in the pitch angles and the rotor speed between IPC and CPC at the wind speed of 13 m/s are compared in the figure 5.5 and the results at the higher wind speed can be seen in the figure A.6 in the appendix A. Pitch angles in the case of IPC are now varied periodically according to the azimuth angle and the phase shift between the pitch angles of the blades is 120 °.

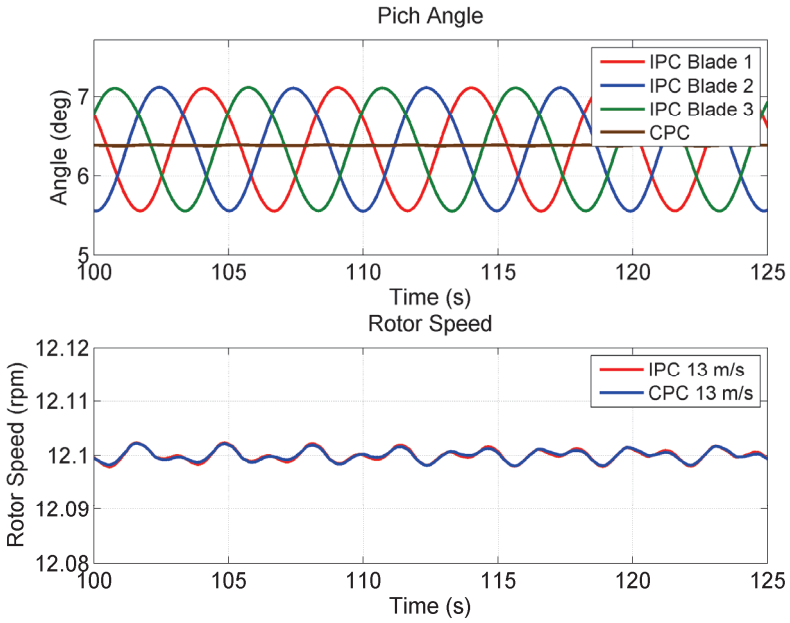

Figure 5.5. *Comparison of the pitch angles and the rotor speed between IPC and CPC at the wind speed of 13 m/s*

It is obvious that the increased pitching activity in the case of IPC leads also to the increased mechanical stress of the pitch actuators. Furthermore, increased pitch activity increases the power usage of the pitch motors which increases the costs of produced energy. Therefore, an optimal solution between load reduction and energy consumption in the terms of pitching activity should always be found. On the other hand, it can be seen in the lower plot of the figure 5.5, that the rotor speed remains nearly the same when adding the IPC to the system. In fact, the oscillations in the rotor speed are decreased slightly at the higher wind speed in the case of IPC. According to Haarnoja [3], this positive effect on the rotor power capture is due to the angle of attack that is kept optimal during the revolution in the presence of IPC.

5.1.3 Performance of the IPC in the presence of Extreme Wind Scenarios

As discussed above, the IPC is able to reduce the amplitude of the 1*P* loading in the out of plane blade moment significantly as well as to drive the mean values of the tilt and yaw moments into zero in the case of normal wind profile. However, the performance of the controller was simulated also in the presence of extreme wind scenarios described in the chapter 4.3. Figure 5.6 illustrates the differences in the out of plane blade moments (upper plot) and in the tilt and yaw moments (lower plot) between IPC and CPC in the presence of extreme operating gust. It can be seen that there is barely any difference in the blade moments between the IPC and CPC. When comparing the performance of the controllers in the terms of tilt and yaw moments only the amplitudes of the moments are comparable, because the mean values of the moments are now zero in the case of IPC. Hence, it can be seen that during the gust, i.e. around 105 seconds, oscillations in the tilt moment are decreased slightly when IPC is used, whereas the yaw moment remains nearly unchangeable.

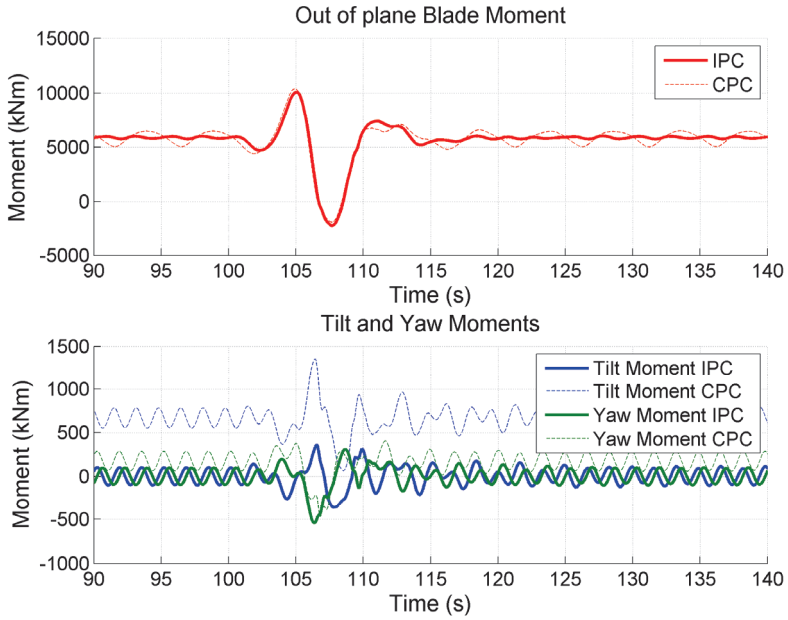

Figure 5.6. *Performance of the baseline IPC in the presence of EOG*

IPC and CPC during the extreme vertical wind shear conditions are compared in the figure 5.7. It can be seen that the effect of EWSV on loads is significantly smoother when the IPC is used. However, some negative overshoot can be seen in the tilt moment after the extreme wind shear has been present, which is though rather small. This reaction of IPC to the wrong direction is probably caused by the slow response of the controller. It might be possible to make the controller slightly faster by tuning the control parameters of the PI controller. However, as described in the chapter 5.1.1, this has to be done carefully in order to maintain the stability of the system.

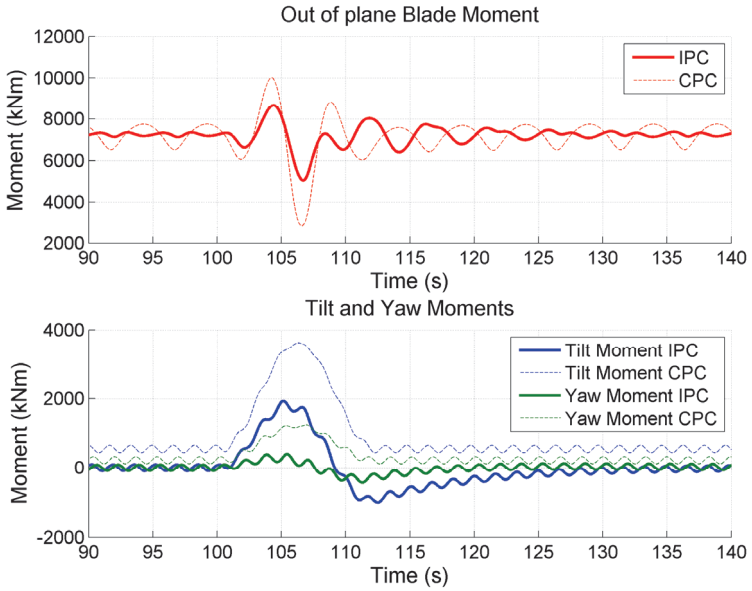

Figure 5.7. *Performance of the baseline IPC in the presence of EWSV*

Furthermore, performances of the IPC and CPC in the presence of extreme horizontal wind shear are compared in the figure 5.8. When IPC is used, the amplitude of the blade moment during the extreme shear is decreased again as well as the effects of extreme shear on the tilt and yaw moments. Nevertheless, the slow response of the controller can be observed again when regarding the behavior of the tilt and yaw moment after the extreme horizontal wind shear was present. Again, it takes some time before the reference value is reached, especially in the case of yaw moment.

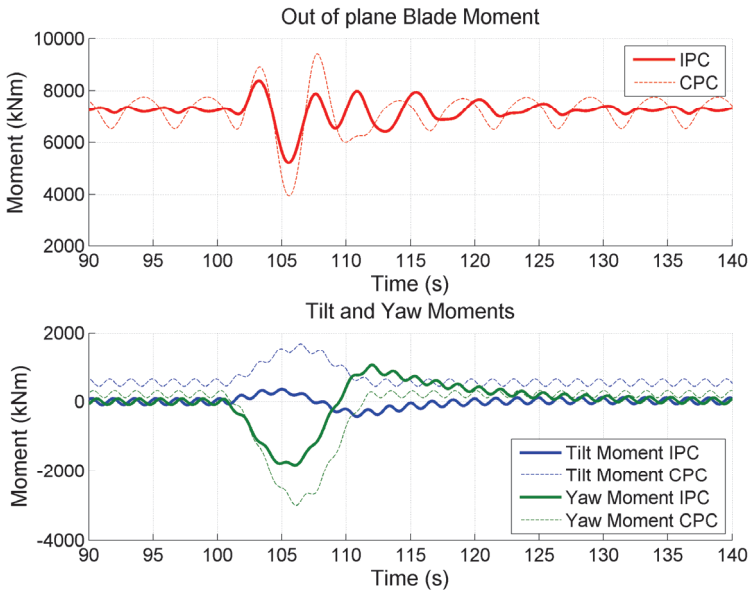

Figure 5.8. *Performance of the baseline IPC in the presence of EWSH*

In conclusion, it can be said the IPC can decrease the loading due to the extreme vertical and horizontal wind shear but only slight load reduction can be attained in the case of extreme operating gust.

5.1.4 Sensitivity of the Controller based on d-q Transformation

When the control algorithms based on the transformation from one coordinate system to another are used the sensitivity issues should always be considered. In other words, how well the algorithm is performing if the measurement signals are noisy, for example. In order to analyze the sensitivity of the IPC based on the d-q transformation described previously in this chapter, white noise was added to the measurement of the azimuth angle that is needed in the transformation. Azimuth angle in the presence of noise is shown in the figure 5.9.

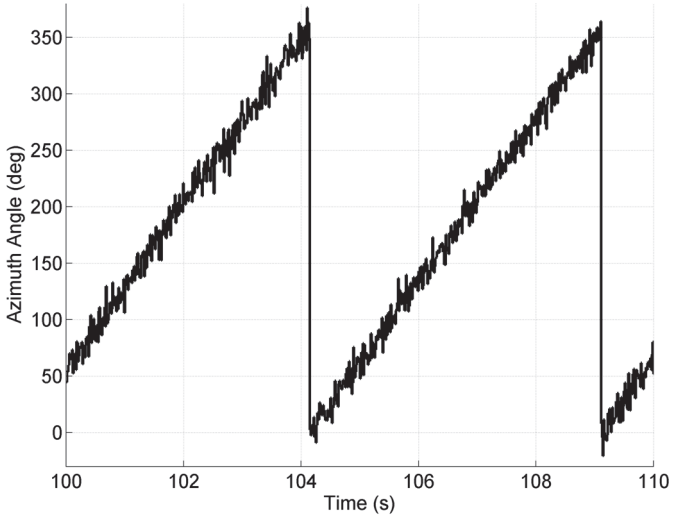

Figure 5.9. *Azimuth angle in the presence of white noise*

Now, when the noisy measurement signal of the azimuth angle is used in the IPC algorithm and hence, in the d-q and inverse d-q transformations, the effect of noise can be seen in the out of blade bending moment and the tilt and yaw moments too. The figures of these moments in the presence of noise are shown in the figures A.7 and A.8 in the appendix A. So, in order to filter out the noise from the azimuth angle measurement, a low-pass filter was added to the system. Azimuth angles at the presence of two different filters, one with the corner frequency of 2.5 Hz on the left and another with the corner frequency of 10 Hz on the right are shown in the figure 5.10. It can be seen in the left plot that the noise is filtered better in the case of the low-pass filter with the lower corner frequency of 2.5 Hz but however, some information is lost because the low-pass filtering also smoothens the jump from 0° to 360°.

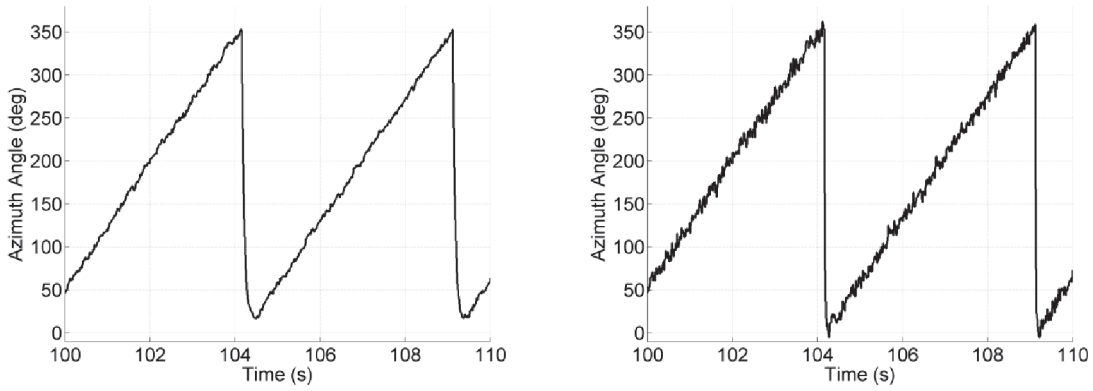

Figure 5.10. *Low-pass filtered azimuth angle in the presence of noise, corner frequency of the filter is 2.5 Hz in the left and 10 Hz in the right plot*

Figure 5.11 shows the out of plane blade bending moment and the tilt and yaw moments in the presence of the filters described above compared to the ideal case, where the measurement signal of azimuth angle is ideal, i.e. it is noiseless and thus unfiltered. Low-pass filtering of the azimuth angle by the lower corner frequency of 2.5 Hz results in peaks in the moments, which is due to the smoothened values of the filtered azimuth angle around the wrapping of the azimuth angle. On the other hand, when the low-pass filter with the larger corner frequency of 10 Hz is used, the differences between the ideal and noisy filtered cases are very small.

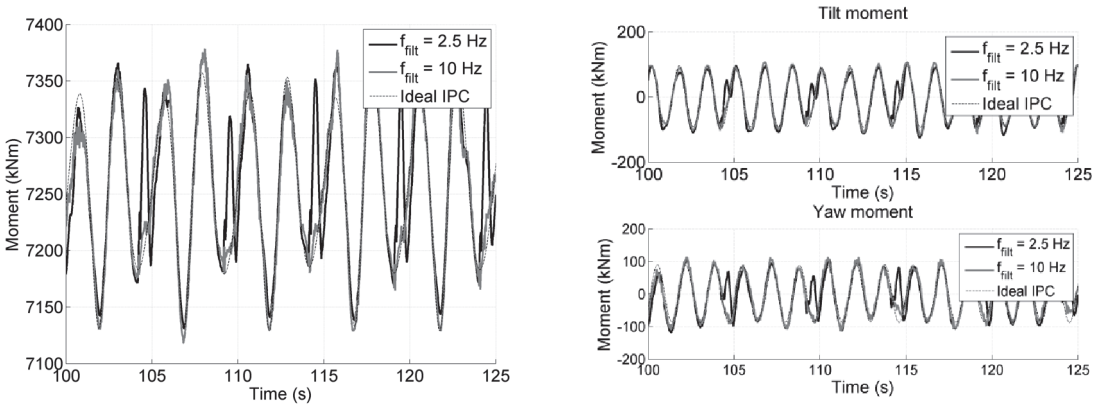

Figure 5.11. *Differences between different filters and the ideal measurement signal of azimuth angle in the terms of out of plane blade bending moment*

In conclusion, it can be assumed that the noise in the measurement signal of the azimuth angle does not significantly worsen the performance of the individual pitch controller. When the noisy signal is filtered by a low-pass filter with a proper corner frequency, results almost identical to the ideal case are gained.

Furthermore, it is worth of noting that significant load reduction is attained compared to the case where only collective pitch controller is used even though the noisy azimuth angle measurement signal was not filtered at all. Furthermore, the mean values of the moments remain the same in the case of too low corner frequency of the low-pass filter and hence, the performance of the controller in load reduction is still rather good. So, the sensitivity of the controller because of the transformations should not be an issue that prevents the utilization of the controller in the real operation conditions in which the measurement signal are often noisy.

5.2 Feedforward Wind Shear Compensation

Utilization of the IPC algorithm described above requires procurement and installation of load sensors which can be expensive. For this reason, load reduction methods that do not require any additional components or installation work would be attractive. Trudnowski and LeMieux [11] have introduced a simple feedforward load reduction method that uses the rotational position of the rotor as a measurement signal. This measurement signal is already available in the control system of the turbine, so no additional sensors are needed and hence, no additional component costs are caused. Furthermore, this method could be added to the control system by only modifying the software remotely and no installation work is then required either. These aspects make this load reduction method attractive and therefore, a controller based on this algorithm was implemented in Simulink and its performance was evaluated through the simulations.

5.2.1 Control System

According to Trudnowski and LeMieux [11], the gravity and shear moments affecting on the turbine blades are a function of the cosine and sine of the rotor position. Hence, for a given blade, the control algorithm, pursuing to the compensation of the loading caused by the wind shear, modulates the pitch angle by

$$\theta_i = \theta_p - \left[q_{p1} \sin(\phi_i + \sigma) + q_{p2} \cos(\phi_i + \sigma)\right], \tag{5.3}$$

Where ϕ_i is the azimuth angle position for that blade, θ_p is the pitch angle from the collective pitch controller and σ is a phase correction factor. The control parameters q_{p1} and q_{p2} and the phase correction factor σ are selected by defining which fatigue loads, either the out of plane or in-plane loads, are to be minimized. According to Trudnowski and LeMieux [11], very little reduction can be gained in the in-plane loading and therefore, only the control algorithm aspiring to the minimization of the out of plane loading was implemented and investigated in this thesis. In addition, it can be seen in the simulation results regarding the IPC based on load sensors, that no load reduction can be gained in the in-plane loading by that control algorithm either.

Only a brief overview of the work of LeMieux et al [11] is given here and more detailed information can be found from [11]. According to their work [11], cyclic moment caused by the wind shear is the primary cause for the out of plane vibrations causing fatigue loading of the blades. This shear moment can be defined as

$$M_{Shear} = -K_2 K_1 f_{\beta 2} \cos \phi, \tag{5.4}$$

where K_2 and $f_{\beta 2}$ depend on the turbine characteristics and K_1 is a wind-shear gradient with respect to the length of the blade and the hub-height wind velocity. To be able to cancel this shear moment, a counter moment, which depends on the pitch angle θ, is introduced in [11]:

$$M_{Counter} = K_2 f_{\beta 3} \theta, \tag{5.5}$$

Now, it can be derived from the out of plane moments affecting on the blade:

$$M_{Shear} = M_{Counter} = -K_2 K_1 f_{\beta 2} \cos \phi = K_2 f_{\beta 3} \theta, \tag{5.6}$$

where

$$f_{\beta 2} = \frac{\Omega V}{4}, \tag{5.7}$$

and

$$f_{\beta 3} = \frac{R \Omega^2}{4}, \tag{5.8}$$

in which Ω is the rotor speed, R is the length of the blade and V is the wind speed. Cancellation of the shear moment is done by using the control functions q_{p1} and q_{p2} from the (5.3)

$$q_{p1} = 0, \tag{5.9}$$

q_{p2} can be derived from the (5.5) by solving the pitch angle θ:

$$\theta = -\frac{K_2 K_1 f_{\beta 2} \cos \phi}{K_2 f_{\beta 3}} = -\frac{K_1 f_{\beta 2} \cos \phi}{f_{\beta 3}} = -q_{p2} \cos \phi \tag{5.10}$$

and taking (5.6) and (5.7) into account

$$q_{p2} = \frac{K_1 f_{\beta 2}}{f_{\beta 3}} = \frac{K_1 V}{R\Omega} = \frac{K_1}{\lambda}, \tag{5.11}$$

where λ is the tip-speed ratio and K_1 is the wind-shear gradient with respect to the blade length and the hub-height wind velocity. K_1 defines the difference between the wind velocity at the top and the bottom of the blade sweep with respect to the hub-height wind velocity. For example, if $K_1 = 0.1$, then the wind speed at the top of the blade sweep is 10 % greater than the hub-height wind speed and the wind speed at the bottom of the blade sweep is 10 % less than the hub-height wind speed. The simplest approach is to select the q_{p2} to be a constant value using the typical values of the tip-speed ratio and the wind-shear gradient. So, the control algorithm for a given blade can now be expressed as

$$\theta_i = \theta_p - q_{p2} \cos(\phi_i + \sigma). \tag{5.12}$$

The equations expressed above are derived in detail in [11].

When considering the definitions of azimuth angle ϕ and the pitch angle θ in the simulation software [35] used in these simulations and the fact that the reference pitch angle is gained from the collective pitch controller, the control algorithm for an ith blade can be expressed as

$$\theta_i = \theta_{CPC} - q \cos\left(\phi + \pi + (i-1)\frac{2\pi}{3} + \sigma\right). \tag{5.13}$$

where ϕ is the azimuth angle for blade 1 and i gets the values 1, 2 and 3 corresponding to the blade 1, blade 2 and blade 3, respectively. From now on, only the symbol q is used when referring to the gain q_{p2} in (5.12) because only one gain is used. Azimuth angle is defined in [35] such, that at the azimuth angle of 0 °, the blade 1 is pointing up (looking downwind) and the order of blades passing through a given azimuth angle is 3-2-1. For this reason, π has to be added to the azimuth angle ϕ in (5.13) in order to get correct results considering the definitions in [35].

First, the control algorithm defined in (5.12) was used as its simplest form by using a constant gain q and setting the phase correction factor σ to zero. The constant value of the tip-speed ratio λ in (5.10) was gained by using the rated values for the speeds of the rotor and the wind. These rated values can be seen in the Table 4.1. Another term in the equation of q, namely the wind shear gradient K_1, was set to be 0.112. This value was gained by striving to derive a connection between the wind shear gradient defined in [11] and the normal vertical power law shear, VSHR of 0.14.

Taking a look into the equation (4.6), one can derive that the wind speed at the tip of the blade when facing up can be expressed as

$$V_{top} = V_{hub}\left(\frac{Z_{hub}+R}{Z_{hub}}\right)^{VSHR} = V_{hub}\left(1+\frac{R}{z_{hub}}\right)^{VSHR} \tag{5.14}$$

and the wind speed at the tip of the blade when facing down

$$V_{bottom} = V_{hub}\left(\frac{Z_{hub}-R}{Z_{hub}}\right)^{VSHR} = V_{hub}\left(1-\frac{R}{z_{hub}}\right)^{VSHR}, \tag{5.15}$$

where R is the length of the blade. Now, using the blade length and hub-height of the 5 MW reference turbine, R = 61.5 and Z_{hub} = 90 m [5] and the value of 0.14 for *VSHR* in the equations (5.13) and (5.14), one gets that the wind speed at the top of the blade is

$$V_{top} \approx 1.0756 * V_{hub} \tag{5.16}$$

and the wind speed at the bottom of the blade is

$$V_{bottom} \approx 0.8513 * V_{hub}. \tag{5.17}$$

It can be seen, that V_{top} is now approximately 7.6 % greater than the hub-height wind speed and V_{bottom} is approximately 14.9 % less than the hub-height wind speed. Therefore, the wind shear gradient K_1 was simply set to be the average value of these values to correspond to the normal vertical power law shear of 0.14.

The Simulink model of the feedforward controller based on the control algorithm of (5.13) is illustrated in the figure 5.12. Collective pitch controller is the same as used in the previous simulations.

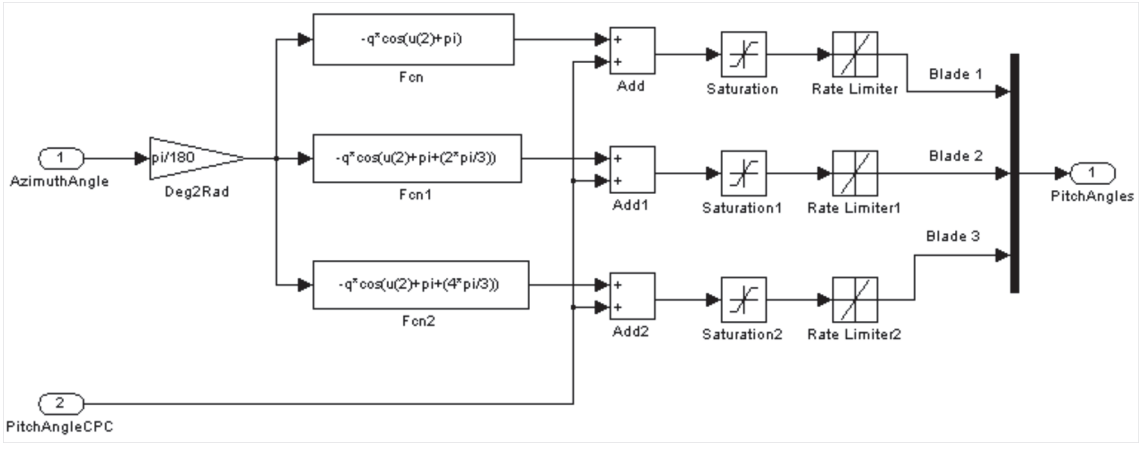

Figure 5.12. *Simulink model of the feedforward individual pitch controller*

Performance of this simple feedforward IPC in load reduction was evaluated through the simulations, which will be discussed next.

5.2.2 Simulation Results

Operation of the feedforward IPC in load reduction was simulated at the wind speeds of 13 m/s and 23.7 m/s. Simulation results in the terms of out of plane blade bending moment as well as the tilt and yaw moments at the wind speed of 13 m/s are shown in the figures 5.13 and 5.14. Corresponding figures at the wind speed of 23.7 m/s can be seen in the figures A.9 and A.10 in the appendix A.

Taking a look into the figure 5.13, it seems like the feedforward IPC is operating nearly as well as the IPC based on load sensors. The amplitude of the oscillations in the out of plane blade bending moment is decreased significantly compared to the situation where only the collective pitch controller is used. Furthermore, reduction in the out of plane blade moment leads to the near zero average tilt and yaw moments, which can be seen in the figure 5.14.

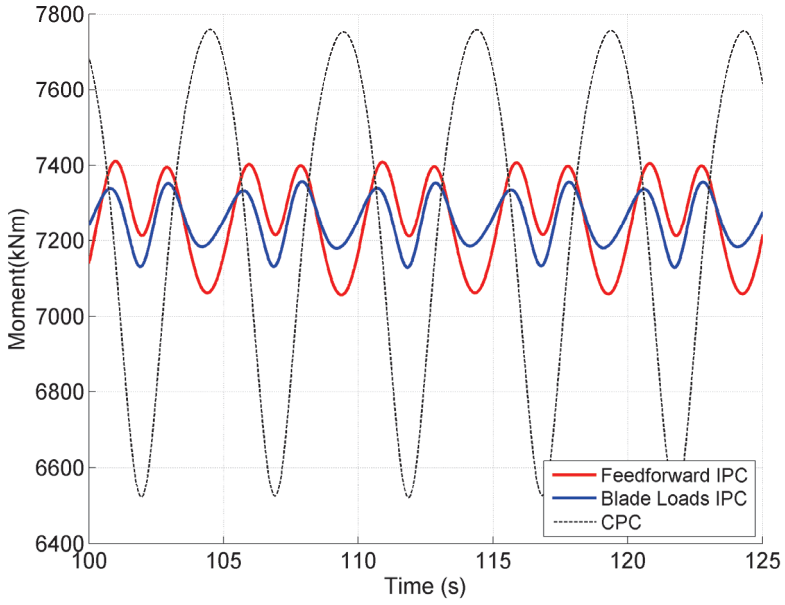

Figure 5.13. *Out of plane blade bending moment for the different controllers at the wind speed of 13 m/s*

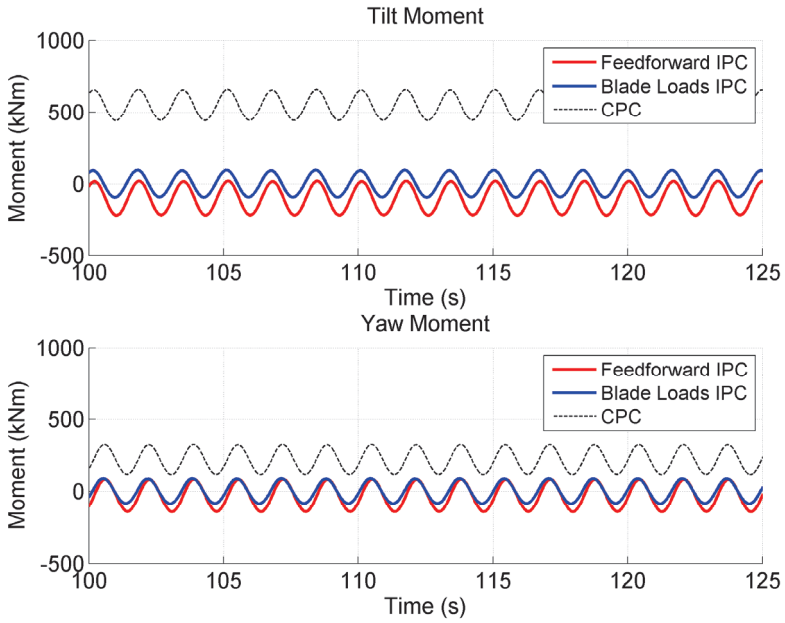

Figure 5.14 *Tilt and yaw moments for the different controllers at the wind speed of 13 m/s*

Unfortunately, the performance of the feedforward IPC becomes much poorer as the wind speed increases. As shown in the figure A.9 in the appendix A, the amplitude of the oscillations in the out of plane blade moment is still decreased at the wind speed of 23.7 m/s but significantly less than in the case of IPC based on load sensors. Furthermore, the static component of the tilt moment is decreased but the zero level is not reached with this simple feedforward IPC, which can be seen in the figure A.10 in the appendix A. Furthermore, the static component of the yaw moment is actually increased compared to the case of CPC only. The yaw moment at the higher wind speed is already negative near the zero and the feedforward wind shear compensation algorithm changes the yaw moment into the wrong direction and hence, the absolute value of the static component of the yaw moment increases.

Based on the simulation results introduced above, it can be assumed that the simplest form of the control algorithm based on rotor position measurement is not effective enough in the load reduction as the wind speed increases. So, some kind of adaptive control is needed in order to adjust the control parameter as the wind speed increases. Pitch angles of the baseline IPC, that utilizes the blade load sensors, and the feedforward IPC are compared in the figure 5.15, in which one can see that the pitch activity in the case of feedforward IPC is too low in order to decrease the loading enough. In addition, the pitch angle of the feedforward IPC is lagging the pitch angle of baseline IPC. So, the gain q at the wind speed of 23.7 m/s should be approximately 1.4 times q_{rated} and a phase correction factor of 0.6335 is needed in order to get same amount of pitching activity as in the case where the load sensors are used.

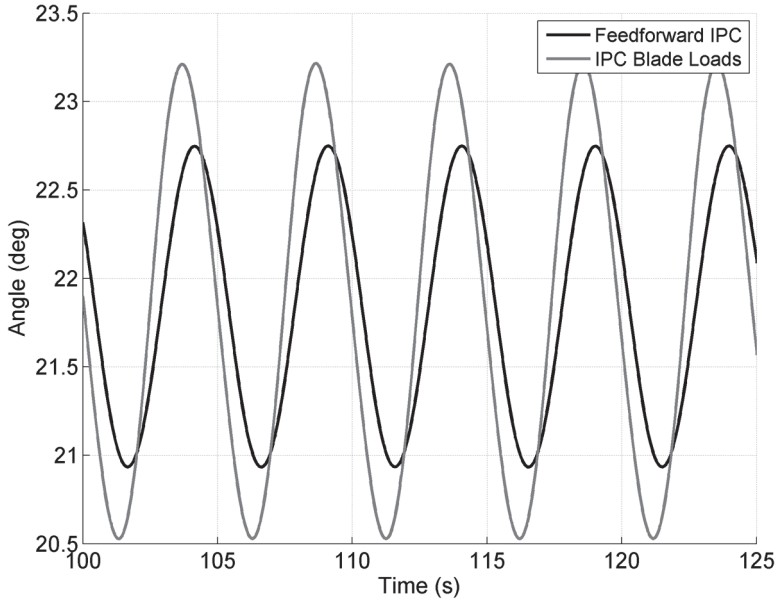

Figure 5.15. *Comparison of the pitch angles between different IPC controllers at the wind speed of 23.7 m/s*

In conclusion, the gain q as well as the phase correction factor σ should be adapted as the wind speed increases. Therefore, a gain scheduled feedforward controller is introduced next.

5.3 Gain Scheduled Feedforward IPC

In order to improve the performance of the feedforward IPC based on the measurement of the rotor position at the wind speeds above rated, the gain and the phase of the control algorithm should be adapted as the wind speed changes. Based on the observations in the previous chapter, this can be done by multiplying the constant gain q in (5.13) by a constant k and modulating the phase by a phase correction factor σ in order to get the pitch angle similar to the case where blade load sensors are used (see the figure 5.15). Hence, the control algorithm can be expressed as

$$\theta_i = \theta_{CPC} - k(V) q_{rated} \cos\left(\phi + \pi + (i-1)\frac{2\pi}{3} + \sigma(V)\right), \tag{5.18}$$

in which q is the constant gain in the case of simple feedforward IPC described in the previous chapter, $k(V)$ is the gain correction factor and $\sigma(V)$ the phase correction factor which both depend on the wind speed V. Simulations at different wind speeds with both IPC controllers described previously in this thesis were run in order to define the differences in the pitch angles between the two controllers.

Parameters for the phase and gain correction factors can be derived from the differences in the pitch angles at different wind speeds and they are shown in the table 5.1. When the phase and gain correction factors are plotted as a function of wind speed, it can be noted that the both of them increase almost linearly as the wind speed increases. The figures concerning the linear relation between the wind speed and the correction factors are shown in the figures A.11 and A.12 in the appendix A.

Table 5.1. *Gain and phase correction parameters as the wind speed increases*

Wind Speed (m/s)	***Phase Correction σ(V) (rad)***	***Gain Correction k(V)***
11.5	0	1
13.0	0	1
15.0	0.1267	1.073
17.0	0.2534	1.0385
18.0	0.2661	1.0989
20.0	0.3801	1.2376
22.0	0.5068	1.3536
23.7	0.6335	1.4121
25.0	0.7603	1.5525

Simulink model of the gain scheduled feedforward IPC based on the control algorithm of the equation (5.18) is shown in the figure 5.16, where *c* refers to the phase correction factor *σ*.

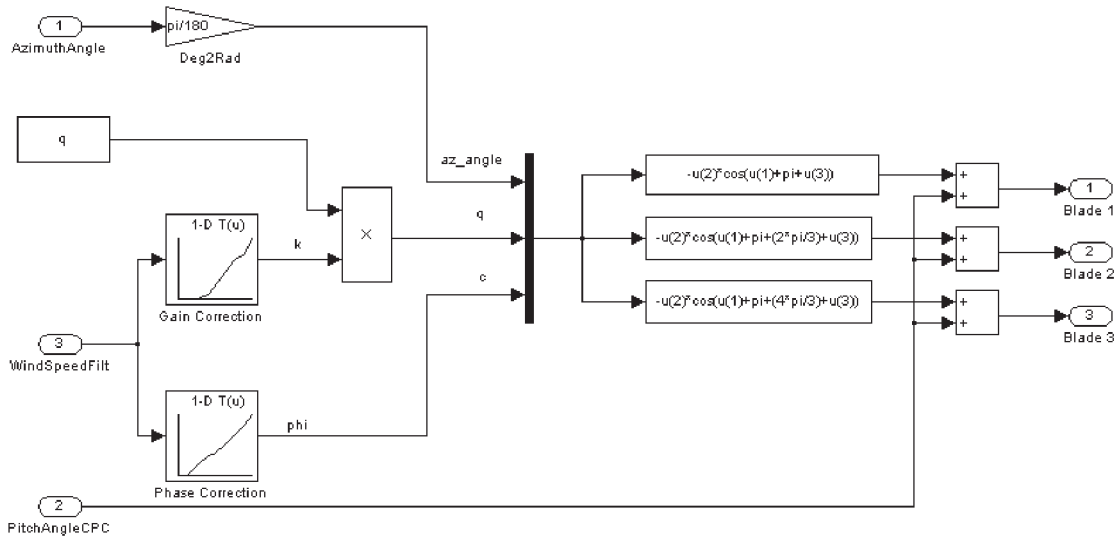

Figure 5.16. *Gain scheduled feedforward IPC*

Gain scheduling of the control parameters in the Simulink model is done by simple look up tables that uses the linear interpolation between data points. Simulations were made at different wind speeds and the performance of the gain scheduled feedforward IPC was only slightly poorer than the IPC with load sensors. Out of plane blade bending moment as well as tilt and yaw moments at the wind speed of 23.7 m/s are shown in the figures 5.17 and 5.18.

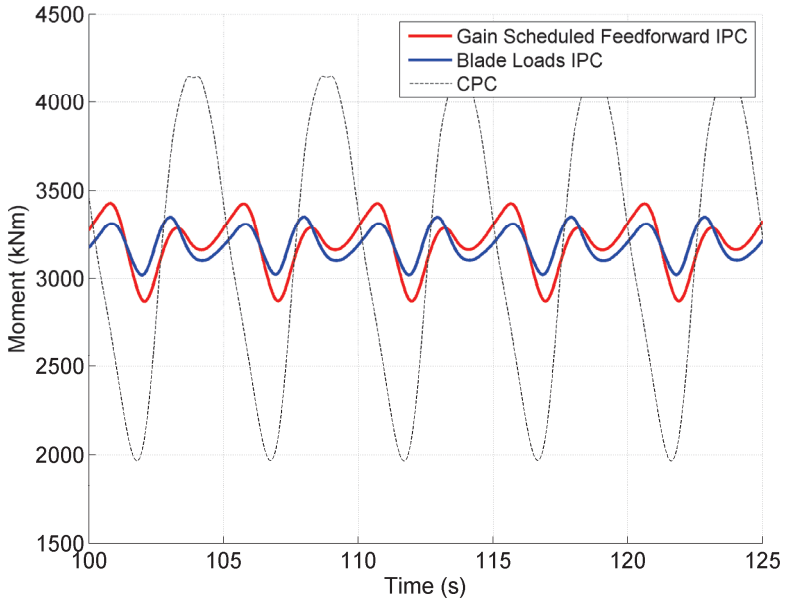

Figure 5.17. *Performance of the gain scheduled feedforward IPC in the terms of out of plane bending moment at the wind speed of 23.7 m/s*

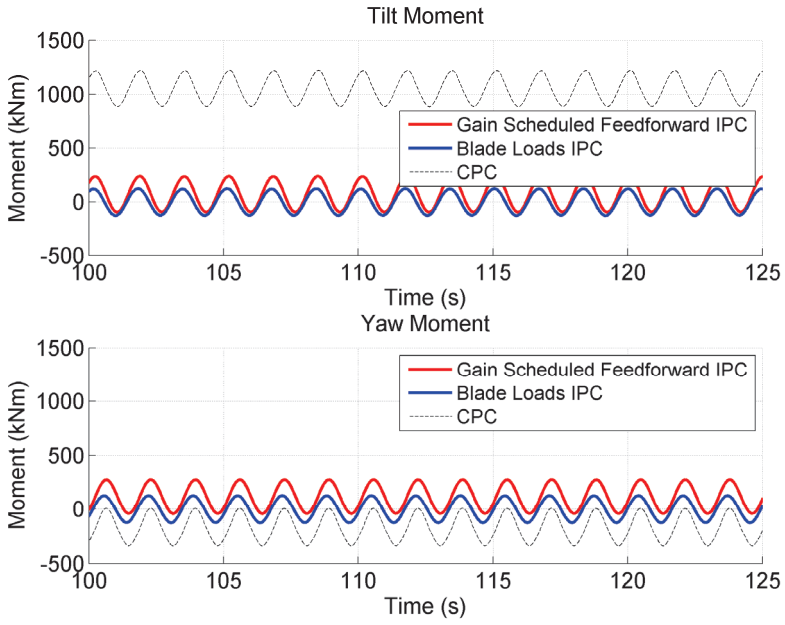

Figure 5.18. *Performance of the gain scheduled feedforward IPC in the terms of tilt and yaw moments at the wind speed of 23.7 m/s*

Even though the gain scheduling improves the performance of the feedforward IPC, there is also one significant drawback in gain scheduling. Measurements for the real wind turbine are needed in order to get the parameters for the gain and phase correction factors. Therefore, the load sensors are needed at least in the prototype of a turbine. Furthermore, measurements at different wind speeds are always challenging because the wind speeds cannot be chosen and it can take for long before all the wind speeds needed appear. However, because of the nearly linear relation between the wind speed and correction factors, the amount of needed measurements can be decreased. For example, the simulation at the wind speed of 19 m/s was not made in order to define the control parameters needed in (5.19), but the values for k and σ gained by linear interpolation seem to operate well as it can be seen in the figure 5.19. Corresponding tilt and yaw moments are shown in figure A.13 in the appendix A.

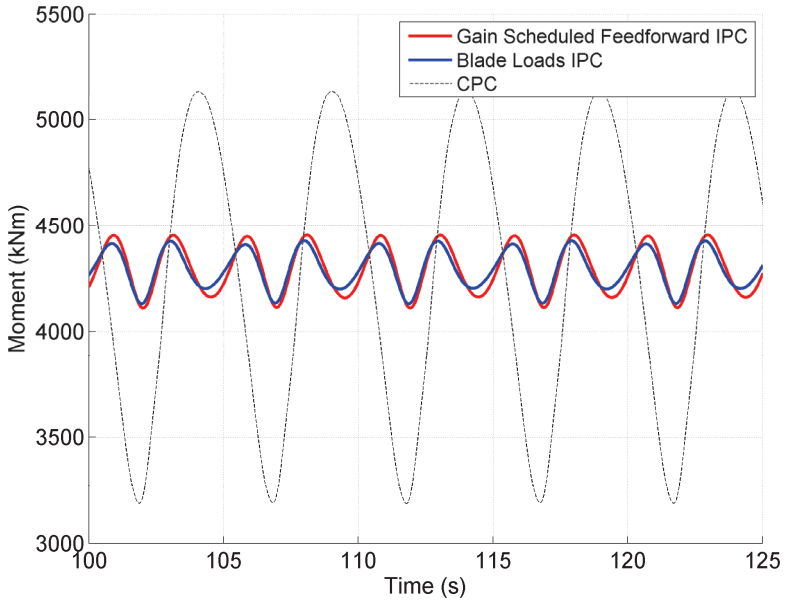

Figure 5.19. *Performance of the gain scheduled feedforward IPC with interpolated control parameter in the terms of out of plane blade bending moment at the wind speed of 19 m/s*

Despite of the relatively good performance of the gain scheduled feedforward IPC, the benefit of load sensors should not be underrated. This means that feedforward IPC as such can be used only in wind shear compensation but load sensors can be used in other purposes too. According to Bossanyi [15], signals from the load sensors can, for example, be readily used to estimate rotor torque and thrust, which can then be added to the collective pitch control algorithm in order to improve the performance of the controller.
It is worth of noting that despite the good simulations results concerning the load reduction neither the baseline IPC nor the gain-scheduled feedforward IPC is able to mitigate the 3P loading in the tilt and yaw moments. Therefore, the control algorithm has to be modified somehow to be able to affect on the 3P loading which is the topic of the next chapter.

6 3*P* COMPENSATION

As discussed in the previous chapter, significant load reduction can be gained in the 1*P* component of the out of blade bending moment and hence, in the mean value of the tilt and yaw moments by baseline individual pitch controller. However, the 3*P* loading in the tilt and yaw moments cannot be affected by this control scheme. Therefore, different additional control algorithms have been introduced in the literature in order to decrease this remaining 3*P* loading in the tower top moments. In the reports of Chen et al. [13], van Engelen [14] and Bossanyi [15], the 3*P* load reduction is gained by extending the baseline IPC algorithm whereas the utilization of the higher harmonic control borrowed from helicopter control is introduced in the report of Haarnoja [3]. Feedforward filter method, introduced in the Bossanyi's report and the higher harmonic control are only introduced briefly but the extended IPC described in the report of Chen et al. [13] was also implemented and evaluated in Simulink.

6.1 Feedforward Filter

In most reports dealing with the cyclic individual pitch control, which is based on the d-q transformation, the control scheme includes a notch filter in the series with the PI controllers of the d- and q-axis. According to Bossanyi [2], some filtering of the d- and q-axis loads, i.e. tilt and yaw moments, is needed after the d-q transformation in order to remove the high-frequency disturbances from the signals. In the later publication from the same author [15] it is expressed that without the filter the individual pitch control action tends to increase the 3*P* loads in the non-rotating frame loads which can be prevented by using a notch filter. However, disturbing amplification in the fixed part loads has not been pointed out within the simulations related to this thesis and therefore, a notch filter was not used in the simulations of the previous chapter.

Bossanyi [15] states that the filter could not only be used for the filtering of the disturbances but also for the 3*P* load reduction. This can be done by adding a feedforward filter into the system which adjusts the amplitude and the phase of the 3*P* response in a way that 3*P* component of the tower top loading is reduced. This feedforward filter is shown in the figure 6.1. The filter selects the 3*P* component in the load and adjusts the phase in a way that an additional contribution to the individual pitch angle demand is generated. Therefore, the final pitch angle demand consists of a 1*P* component gained from the baseline IPC and 3*P* reduction component gained from the feedforward filter.

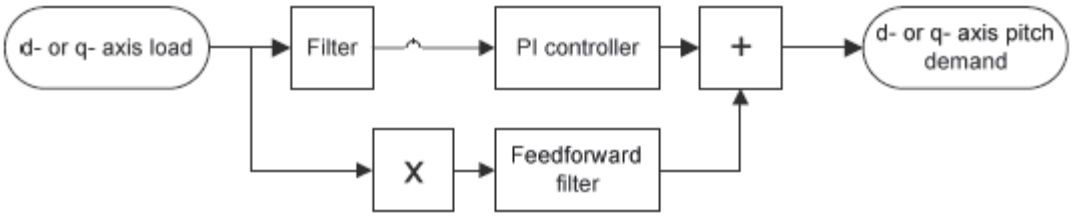

Figure 6.1. *IPC that uses a feedforward filter for 3P load reduction [15]*

According to Bossanyi [15], tuning of the feedforward filter is quite complicated and some sophisticated method, for example numerical optimization technique operating in the frequency domain, is needed. Therefore, a controller based on this method was not implemented within this thesis. However, based on the simulation results introduced in [15], 3*P* tower top loading can be reduced by using this control scheme and in addition, some load reduction in the rotating blade moments is gained too. Simulation results introduced there are for the 2 MW three-bladed wind turbine but there is no reasons expressed why this method would not work for the larger wind turbines too. Nevertheless, it is again worth of noting that the fast response of the pitch actuator is needed in order to attain significant load reduction [15].

6.2 Higher Harmonic Control

In Haarnoja's report [3], a totally different method for overall load reduction is introduced. This method, higher harmonic control (HHC), is originally introduced in the helicopter applications but can also be applied to the wind turbine control [43, see 3]. In the case of IPC algorithms using d-q transformation, the blade pitch angles are always coupled through the coordinate transformation whereas HHC allows actual independent control of the pitch angles. Only a brief overview of the method is given here and more detail information can is expressed in [3; 43].

According to Haarnoja [3], the idea of HHC is based on the assumption that on the bandwidth of the controller, the system can be considered to be in steady state. In general at a given frequency, the closed loop system can be expressed as

$$\boldsymbol{z} = \boldsymbol{T}\boldsymbol{u} + \boldsymbol{z_0}, \tag{6.1}$$

where $\mathbf{z}$ includes the sine and cosine components of the blade vibration at the certain frequency, $\mathbf{z_0}$ defines the corresponding vibration amplitude for the nominal pitch angle that is got from CPC, $\boldsymbol{u}$ is the amplitude of the control signal and $\boldsymbol{T}$ is *a constant control response matrix*. Equation above describes a general situation including and therefore, the variables $\boldsymbol{z}$ and $\boldsymbol{u}$ are defined to be vectors.

$\boldsymbol{T}$ contains the gain of the system at the frequency of interest and the need of knowing the overall transfer function of the system can be avoided by using it. According to Haarnoja [3], a simple feedback loop

$$\boldsymbol{u_{n+1} = u_n - T^{-1} z_n,} \tag{6.2}$$

should lead to a deadbeat control. To be able to implement this control algorithm for the system, the output signal of the system has to be first multiplied by cosine and sine signals that have the given frequency. Then, the product is integrated over one or more periods of the disturbance frequency in order to define the Fourier components $\boldsymbol{z_n}$. Corresponding change needed in the input signal is gained by multiplying these coefficients by the inverse of $\boldsymbol{T}$. As mentioned earlier, $\boldsymbol{T}$ describes the characteristics of the system and can be identified from the transfer function of the system. When this method is applied to the wind turbine application, the output of the system is the out of plane blade root bending moment and the input is the desired pitch angle related to the nominal pitch angle set by CPC. Furthermore, each one of the three blades needs to have their own controller. [3].

Expressed in the Haarnoja's report [3], this method is able to alleviate the desired components in the blade root bending moment and the controller can be implemented to alleviate different disturbance frequencies or their harmonic components. It is though worth of noting that the good load reduction results expressed in [3] were gained by assuming that the blades were rigid by totally disabling the degrees of freedom of the blades. This was necessary because the HHC that was designed to alleviate higher order frequency components tended to excite certain blade vibrations. [3]. Due to this and the relatively complicated structure of the controller, it would probably be challenging to apply this method for a real wind turbine.

6.3 Extended Cyclic Pitch Control

According to Chen et al. [13], the 3*P* loading in the tilt and yaw moments is mainly caused by the 2*P* and 4*P* components in the out of plane blade root bending moments. Therefore, the 3*P* loading in the tilt and yaw moments can be decreased by reducing the 2*P* and 4*P* loading in the blade moments. Same kind of approach based on d-q transformation can be used as in the case of baseline IPC. Tilt and yaw moment components M_{d2} and M_{q2} which are caused by the 2*P* component in the blade moment can be defined as:

$$\begin{bmatrix} M_{d2} \\ M_{q2} \end{bmatrix} = \frac{2}{3} \begin{bmatrix} \cos(-2\phi) & \cos\left(-2\phi + \frac{2\pi}{3}\right) & \cos\left(-2\phi + \frac{4\pi}{3}\right) \\ \sin(-2\phi) & \sin\left(-2\phi + \frac{2\pi}{3}\right) & \sin\left(-2\phi + \frac{4\pi}{3}\right) \end{bmatrix} \begin{bmatrix} M_1 \\ M_2 \\ M_3 \end{bmatrix}, \tag{6.3}$$

in which ϕ is the azimuth angle and M_1, M_2 and M_3 are the out of plane blade root bending moments for the blades one, two and three, respectively.

As in the case of baseline IPC described in the chapter five, two independent PI controllers can be used in order to drive M_{d2} and M_{q2} into zero. Furthermore, an inverse d-q transformation is again needed before control signals can be fed to the pitch actuators:

$$\begin{bmatrix}\theta_{2P1}\\ \theta_{2P2}\\ \theta_{2P3}\end{bmatrix} = \begin{bmatrix}\cos(-2\phi) & \sin(-2\phi)\\ \cos\left(-2\phi+\frac{2\pi}{3}\right) & \sin\left(-2\phi+\frac{2\pi}{3}\right)\\ \cos\left(-2\phi+\frac{4\pi}{3}\right) & \sin\left(-2\phi+\frac{4\pi}{3}\right)\end{bmatrix}\begin{bmatrix}u_{d2}\\ u_{q2}\end{bmatrix}, \tag{6.4}$$

where θ_{2P1}, θ_{2P2} and θ_{2P3} are the pitch angle demands for the blades one, two and three and u_{d2} and u_{q2} are the outputs of the tilt and yaw moment controllers, respectively.

In addition to the algorithm that is striving to mitigate the loading caused by the 2*P* component of the blade moment, similar approach can be used in the case of the 4*P* blade loading [13]. M_{d4} and M_{q4} can be defined by using (6.3) and the pitch angle demands θ_{4P1}, θ_{4P2} and θ_{4P3} are again gained by inverse d-q transformation through (6.4). Same PI controller can be used as in the case of baseline IPC and 2*P* reduction algorithm.

$$\begin{bmatrix}M_{d4}\\ M_{q4}\end{bmatrix} = \frac{2}{3}\begin{bmatrix}\cos(-4\phi) & \cos\left(-4\phi+\frac{2\pi}{3}\right) & \cos\left(-4\phi+\frac{4\pi}{3}\right)\\ \sin(-4\phi) & \sin\left(-4\phi+\frac{2\pi}{3}\right) & \sin\left(-4\phi+\frac{4\pi}{3}\right)\end{bmatrix}\begin{bmatrix}M_1\\ M_2\\ M_3\end{bmatrix}, \tag{6.5}$$

$$\begin{bmatrix}\theta_{4P1}\\ \theta_{4P2}\\ \theta_{4P3}\end{bmatrix} = \begin{bmatrix}\cos(-4\phi) & \sin(-4\phi)\\ \cos\left(-4\phi+\frac{2\pi}{3}\right) & \sin\left(-4\phi+\frac{2\pi}{3}\right)\\ \cos\left(-4\phi+\frac{4\pi}{3}\right) & \sin\left(-4\phi+\frac{4\pi}{3}\right)\end{bmatrix}\begin{bmatrix}u_{d4}\\ u_{q4}\end{bmatrix}, \tag{6.6}$$

Finally, the total individual pitch angle demand for a given blade is gained by summing up the three angle demands got from the IPC_{1P}, IPC_{2P} and IPC_{4P}. Now, the baseline individual pitch controller, IPC_{1P}, is taking care of the mitigation of the 1*P* component in the out of plane blade moment and driving the mean values of the tilt and yaw moments into zero. Additional controllers, IPC_{2P} and IPC_{4P} are used to reduce the remaining 3*P* loading in the tilt and yaw moments. [13].

This so called extended individual pitch controller based on the descriptions above was implemented in Simulink in order to evaluate its effectiveness in the reduction of 3*P* loading of the tower top moments. Two different versions of the controller was implemented, one that combines only the baseline 1*P* and 2*P* load reduction and another that utilizes all the three load reduction schemes described above.

The former controller is illustrated in the figure 6.2 and the simulink model of the latter controller is shown in the figure A.14 in the appendix A. Same values for the control parameters $K_P = 8e^{-6}$ and $T_I = 2$ of the PI controllers are used as in the case of baseline IPC alone discussed in the previous chapter. So, the control parameters are the same for every controller IPC_{1P}, IPC_{2P} and IPC_{4P}. In order to get the final pitch angle for a given blade, the individual pitch angle demands for that blade, gained from the IPCs, are summed up with the collective pitch angle demand.

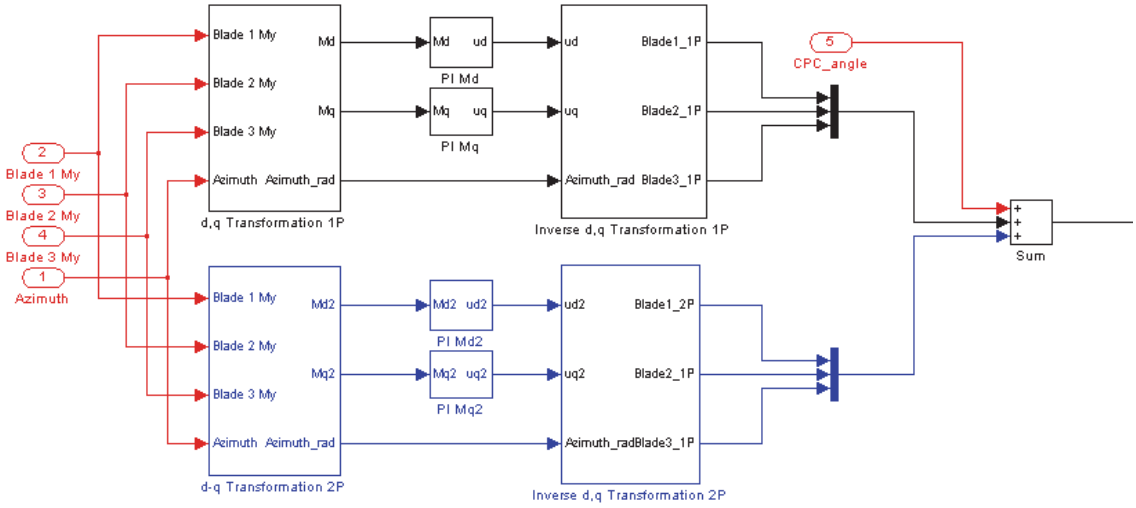

Figure 6.2. *Extended IPC including the 1P and 2P blade load reduction algorithms*

Performances of the different IPCs at the wind speed of 13 m/s are compared in the figures 6.3 and 6.4. The red curve shows the results in the case where only the 2*P* load reduction algorithm was added to the baseline IPC and the blue one illustrates the performance of the controller were both 2*P* and 4*P* load reduction schemes were used. Performance of the baseline IPC is shown green as a reference. Former figure shows the out of plane bending moment and the pitch angle for the blade one and the latter one illustrates the tilt and yaw moments. It can be seen in the figures that both extensive IPCs are able to decrease the amplitude of the out of plane blade moment and therefore, reduce the 3*P* loading in the tilt and yaw moments. However, it seems that the 3*P* loading in the tilt and yaw moments is mainly caused by the 2*P* loading in the blade moment because the activation of the IPC_{4P} does not notably contribute to the performance of the controller. The figures below show that the extended IPC is able to reduce the 3*P* loading in the tilt and yaw moments significantly and nevertheless, pitch angle is changed rather little compared to the case of baseline IPC. Actually, the amplitude of blade pitch angle is slightly smaller in the case of extended IPC than in the case of baseline IPC.

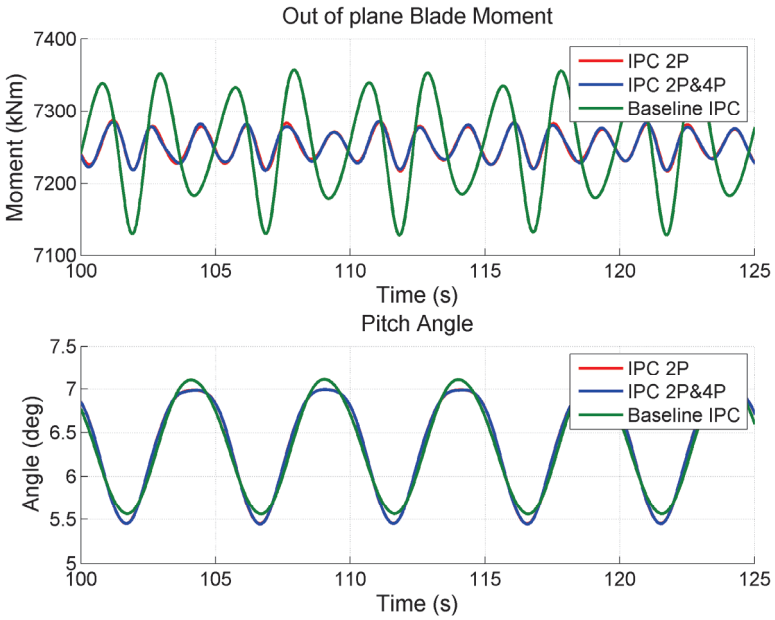

Figure 6.3. *Comparison of the different IPCs in the terms of blade bending moment and the pitch angle for the blade one*

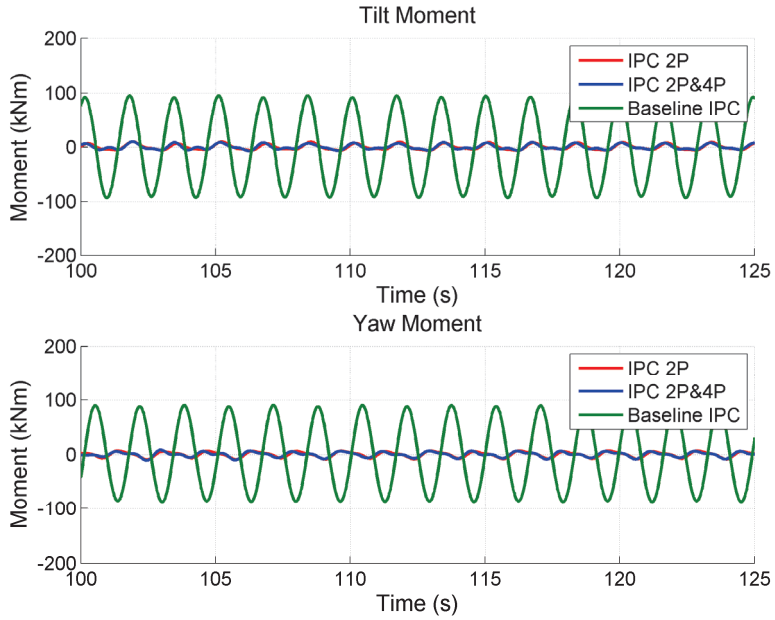

Figure 6.4. *Comparison of the different IPCs in the terms of tilt and yaw moments*

Simulations were run also at the wind speed of 23.7 m/s in order to evaluate how the extended IPC is performing at the higher wind speed. Corresponding figures are shown in the figures A.15 and A.16 in the appendix A. IPC_{2P} that combines the baseline IPC and the 2*P* blade load reduction is performing well at the higher wind speed too, but the performance of the controller that considers also the 4*P* loading is only slightly better than the performance of the baseline IPC.

Therefore, it seems that the best load reduction in the case of cyclic pitch schemes is gained by combining the baseline IPC with the 2*P* load reduction algorithm. Nevertheless, it is important to consider that the rapid response of the pitch actuator is essential in order to gain the load reduction of this scale. The dynamics of the pitch actuators has not been considered carefully in the model used in the simulations and hence, the actual load reduction that is possible to gain would be somewhat smaller. However, the pitch rate is limited to 8 deg/seconds in the model which defines how fast the blades can be pitched. Figure 6.5 shows the pitch rate when the extended IPC is used and it can be seen that there is still rather wide margin before the saturation limit, even at the high wind speed of 23.7 m/s.

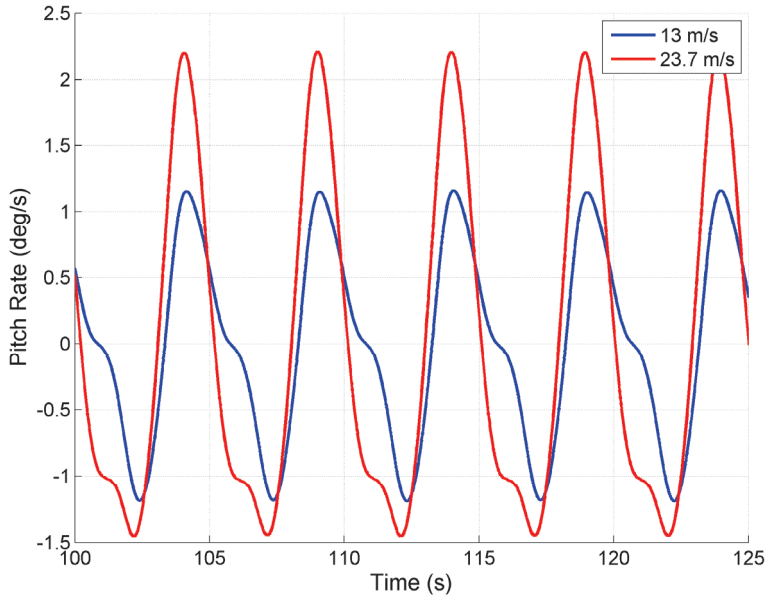

Figure 6.5. *Pitch rate (deg/sec) in the case of extended IPC at wind speeds of 13 m/s and 23.7 m/s*

In summary, it can be said that the 3*P* loading in the tilt and yaw moments, which remains unchangeable in the case of baseline IPC, can be alleviated by extending the algorithm to include the 2*P* load reduction scheme. Comprehensive conclusions cannot be made regarding the effectiveness of the other methods described at the beginning of this chapter because no simulations for the 5-MW reference turbine were made with these methods. However, based on the results from other authors [15; 3], 3*P* loading can be decreased by feedforward filter or higher harmonic control too.

7 TOWER SHADOW COMPENSATION

As discussed previously in the chapters four and five, wind shear has significant effect on the varying loads affecting on the wind turbine. However, there is also another deterministic component in the wind experienced by the turbine that causes the uneven distribution of the wind through the blades. This component is called tower shadow effect and it is caused by the difference in the wind flow due to the tower. In the case of a three-bladed upwind turbine, each of the blades experiences the minimum wind when it is directly in front of the tower and thus, the effect of tower shadow is present three times in a complete rotation. For this reason, the tower shadow contributes to the 3*P* effect which refers to the short term fluctuations of the output power of the turbine at 3*P* frequency. [44].

There are many reports concerning the 3*P* effect, for example, [10; 45; 46; 47], which contributes to the voltage flicker which decreases the quality of the power produced by wind turbines. However, the effect of the tower shadow on the wind turbine loading has not gained that much attention in the researches and literature. For this reason, the effect of the tower shadow on the blade and tower top loading was evaluated through the simulations. Furthermore, two different load reduction controllers striving to the compensation of the tower shadow were implemented. This chapter begins with the evaluation of the effect of the tower shadow on wind turbine loading. Then, feedforward tower shadow compensation algorithm is introduced and a controller based on this is implemented in Simulink. At the end of the chapter, feedback tower shadow compensation scheme that utilizes the blade load sensors is discussed.

7.1 Effect of Tower Shadow on the Wind Turbine Loading

Similar to the wind shear, the effect of tower shadow can be simulated in the wind turbine simulation software FAST too. Hence, the simulation at the wind speed of 13 m/s was run in order to evaluate the effect of wind shear on the wind turbine loading. Only the collective pitch controller was active during the simulation, so no wind shear compensation is done. The effect of tower shadow on the blade loading is shown in the figure 7.1, in which the steady wind, i.e., neither tower shadow nor wind shear are present, are shown as a reference. Comparing the out of plane blade bending moments between the steady and tower shadow cases in the upper plot of the figure 7.1, it can be seen that there is a dip in the moment always when the blade is directly in the front of the tower. On the other hand, the tower shadow does not increase the amplitude of this moment, unlike the wind shear. In addition, tower shadow, neither the wind shear, does not affect on the in-plane blade moment, which can be seen in the lower plot of the figure 7.1.

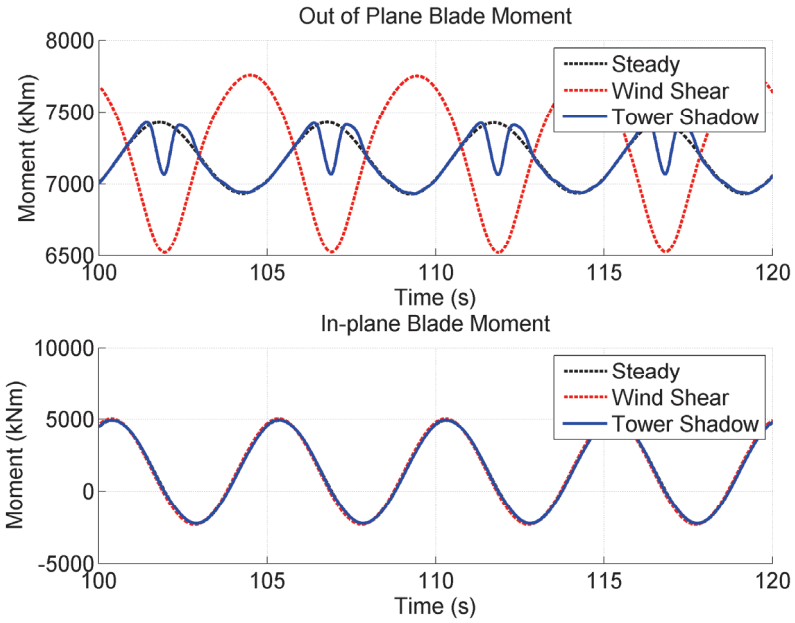

Figure 7.1. *The effect of tower shadow on the blade loading*

The dip in the out of plane blade moment results in a peak in the tilt moment at 3*P* frequency which can be seen in the figure 7.2. In addition, there is some difference in the yaw moments between the steady and tower shadow cases, but the difference is less significant than in the case of tilt moment. However, tower shadow has a minor effect on the static component of tilt and yaw moments, which in turn is the most detrimental consequence of wind shear.

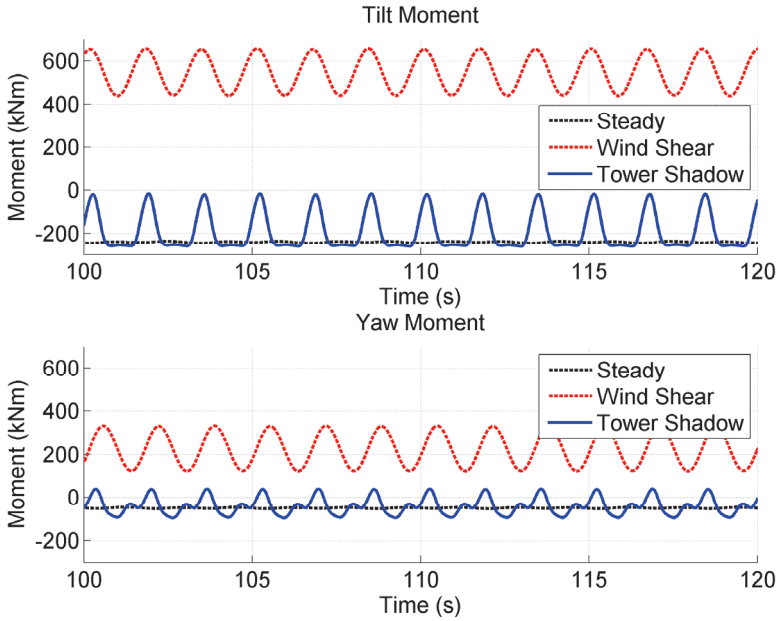

Figure 7.2. *The effect of tower shadow on tower top loading*

Even though the effect of the tower shadow on the wind turbine loading is quite small compared to the influence of wind shear, it could still be useful to try to compensate it. Because the wind speed experienced by the blade decreases in the front of the tower due to tower shadow, the pitch angle of the given blade should be decreased too. By this way, the drop in the blade moment should become smaller.

7.2 Feedforward Tower Shadow Compensation

As discussed above, wind speed is decreased in the front of the tower due to the tower shadow effect. To be able to compensate this decrease by adjusting the pitch angle of the blade, which is directly in front of the tower, the profile of the decreased wind should be modeled. Based on the reports of Karnik et al. [44], Hansen et al [48] and Peng [10], the effect of tubular tower on the wind speed experienced by the blades can be modeled based on the potential flow theory around a cylinder. Hence, the wind speed in the front of the tower can be expressed using the following equation:

$$V_{tower} = BV_{hub}, \tag{6.1}$$

where B so called tower-shadow coefficient and can be defined by

$$B = 1 - R_{tower}^2 \frac{x^2 - y^2}{(x^2 + y^2)^2}, \tag{6.2}$$

Where x and y are the longitudinal and lateral distances between a given point in the rotor plane and the rotor center, respectively and R_{tower} is the radius of the tower at the height of interest. Furthermore the y can be expressed in the terms of azimuth angle ϕ and the radial distance from the rotor axis r:

$$y = r \sin \phi \tag{6.3}$$

It should be noted that (6.1) is valid only when the blade is in the tower shadow area, i.e., $\phi = \pm 60°$ to the right and left from the rotor center.

In order to compensate the effect of the decreased wind speed experienced by the blade due to tower shadow, a simple feedforward controller was implemented. The hub-height wind speed V_{hub} and azimuth angle ϕ are measured, from which the tower-shadow coefficient B and hence, the wind speed in the front of the tower V_{tower} can be calculated. Pitch angle that corresponds to the decreased wind speed V_{tower} is then chosen based on the relation between the wind speed and the pitch angle that gives the rated rotor speed. Therefore, the same table (see table 4.2) as in the collective pitch controller is used in this controller too.

Beginning with the simplest option, R_{tower}, x and r in the (6.2) and (6.3) were chosen to be constant. Actually, the width of the tower of the 5-MW reference turbine decreases from *6 m* at the bottom to *3.87 m* at the top of the tower, but at the beginning, the average value of *5 m* for the tower width was chosen. The longitudinal distance from the rotor plane to the rotor center, x, remains close to constant at *5.01910 m*. Different values of the radial distance r produce different curves for the tower shadow coefficient B which can be seen in the figure 7.3. It is worth of noting that the tower shadow coefficient considers also the slight increase in wind speed in the sides of the tower. A certain blade element is affected by the tower shadow as longer and closer the element is to the hub. For example, the blade element at the tip of the blade ($r = 61.5$ *m*) is shadowed by the tower shorter period of time than the blade element at the center of the blade ($r = 30$ *m*). At the beginning, r was set to be *30 m* that is approximately the mean value of the blade length.

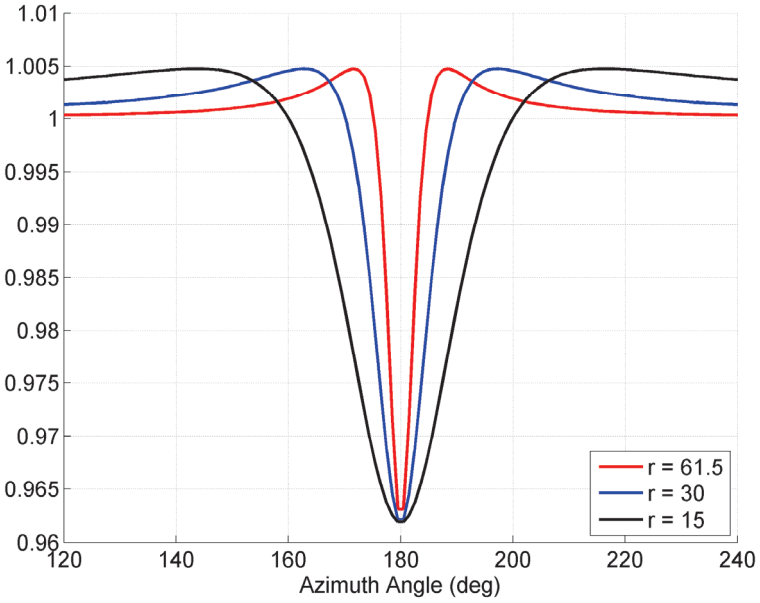

Figure 7.3. *Tower shadow coefficient at different values of r*

Simulink model of the implemented controller is shown in the figure 7.4. Tower shadow coefficient B is calculated based on the measurement of the azimuth angle, then the measured wind speed is multiplied by B to get the $V_{tower.}$ Smaller one of the measured hub-height wind speed and the modified wind speed due to tower shadow is chosen. This is done because the wind speed increases around the sides of the tower and therefore, the controller would increase the pitch angle at the sides of the tower shadow area. However, this is not desired because too high pitching activity back and forth is to be avoided. Now when the decreased wind in steady state speed is known, look-up table is used in order to get the corresponding pitch angle. Operation pitch angle, i.e. the pitch angle that corresponds to the hub-height wind speed is then subtracted from the pitch angle gained from the look-up table.

By this way, the small feedforward term of the pitch angle is gained. Finally, the feedforward term is added to the pitch angle demand set by the collective pitch controller. It is worth of noting that for the given blade, the compensation of tower shadow is done only if the blade is in the tower shadow area, i.e. the azimuth angle for the given blade is ± 60° from the angle at which the blade is pointing down direct in the front of the tower. In the case of FAST simulation software, this means the azimuth angle is between 120° and 240° for the blade one, 0° and 120° for blade two and 240° and 360 ° for blade three. If the azimuth angle is outside the limits, the value of *B* will be one and the controller has no effect on the operation of the system.

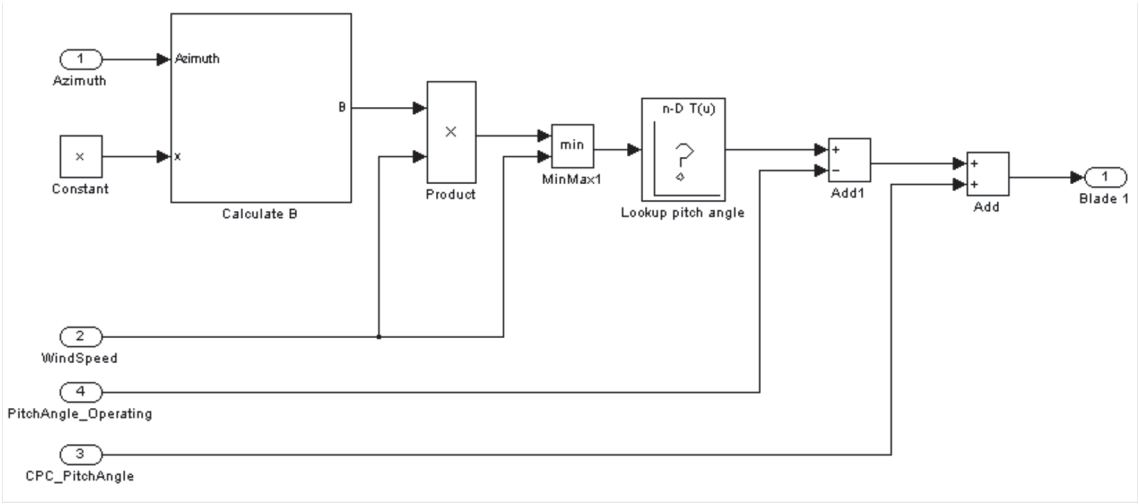

Figure 7.4. *Simulink model of the feedforward tower shadow compensation controller*

When the simple average values are used for the parameters in (6.2), the controller is decreasing the pitch angle too much, which leads to the significant overshoot in the blade moment. This effect at the wind speed of 13 m/s is illustrated in the upper plot of the figure 7.5. Furthermore, the lower plot of the figure shows that the pitch angle is changed rapidly which leads to the very high pitching activity as well as to the attainment of the pitch rate limitation. Therefore, the profile of the tower shadow coefficient has to be modified in order to get the shape of the pitch angle modulation smoother.

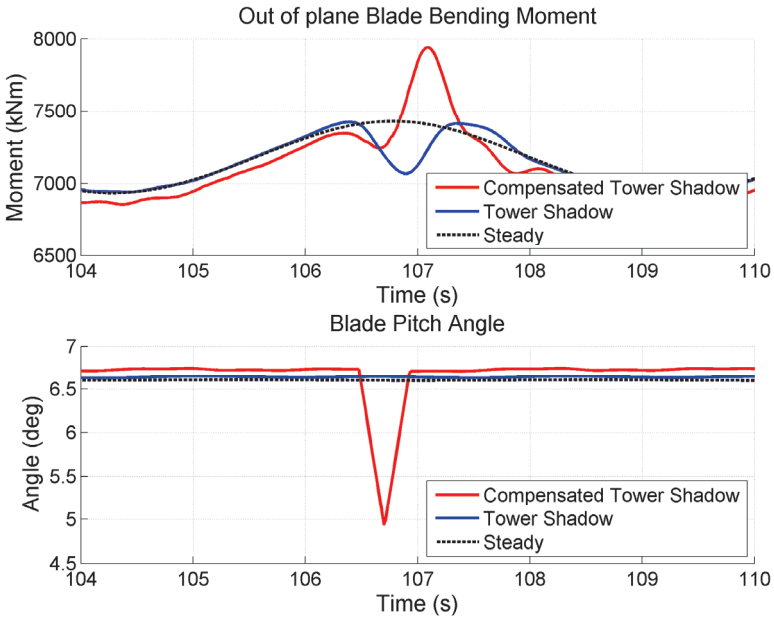

Figure 7.5. *Performance of the feedforward tower shadow compensation at the constant average parameters at the wind speed of 13 m/s*

It pointed out through the simulations that it is better to not consider the width of the tower in the calculation of tower shadow coefficient B. It is better to replace R_{tower} by a small gain term G in (6.2) to be able to modify the profile of the pitch angle. So, the calculation of B is based on following equation:

$$B = 1 - G\frac{x^2 - y^2}{(x^2 + y^2)^2}, \tag{6.4}$$

Several simulations at different parameter combinations were run but the most satisfying results at the wind speed of 13 m/s are gained by using the value of 15 m for r and 0.3 for the gain G. The smaller effective radius r leads to a larger pitching interval, because the modeled wind speed decrease is then wider (see figure 7.3). Therefore, pitch angle demand from the tower shadow compensation controller is smoother and the limitation of the pitch rate is not reached. When the controller based on (6.4) and the descriptions above are used, simulation results consisted with the figures 7.6 and 7.7 are gained. It can be seen in the figure 7.6 that the decrease in the pitch angle when the blade is in the tower shadow area results in the smaller dip in the blade moment compared to the case where no tower shadow compensation was made.

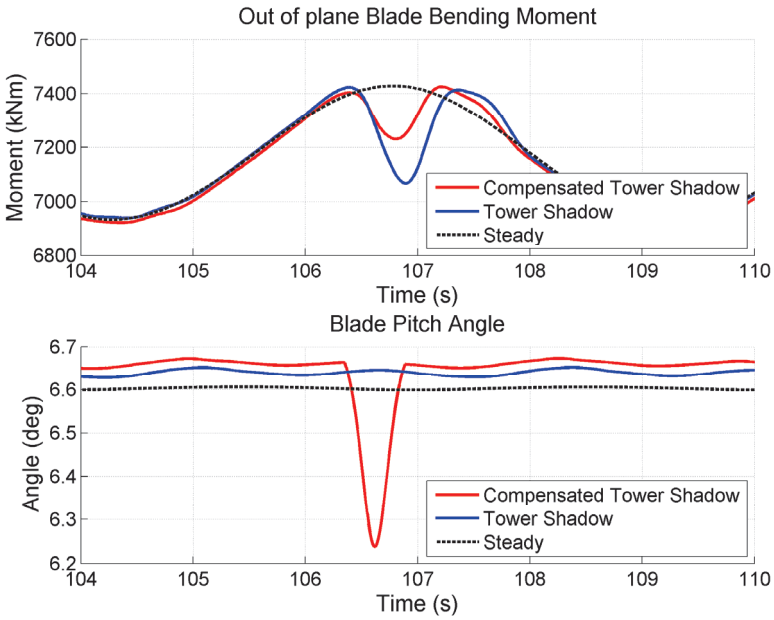

Figure 7.6. *Out of blade bending moment and the blade pitch angle for the blade one when the feedforward tower shadow compensation is used*

The smaller dip in the blade moment results some reduction in the amplitude of the peak in the tilt moment which can be seen in the upper plot of the figure 7.7. In addition, the yaw moment becomes smoother too even though the effect of tower shadow on it is not so significant without the compensation either.

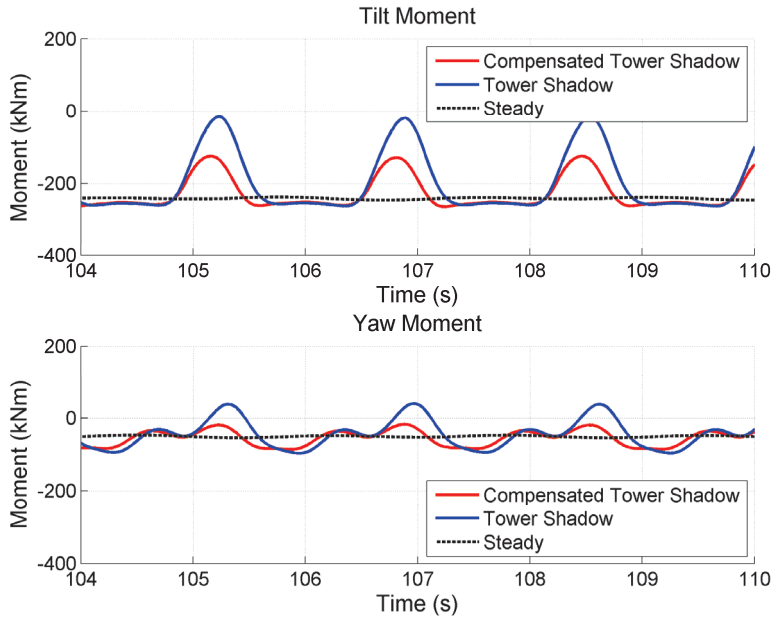

Figure 7.7. *Tilt and yaw moments when the feedforward tower shadow compensation is used*

It seems that the pitch angle should be reduced more to be able to completely compensate the dip in the blade moment, which would then result in the constant tilt and yaw moments. However, the increase in the gain G in (6.4), which leads to the greater decrease in the wind speed in the front of tower and thus, smaller pitch angle demand, does not contribute to the better tower shadow compensation. Only the overshoot in the blade moment after the dip becomes more significant which leads to the undesirable back and forth movement in the tilt moment. The effects of different values of G and r on the tower shadow compensation are illustrated in the figures A.17 and A.18 in the appendix A.

Even though some tower shadow compensation can be made by this simple feedforward control algorithm at the wind speed of 13 m/s, the performance of the controller becomes significantly poorer as the wind speed changes. Upper plot of the figure 7.8 shows the performance of the controller at the wind speed of 20 m/s in the terms of out of plane blade moment. Now, the reduction in the dip in the moment is significantly smaller than at the wind speed of 13 m/s and in addition, the overshoot after the dip becomes even greater than in the case where no tower shadow compensation was made. Besides, it is worth of noting that the location of the dip caused by the tower shadow is different than at the lower wind speed because it is now shifted to the left. It seems that as the wind speed increases the azimuth angle, at which the maximum value of the out of plane blade moment is reached, increases too. This phase shift might be due to the larger pitch angle which changes the aerodynamic properties of the turbine more. Based on this phase shift, the dip due to tower shadow is not anymore located directly under the maximum value of the blade moment.

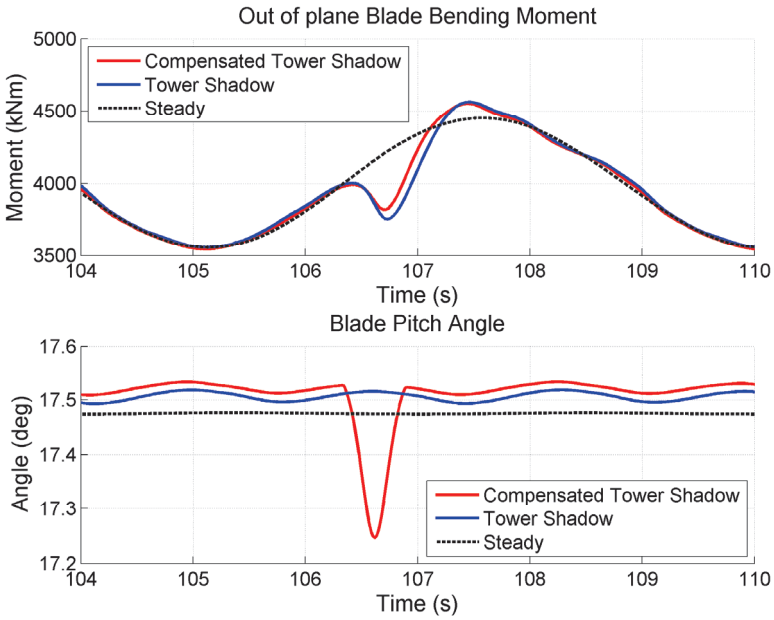

Figure 7.8. *Performance of the feedforward tower shadow compensation at the wind speed of 20 m/s*

In conclusion, control parameters of the simple feedforward tower shadow compensation controller should be adapted as the wind speed changes, so some kind of gain scheduling tables would be needed again. Furthermore, it is not enough to modify the gain *G,* because the shape of the so called tower shadow dip changes along the wind speed. Therefore, some kind of phase correction would be needed too. To produce gain scheduling tables needed, several simulations and manual tuning of the control parameters would be needed. Furthermore, additional gain scheduling tables do not contribute to the utilization of the control algorithm in the real wind turbine because they demand more measurements at various wind speeds. As mentioned earlier in this thesis, these kinds of measurements are always challenging to arrange. For these reasons, the feedforward tower shadow compensation is not dealt further within this thesis.

7.3 Tower Shadow Compensation based on Load Sensors

Due to the nonlinear characteristics of the wind turbines, it seems that some kind of gain scheduling is always needed in the case of feedforward control algorithms. Therefore, the possibility to utilize the blade load sensors in the tower shadow compensation was evaluated too. However, methods based on d-q transformation are not suitable for the tower shadow compensation purpose because the pitch angles of the three blades are always coupled due to the d-q transformation. In order to compensate the tower shadow, the pitch angle of the blade which is in the tower shadow area at the given time should be affected independently.

As discussed earlier in this chapter, tower shadow causes a notch in the out of plane blade moment. Taking a look into figure 7.1, it seems that it might be possible to compensate the effect of tower shadow by pitching the blade in a way that the blade moment is kept constant through the tower shadow area. Based on this assumption, a feedback tower shadow compensation controller was implemented. Even though, the performance of the controller was not assumed to be equally good at different wind speeds due to the different shape of the moment at the higher wind speed (see the figure 7.8).

The control purpose of the feedback tower shadow compensation is to keep the blade moment constant at the same value as before the blade comes to the tower shadow area. The idea of the control scheme is illustrated in the figure 7.9 in which the grey arrow refers to the value of the moment which is caught and used as a reference value for the controller. So, the thought is to control the blade pitch angle in a way that the moment is kept constant.

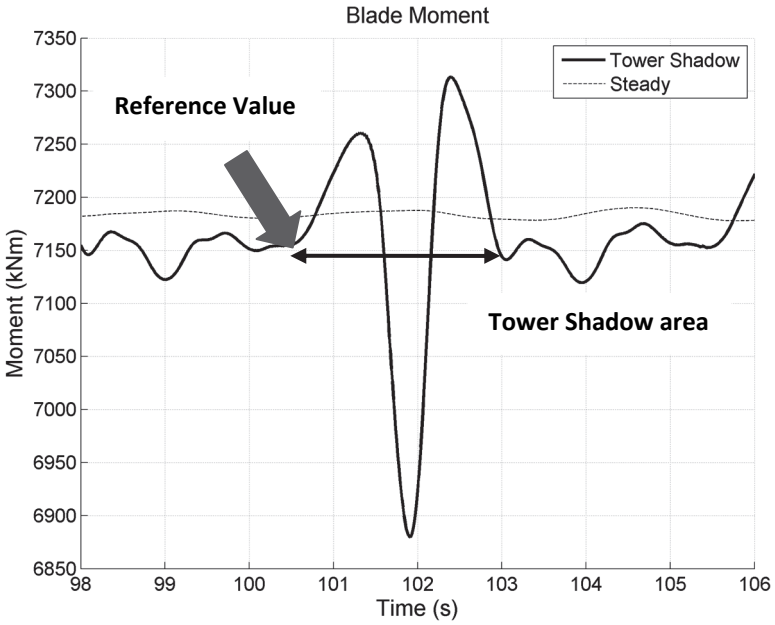

Figure 7.9. *Idea of the feedback tower shadow compensation controller*

Consequently, a PI controller that generates an additional tower shadow compensation term to the pitch angle demand was implemented. Each of the blades needs their own tower shadow controller that uses the out of plane blade moment for that given blade as measurement signal in order to create the additional pitch angle demand for that blade. These additional pitch angle demands are then summed up with the angle demand gained from the baseline IPC. This tower shadow compensation method was implemented based on the baseline IPC because the blade load sensors are needed anyway and hence, the sinusoidal blade loading due to gravity can be decreased too. This tower shadow compensation controller for the blade one is shown in the figure A.19 in the appendix A. Same kind of controllers are used for the blades two and three, only the values of the azimuth angle defining the tower shadow area are different. Reference value of the blade moment for the PI controller is generated by catching the value of the moment at the azimuth angle of 120° through a triggered sub-system. Again, the additional tower shadow compensation term is added to the final pitch angle demand only if the blade is in the tower shadow area. Otherwise, the pitch angle demand from the tower shadow compensation will be zero. The subsystem that defines the tower shadow zone returns value 1 if the blade is between 120 ° and 240 °, otherwise it returns 0. Integrator of the PI controller is also reset when the subsystem returns value zero in order to avoid problems caused by the integrator wind up.

Nevertheless, this feedback tower shadow compensation controller based on the blade load sensors is not performing very well. Figure 7.10 shows the performance of the controller at the wind speed of 13 m/s in the terms of the out of plane blade moment and the pitch angle for the blade one at different values for the control parameters K_P and K_I.

Black dashed curve shows the effect of the tower shadow when the baseline IPC is used alone and no tower shadow compensation is done. One can see on the lower plot of the figure that the shape of the blade pitch angle is not purely sinusoidal even though no tower shadow compensation is made. So, the effect of the tower shadow on the blade moments affects also on the individual blade pitch angles through the transformation that utilizes the measurements of the blade loads. Furthermore, different values for the control parameters do not contribute to the performance of the controller. In the case of loose tuning of the PI controller *(red curve)*, the controller is hardly doing something but when the tuning is tightened *(blue curve)*, the overshoot after the drop in the blade moment increases. It can also be seen that there is hardly no difference between the P and PI controller *(green and blue curve)*. The time period during which the blade is in the tower shadow area is only around two seconds which may be one of the reasons why I-part does not enhance the performance of the controller. Other combinations for the control parameters were tested too but none of them contributed to the performance of the controller. It is worth of noting that the negative values are needed for the control gain K_P because the relation between the blade moment and the pitch angle is inverse i.e., larger pitch angle causes smaller moment.

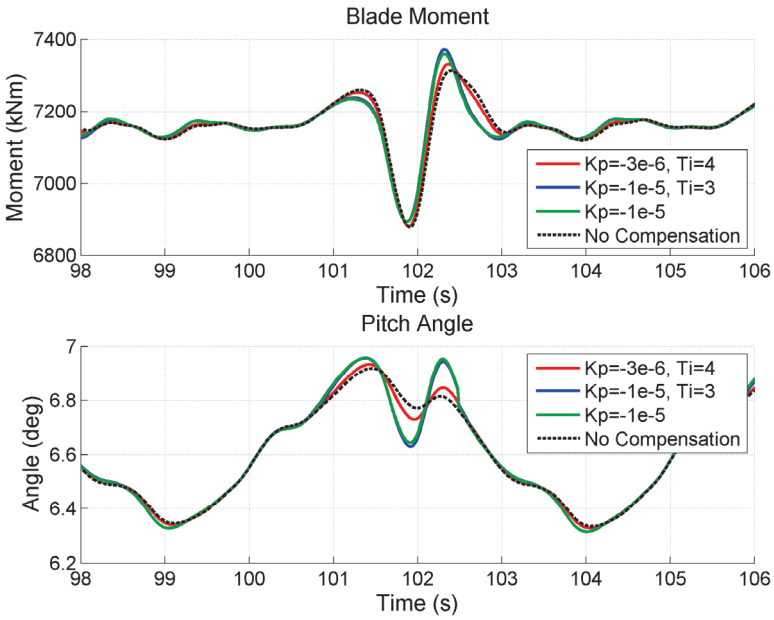

Figure 7.10. *Performance of the feedback tower shadow compensation at different values for the control parameters*

Because of the poor performance of the controller described above, the tower shadow area in which the controller is active was made narrower in order to see whether the overshoot in the moment could be decreased by this way. Instead of from 120 ° to 240 °, the tower shadow zone was defined to be from 170° to 215° which is roughly the area of the drop in the blade moment.

However, as the figure 7.11 shows, the effect of the tower shadow cannot be compensated more effectively than in the case of wider tower shadow area. There is hardly no difference between the red and blue curve, in other words the wider and narrower tower shadow zone at the same control parameters (K_P = -3e^{-6} and T_I = 4). And again, when the gain K_P is increased to the value -1e^{-5}, only the overshoot in the moment becomes larger.

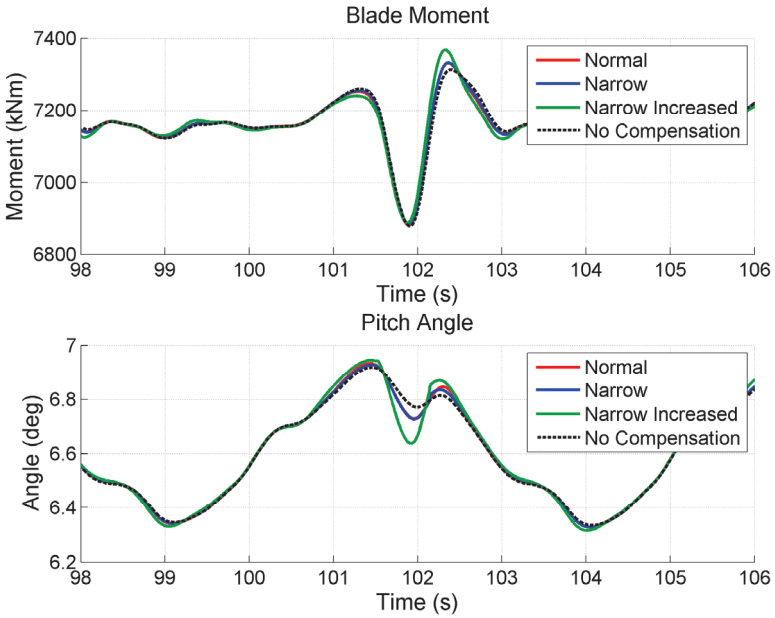

Figure 7.11. *Effect of narrower tower shadow area on the performance of the feedback tower shadow compensation*

As a conclusion, it can be assumed that the pitch angle demand from the baseline IPC and the additional term from the tower shadow compensation are someway interrupting each other and the method described above cannot be used. Another reason could be the fact that the shapes of the blade pitch angles are disturbed by the tower shadow which may affect on the performance of the IPC and by this way makes the situation more complicated. In order to overcome the problems described above, the controller that strives to keep blade moment constant through the tower shadow area was applied to the CPC too. However, good compensation results were not gained by this way either. Figure 7.12 shows that again in the case of so called normal tower shadow area *(red curve)* i.e., from 120° to 240 °, the control activity is too low and the drop in the blade moment is not compensated at all. Furthermore, only the overshoot after the drop is increased when the tower shadow area is narrowed *(blue curve)*. Loosening the tuning of the PI controller in the case of narrowed tower shadow area decreases the overshoot but however, at the cost of decreased compensation of the drop in the moment. Other parameters for the PI controller were tested in the case of this tower shadow compensation algorithm too but better compensation results were not attained.

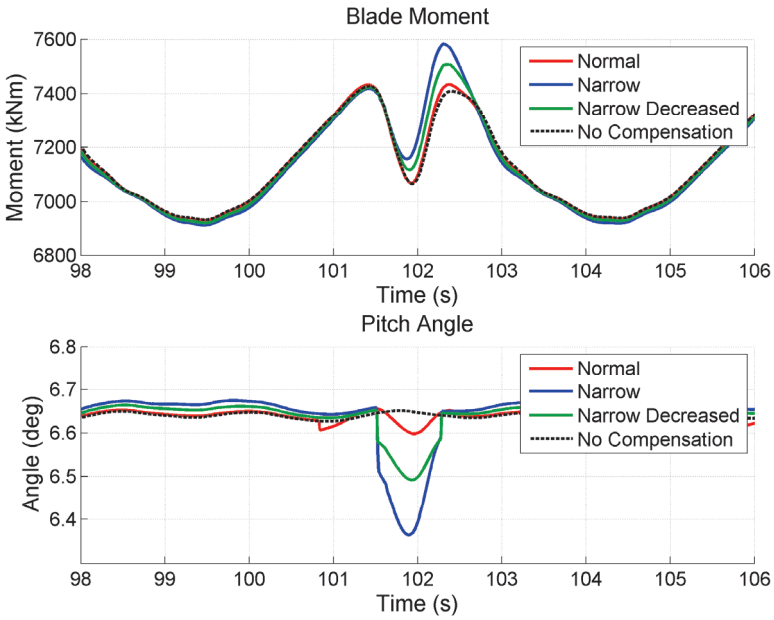

Figure 7.12. *Performance of the feedback tower shadow compensation based on CPC*

It seems that the control algorithm that strives to keep the blade moment constant through the tower shadow is not suitable for the tower shadow compensation purpose. As mentioned before, the blade is in the tower shadow area only roughly two seconds which demands extremely fast response from the compensation algorithm. However, the controller described above cannot be tuned fast enough without causing significant overshoot in the blade moment after the drop caused by tower shadow. Therefore, in the case of tower shadow compensation, it seems that no additional value is gained by using load sensors compared to the feedforward method described in the beginning of this chapter. Of course, there might be other kind of methods utilizing load sensors that could be used for the tower shadow compensation and thus, achieve better compensation than the feedforward method.

8 COMPARISON OF THE DIFFERENT LOAD REDUCTION METHODS

Different control algorithms for the load reduction due to wind shear and tower shadow have been introduced in the previous chapters. Different methods are now compared considering not only the load reduction results but also the other issues affecting on the eventual utilization of the methods in the real wind turbines. First, different methods for the reduction of the loading caused by the wind shear are discussed. Then, control schemes for tower shadow compensation are compared.

8.1 Wind Shear Compensation

Four different control algorithms striving to the alleviation of the loading caused by the wind shear have been implemented within this thesis. First, baseline IPC based on blade load sensors was discussed. Then, two feedforward IPCs, one simple with constant gains and another gain-scheduled one were introduced. Furthermore, an extension to the baseline IPC for the reduction of remaining 3*P* loading in the tilt and yaw moments was implemented. Capabilities of these controllers for load reduction at the wind speed of 18 m/s are compared in the terms of blade moment in the figure 8.1 and in the terms of tilt and yaw moments in the figure 8.2. Moments in the case of collective pitch control only are shown (black curve) as a reference value in both figures.

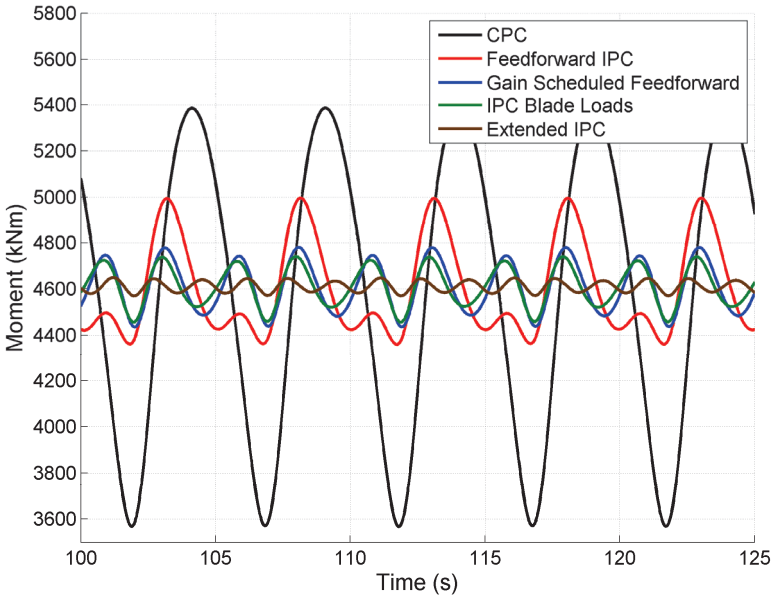

Figure 8.1. *Comparison of the performances of the different IPCs at the wind speed of 18 m/s in the terms of out of plane blade moment*

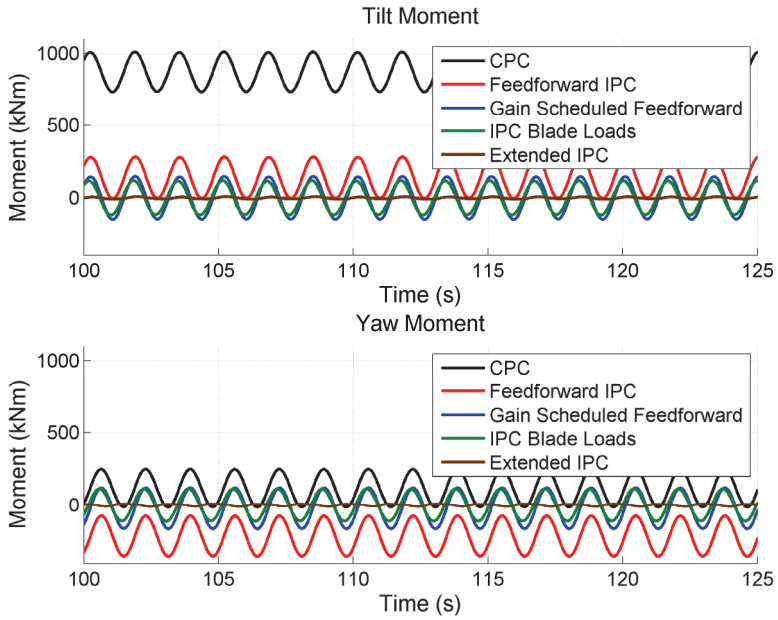

Figure 8.2. *Comparison of the performances of the different IPCs at the wind speed of 18 m/s in the terms of tilt and yaw moments*

In order to get more comprehensive view of the performances of the different controllers, numerical values of the disturbing moments at the wind speed of 18 m/s are compared in the table 8.1. Amplitudes of the blade and tilt and yaw moments are compared as well as the mean values of the tilt and yaw moments. In addition to the absolute values, the table shows also the percentage values related to the values of CPC. Same results can be seen in the table as in the figures above.

Table 8.1. *Comparison of the different methods for wind shear compensation at the wind speed of 18 m/s*

Moment (kN)	**CPC**	**IPC Blade Loads**	**Simple Feedforward IPC**	**Gain Scheduled Feedforward IPC**	**Extended IPC**
Blade Moment Amplitude	1815 (100 %)	267 (15 %)	637 (35 %)	342 (19 %)	78 (4 %)
Tilt Moment Mean Value	870 100 %	3 (0.2 %)	140 (16 %)	5 (0.6 %)	-0.5 (0.06 %)
Tilt Moment Amplitude	275 100 %	295 (107 %)	285 (104 %)	290 (105 %)	17 (6 %)
Yaw Moment Mean Value	115 100 %	-3 (0.2 %)	-215 (187 %)	-25 (22 %)	-3 (0.2 %)
Yaw Moment Amplitude	265 100 %	275 (104 %)	275 (104 %)	275 (104 %)	14 (5 %)

All IPCs can decrease the amplitude of the blade moment as well as the mean value of the tilt moment significantly. However, performance of the simple feedforward IPC is poor in the case of yaw moment because the absolute value of the moment is increased significantly. As discussed in the chapter five, poor performance of the simple feedforward controller at the higher wind speeds is probably due to the fact that the yaw moment at the higher wind speed is already negative near the zero and the feedforward wind shear compensation algorithm changes the yaw moment into the wrong direction. Hence, the absolute value of the static component of the yaw moment increases.

Furthermore, it is important to note that all IPCs, except the extended IPC, are actually increasing the amplitude of the tilt and yaw moments. However, the increase is rather small compared to the load reduction in the mean values attained by IPC blade loads and gain scheduled feedforward IPC. Furthermore, it is mentioned in the report of Bossanyi [15] that the individual pitch control action may amplify the 3*P* component, i.e. the amplitude of the oscillations, in the tilt and yaw moments which can be prevented by low-pass filtering the d- and q axis moment signals after the transformation. However, no filtering was made within the simulations of this thesis. So, the amplitude of the oscillations in the tilt and yaw moments could probably be decreased by low-pass filtering of the signals. Nevertheless, the amplitude decrease in the case of feedforward methods cannot be affected by this way. Despite the poor performance of the other controllers in the case amplitudes of the tilt and yaw moments, the extended IPC is able nearly to eliminate the 3*P* loading from them. Furthermore, the overall performance of this controller seems to be very good.

In addition to the capabilities of the controllers in the load reduction, there are also other issues that should be considered before overall conclusions can be made. As discussed earlier, pitching of the blades always increases the mechanical stress of the pitch actuators. Furthermore, power usage of the pitch motors is increased which leads to the higher costs of the energy produced by the wind turbines. According to Haarnoja [3], a rough estimation of the power consumption can be made by assuming that the pitch motor is working only against the moment of inertia of the blade and not considering the forces caused by the rotational motion and the interaction with the wind. Therefore, the power needed can be expressed as

$$P = \dot{\theta}T = \dot{\theta}\ddot{\theta}I_{rot}$$

where θ is the pitch angle, T is the torque of the pitch motor, and I_{rot} is the moment of inertia around the blade axis. Hence, the power consumption of the pitch motors can be assumed to be directly proportional to the product of the first and second derivatives of the pitch angle

$$P \propto \dot{\theta}\ddot{\theta}.$$

Now, power consumption of the different methods can be compared which is shown in the case of constant wind speed of 18 m/s in the figure 8.3. Red curve refers to the simple feedforward IPC (FF), blue curve to the gain scheduled feedforward IPC (FFGS), green one to the extended IPC including the 2P blade load reduction (2P) and the purple curve describes the baseline IPC based on blade load sensors (BL). It is extremely important to consider that the power consumption of CPC, which is shown black, is zero only because the wind speed is completely constant. Of course, this is very ideal assumption and the wind speed affecting on the real wind turbine would never be totally constant due to turbulence and other stochastic variations in the wind. However, because the effect of wind shear on the turbine loading and methods to compensate have been discussed, it is justifiable to use this kind of wind profile. Otherwise, it might be difficult to evaluate the performances of the controllers in the purpose in which they were implemented for, namely the alleviation of the loading caused by wind shear. Due to the derivative blocks in the simulink model, which were used in order to define $\dot{\theta}$ and $\ddot{\theta}$, power estimation curves for the baseline IPC blade loads and the extended IPC include high frequency noise components. The signals could be low-pass filtered but in this case it has not been done in order to guarantee the preservation of all information.

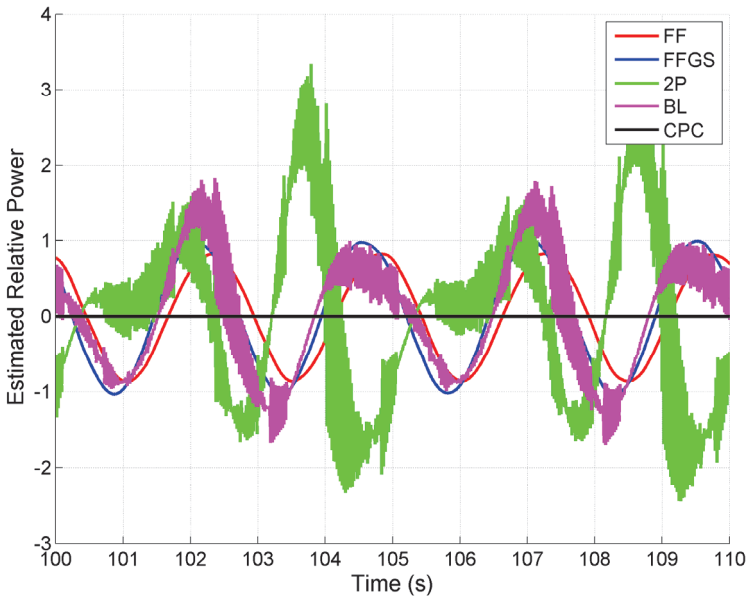

Figure 8.3. *Rough estimation of the power consumption of the different controllers at the constant wind speed of 18 m/s*

According to Haarnoja [3], if only the positive instantaneous power consumption is considered, it is possible to calculate a rough estimation about the relative average power consumption. Power consumptions of the different methods are thus compared in the table 8.2. Most well-known method in the literature, namely the IPC blade loads, is considered as a reference and other methods are then compared to that.

This table together with the figure above suggests that the relative power consumptions of the feedforward methods are slightly smaller but it is worth of noting that the load reduction, especially in the case of simple feedforward IPC, is also milder. Furthermore, it seems that when the baseline ICP is extended to include also the 2*P* blade load reduction algorithm, the power consumption is increased approximately by 44 %. Nevertheless, it can be derived from the table 8.1, that the blade load alleviation is increased 71 % and the tilt and yaw moment are decreased more than 90 % compared to the baseline IPC. So, comprehensive calculations are needed in order to find the optimum compromise between load reduction and the increased power consumption of the pitch motors.

Table 8.2. *Relative average power consumption of the different methods for wind shear compensation*

Controller	***Relative Power Consumption***
IPC Blade Loads	1.0
Feedforward IPC	0.81
Gain Scheduled Feedforward IPC	0.97
Extended IPC	1.44

In conclusion it can be said, that every controller is able to decrease the amplitude of the out of plane blade moment and hence, decrease the loading of the blades. However, the simple feedforward IPC has an opposite effect on the yaw moment and the utilisation of this method should thus be considered carefully. Nearly equally good load reduction can be attained by the baseline IPC based on blade load sensors and the gain scheduled feedforward IPC. Furthermore, estimated average power consumption of these methods is almost equal. However, challenging measurements at different wind speeds are needed in order to get the control parameters for the gain scheduled feedforward IPC. Most superior load reduction seems to be attained by extended IPC but however, the power consumption is also higher.

8.2 Tower Shadow Compensation

In addition to the methods striving to alleviation of the loads caused by wind shear, different methods for the tower shadow compensation have been discussed within this thesis. Unlike the methods for the load reduction due to wind shear, good load reduction at different wind speeds was gained by none of the tower shadow compensation schemes described in the chapter seven. However, all methods are compared in the figure 8.4 in the terms of tilt moment at the wind speed of 13 m/s. Only the amplitude and the shape of the moment are comparable because the feedback method based on baseline IPC is affecting also on the mean value of the tilt moment. Results concerning feedback methods, which are based on blade load sensors, green and blue curve, describe the cases in which there is no overshoot in the blade moment (see red curve in the figures 7.11 and 7.12). It can be seen that only the feedforward method, shown in red, can really somewhat compensate the effect of tower shadow. By this method, the amplitude of the peak in the tilt moment, caused by tower shadow, can be decreased approximately 50 % at the wind speed of 13 m/s.

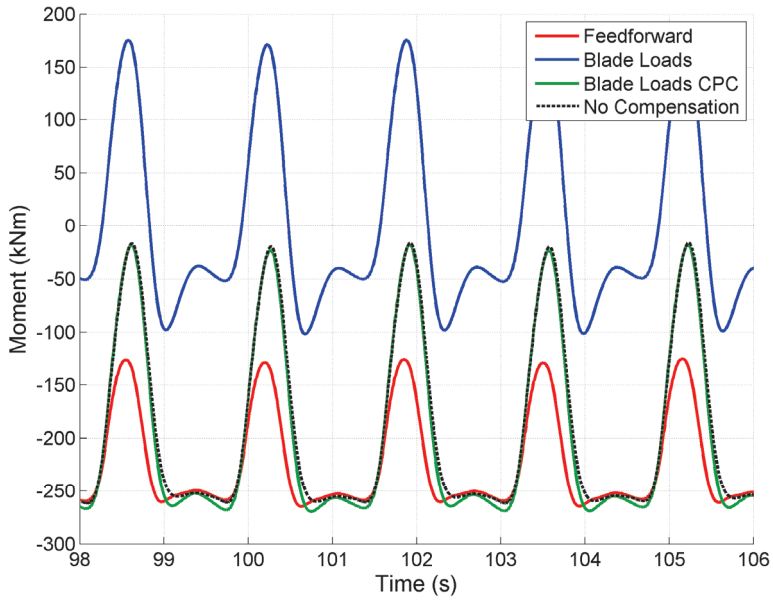

Figure 8.4. *Comparison of the different tower shadow compensation methods in the terms of tilt moment at the wind speed of 13 m/s*

However, in the case of feedforward tower shadow compensation, different control parameters are needed at different wind speeds and therefore, conclusions about the overall performance of the controller cannot be made. In addition, as always in the case of feedforward methods, the accuracy of the model, through which the decrease in wind speed is calculated, is crucial.

9 CONCLUSIONS

Purpose of this thesis was to implement and evaluate different methods for the blade pitch control of the wind turbines. Performance of the collective pitch controller (CPC) in extreme wind conditions was evaluated through the simulations. Furthermore, wind turbine loading and different methods for the alleviation of these loads have been discussed in this thesis. It has been pointed out that the wind shear has more significant effect on the loading of the turbine compared to the effect of the tower shadow. Furthermore, simulation results have shown that significant reduction of the loading caused by wind shear can be attained by individual pitch control (IPC) schemes. However, control algorithms for comprehensive tower shadow compensation were not found within the simulations.

In the third chapter, performance of the collective pitch controller in extreme wind conditions was investigated. It pointed out that the extreme operating gust has the most significant effect on the rotor speed and hence, on the generator power. However, only the simple generator torque controller available in the simulation environment FAST was used in the simulations. Therefore, it could be possible to decrease the effect of extreme operating gust (EOG) by more sophisticated control scheme. In addition, simulation results suggest that the speed of the wind speed measurement has a major impact on the performance of the CPC at the presence of EOG. This means that if the wind speed could be measured in real time, power fluctuations due to EOG could be decreased significantly. This contributes to the utilization of light detection and ranging (LIDAR) technology in the wind speed measurements by which the current wind speed could be measured every second instead of average speed of 5-10 minutes that is typically used in the case of conventional wind vanes. For this reason, further research concerning the utilization of LIDAR techniques would be useful.

Wind shear seems to have a major impact on the wind turbine loading. It has been pointed out through the simulations that this loading can be decreased significantly by individual pitch control. Remarkable alleviation in the blade loading as well as in the tower top loading can be gained by baseline IPC that is a well-known method in the literature. This method is based on the measurement of the blade loads and hence, blade load sensors are needed in order to utilize this method in the real wind turbine. Nevertheless, nearly as good alleviation of the loads caused by wind shear was gained by gain-scheduled feedforward IPC which needs only the measurement of the rotor position.

On the other hand, load sensors are needed anyway at least in the prototype of the turbine in order to define the control parameters at different wind speeds for the gain scheduling. Furthermore, measurements at several wind speeds are always challenging due to the stochastic nature of the wind. Performance of the simple feedforward IPC, that uses the constant control parameters, was evaluated too, but the controller was operating satisfyingly only near the rated wind speed. In addition, the controller was actually exciting some of the loads at higher wind speeds. Therefore, utilization of this control scheme as such is not recommended. Even though good wind shear compensation was gained by the gain scheduling feedforward IPC within the simulations, benefits of the load sensors should not be underrated because they can be used for other purposes too.

Even though the baseline IPC and the gain scheduled feedforward IPC can decrease the blade loading as well as the mean value of the tilt and yaw moments, they cannot affect on the fluctuating loading at 3P frequency (three times the rotor frequency P) in the tilt and yaw moments. Therefore, so called extended IPC striving to the alleviation of the remaining 3P loading was introduced. It can be said that the 3P loading in the tilt and yaw moments is mainly caused by the 2P component in the blade loads. Therefore, by extending the baseline IPC to include another control loop affecting on the 2P loading of the blades oscillations at the 3P frequency in the tower top moments can be decreased notably. As a drawback, power consumption of the pitch motors is increased roughly 45 % compared to the baseline IPC.

Effect of tower shadow on wind turbine loading and methods for its compensation have also been discussed in this thesis. It was pointed out through the simulations that the tower shadow causes a drop in the blade moment which leads to the peaks in the tilt moment. However, the loading caused by the tower shadow is smaller than the effect of wind shear. Different control methods striving to decrease the loading by adjusting the blade pitch angle on the decreased wind speed due to tower shadow were implemented. However, none of the discussed methods were able to compensate the drop in the moment effectively. Feedforward method was the only method that was able to compensate the tower shadow at same rate at certain wind speed. However, some kind of gain scheduling would be again needed in order to get good control results at different wind speeds. Feedback tower shadow compensation controller was implemented too but the controller could not be tuned to operate fast enough without causing oscillations. Poor results concerning the tower shadow compensation may be partly explained by the extremely fast nature of the tower shadow phenomenon. One of the blades is in the front of the tower only approximately 2 seconds which would demand extremely fast pitching activity. Due to this and relatively small impact on the wind turbine loading, the need of tower shadow compensation should be considered carefully.

All simulations within this thesis have been made at ideal wind conditions. In other words, the turbulence and other short term variations in the wind speed have not been considered at all. Therefore, comprehensive simulations at more realistic wind condi-

tions are needed before overall conclusions about the performance of the methods described within this thesis can be made.
In addition, it is important to note that the load reduction results expressed in this thesis should mainly be used to compare the different methods instead of only focusing on the scale of the load reduction gained by individual pitch control. It is obvious that the scale of the load reduction through the methods discussed in this thesis would be smaller in more realistic wind conditions. Furthermore, the dynamics of the pitch actuators should be considered more carefully in the future simulations. Within this thesis, the pitch angle demand is only limited between 0 and 90 ° and the pitch rate is limited to be 8 ° per seconds at highest. However, more comprehensive model for the pitch actuators is needed in order to get more realistic view of the performances of the IPCs for load reduction.

As mentioned in the case of extreme wind scenarios, utilization of LIDAR technology in the wind turbine control would be useful in order to get more accurate information about the wind speed. Furthermore, there are several reports concerning the utilization of LIDAR techniques for load reduction purposes [49; 50; 51; 52]. Therefore, further research within the LIDAR would be meaningful. On the other hand, possibilities to use the measurements, which are already available in the wind turbines, for load reduction purposes would be worth of considering too. In addition to the feedforward method based on rotor position measurement, it might be possible to design a controller utilizing the measurements from the nacelle inertial measurement unit that is usually part of the wind turbine structure. Therefore, further research related to this would be useful too. It is also worth of considering that all simulations within this thesis has been made at the wind speeds above rated wind speed, i.e., in the full load area in which the power is limited by collective pitch control. However, possible load reduction at partial load operation, in other words at the wind speeds below rated, could be worth of evaluate too.

SOURCES

[1] Bianchi, F.D., De Battista, H. & Mantz, R.J. Wind Turbine Control Systems. La Plata 2007, Springer. 205 p.

[2] Bossanyi, E.A. Individual Blade Pitch Control for Load Reduction. Wind Energy (2003)6, pp. 119-128.

[3] Haarnoja, T. Smart Control of Wind Power Plant. Espoo 2011, VTT. 27 p.

[4] Anaya-Lara, N, Cartwright, O., Ekanayake, P., Hughes, J. & Jenkins, M. Wind Energy Generation: Modelling and Control. 1st ed. Chichester West Sussex 2009, John Wiley & Sons, Ltd. 269 p.

[5] Butterfield, G., Jonkman, S., Musial, J., & Scott,W. Definition of a 5-MW Reference Wind Turbine for Offshore System Development. Colorado 2009, NREL. 63 p.

[6] Chen, J-J. & J, Zhi-cheng, J. The gain scheduling control for wind energy conversion systems based on LPV model. IEEE International Conference on Networking, Sensing and Control, Chicago 10-12.4.2010. 2010, IEEE pp. 653-657.

[7] Guo, C-C., Li, Y. & Yao, X-J. LPV H-infinity controller design for variable-pitch variable-speed wind turbine. Power Electronics and Motion Control Conference, IPEMC '09, Wuhan 17.-20.5.2009. 2009, IEEE. pp. 2222 - 2227.

[8] Barone, M.F., Berg, D.E., Berg, J.C., Resor, B.R. & Wilson, D.G. Compined Individual Pitch Control and Active Aerodynamic Load Controller Investigation for the 5MW UpWind Turbine. AWEA Windpower 2009 Conference & Exhibiton, Chicago, Illinois 4.-7.5.2009. pp. 1-12.

[9] Ximei, Z. & Xianfeng, S. Individual Variable Pitch Control of Wind Turbines. Electrical Machines and Systems (ICEMS) International Conference, Beijing 20.-23.8.2011. 2011, School of Electrical Engineering Shenyang University of technology. pp. 1-3.

[10] Peng, G. Influence Analysis of Wind Shear and Tower Shadow on Load and Power Based on Blade Element Theory. 23rd Chinese Control and Decision Conference (CCDC), Mianyang, China 23.-25.5.2011. 2011, IEEE. pp. 2809-2812.

[11] LeMieux, D. & Trudnowski, D. Independent Pitch Control using Rotor Position Feedback for Wind Shear and Gravity Fatigue Reduction in a Wind Turbine. American Control Conference, Anchorage, AK 8.-10.5.2002. 2002, AACC. pp. 4335-4340.

[12] Camblong, H., Nourdine, S., Tapia, G. & Vechiu, I. Comparison of Wind Turbine LQG Controllers Using Individual Pitch Control to Alleviate Fatigue Loads. 18th Mediterranean Conference on Control & Automation, Marrakech Morocco 23.-25.6.2010. 2010, IEEE. pp. 1591-1596.

[13] Cheng, M., Chen, Z., Zhang, J. & Zhang, Y. Mitigation of Fatigue Loads Using Individual Pitch Control of Wind Turbines Based on FAST. 46th International Universities' Power Engineering Conference, Soest Germany 5.-8.9.2011. VDE VERLAG GMBH.

[14] Van Engelen, T.G. Design Model and Load Reduction Assessment for Multi-rotational Mode Individual Pitch Control (Higher Harmonics Control). European Wind Energy Conference 2006, Athens 27.2-2.3.2006.

[15] Bossanyi, E.A. Further Load Reductions with Individual Pitch Control. Wind Energy 8(2005)4. pp. 481-485.

[16] Hombu, M., Sakasegawa, E., Shinohara, K. & Yamamoto, K. Characteristic Analysis of a Wind Power System with Doubly Fed Induction Generator in Considering of the Tower Shadow Effect. IPEC 2010 : International Power Electronics Conference, Sapporo 21.-24.6.2010. pp. 3225 - 3229.

[17] Nelson, V. Wind Energy: Renewable Energy and the Environment. Boca Raton 2009, CRC Press. 304 p.

[18] Enercon E-82 E3/3,000 kW [WWW]. [referred 1.6.2012]. Available in: http://www.enercon.de/en-en/64.htm

[19] Generators for Wind Power, Proven generators - Reliable Power [WWW]. ABB Motors and Generators. ABB Download Center. 2010. [referred 27.06.2012]. Available in: http://www05.abb.com/global/scot/scot234.nsf/veritydisplay/16edc80e7f7d96c4c1257a0f00388631/$file/ABB%20brochure%20Generators%20for%20wind%20power%20LowRes_31052012.pdf

[20] Hodges, D., Lee, D. & Patil, M. Multi-flexible-body dynamical analysis of horizontal axis wind turbines. Wind Energy 5(2002)4. pp. 281-300.

[21] Bossanyi, E., Burton, T., Jenkins, N. & Sharpe, D. Wind Energy Handbook. 1st Edition. 2001, John Wiley & Sons. 643 p.

[22] Hansen, A.C. & Laino, D.J. User's Guide to the Wind Turbine Aerodynamics Computer Software AeroDyn. [WWW]. [referred 1.4.2012]. Available in: http://wind.nrel.gov/designcodes/simulators/aerodyn/AeroDyn.pdf

[23] Kennedy, J., Littler, T., McSwiggan, D. & Morrow, D.J. A Study of Tower Shadow Effect on Fixed-Speed Wind Turbines. UPEC 2008 : 43rd International Universities Power Engineering Conference, Padova 1.-4.9.2008. pp. 1-5.

[24] Hess, F. Benefits from Individual Pitch Control. 2011.

[25] Linh, N.T. Power Quality Investigation of Grid Connected Wind Turbines. 4th IEEE Conference on Industrial Electronics and Applications, Xi'an China 25.-27.5.2009. 2009, IEEE. pp. 2218 - 2222.

[26] Hu, W., Chen, Z., Wang, Y. & Wang, Z. Flicker Mitigation by Active Power Control of Variable-Speed Wind Turbines with Full-Sclae Back-to-Back Power Converters. IEEE Transactions on Energy Conversion 24(2009)3, pp. 640-649.

[27] Bin, L. Wang, H. & Wang, W. Application of Individual Pitch Controller for Flicker Reduction on Variable Speed Wind Turbines. Power and Energy Engineering Conference (APPEEC), Chengdu China 28.-31.3.2010. pp. 1-4.

[28] Amin, M.M.N & Mohammed, O.A. Power Quality Improvement of Grid-Connected Wind Energy Conversion System for Optimum Utilization of Variable Speed Wind Turbines. IECON 2010 - 36th Annual Conference on IEEE Industrial Electronics Society, Glendale AZ U.S.A 7.-10.11.2010. 2010, IEEE. pp. 3287-3292.

[29] Laks, J.H., Pao, L.Y. & Wright, A.D. Control of Wind Turbines: Past, Present and Future. American Control Conference, St. Louis 10-12.6.2009. pp. 2096-2103.

[30] Ahmed-Ali, T., Beltran, B., & Benbouzid, M. Second-Order Sliding Mode Control of a Doubly Fed Induction Generator Driven Wind Turbine. IEEE Transactions on Energy Conversion 27(2012)2, pp. 261 – 269.

[31] Hansen, A., Hansen, M.H., Larsen, T.J., Øye, S., Sørensen, P. & Fuglsang, P. Control design for a pitch-regulated, variable speed wind turbine. Roskilde 2005.

[32] Bu, Feifei., Huang, Wenxin., Hu, Yuwen., Xu, Yunqing., Shi, Kai. & Wang, Qianshuang. Study and implementation of a control algorithm for wind turbine yaw control system. World Non-Grid-Connected Wind Power and Energy Conference, WNWEC 2009, Nanjing 5.-7.11.2009. pp. 1-5.

[33] Choi, Han-Soon., Kim, Jeong-Gi., Cho, Jang-Hwan. & Nam, Yoon-su. Active Yaw Control of MW class Wind Turbine. International Conference on Control, Automation and Systems 2010, Kintex Gyeonggi-do 27.-30.10.2010. pp. 1075-1078.

[34] IEC 61400-1. Wind turbines - Part 1: Design requirements. Switzerland 2005, IEC. 90 p.
Jonkman, J. & Marshall, L.B. FAST User's Guide. [WWW]. NREL. 2005 [referred 15.1.2012]. Available in: http://wind.nrel.gov/designcodes/simulators/fast/FAST.pdf

[35] Jonkman, J. & Marshall, L.B. FAST User's Guide. [WWW]. NREL. 2005 [referred 15.1.2012]. Available in: http://wind.nrel.gov/designcodes/simulators/fast/FAST.pdf

[36] Jonkman, J. NWTC Design Codes FAST. [WWW]. NREL. 2010. [referred 15.1.2012]. Available in: http://wind.nrel.gov/designcodes/simulators/fast/

[37] Laino, D.J. NWTC Design Codes AeroDyn. [WWW]. 2010. [referred 16.4.2012]. Available in: http://wind.nrel.gov/designcodes/simulators/aerodyn/

[38] Germanischer Lloyd Industrial Services GmbH. Guidelines for the Certification of Wind Turbines. Hamburg 2010.

[39] Järvinen, S. Tuulen nopeuden etämittaus LIDAR-teknologian avulla. Master of Science Thesis. Tampere 2011. Tampere University of Technology, Faculty of Science and Environmental Engineering. 73 p.

[40] Hansen, A.G. & Laino, D.J. User's Guide to the Wind Turbine Aerodynamics Computer Software AeroDyn. [WWW]. 2002. [referred 10.2.2012]. Available in: http://wind.nrel.gov/designcodes/simulators/aerodyn/AeroDyn.pdf

[41] Niemann, H., Poulsen, N.K. & Thomsen, S.C. Stochastic wind turbine control in multiblade coordinates. American Control Conference, Marriot Waterfront Baltimore 30.6-2-7.2010. pp. 2772-2777.

[42] Larsen, T.J., Madsen, H.A. & Thomsen, K. Active Load Reduction Using Individual Pitch, Based on Local Blade Flow Measurements. Wind Energy 8(2005)1, pp. 68-80.

[43] Hall, S.R. & Wereley, N.M. Linear Control Issues in the Higher Harmonic Control of Helicopter Vibrations. 45th Annual forum of the American Helicopter Society, Boston MA 22.-24.5.1989. pp. 955-971.

[44] Karnik, N., Santoso, S. & Swagata, D. Time-Domain Modeling of Tower Shadow and Wind Shear in Wind Turbines. Department of Electrical and Computer Engineering, The University of Texas at Austin, 2011.

[45] Bassan, S., Fadaeinedjad, R., Moallem, M. & Moschopoulos, G. Flicker Contribution of a Wind Power Plant with Single and Multiple Turbine Representations. IEEE Canada Electrical Power Conference 2007, Montreal Quebec Canada 25. - 26.10.2007. 2007, IEEE. pp. 74-79.

[46] Chen, Z., Hu, W., Wang, Y. & Wang, Z. Flicker Mitigation by Active Power Control of Variable-Speed Wind Turbines With Full-Scale Back-to-Back Power Converters. IEEE Transactions on Energy Conversion 24(2009)3, pp. 640 – 649.

[47] Bin, L., Wang, H. & Wang, W. Application of Individual Pitch Controller for Flicker Reduction on Variable Speed Wind Turbines. APPEEC 2010 (Asia-Pacific Power & Energy Engineering Conference 2010), Chengdu China 28. - 31.3.2010. 2010, IEEE. pp. 1 - 4.

[48] Hansen, A.C. & Moriarty, P.J. AeroDyn Theory Manual. [WWW]. NREL. 2005. [referred 20.4.2012]. Available in: http://www.nrel.gov/docs/fy05osti/36881.pdf

[49] Dunne, F., Jonkman, B., Kelley, N., Pao, L.Y. & Wright, A.D. Combining standard feedback controllers with feedforward blade pitch control for load mitigation in wind turbines. 48th AIAA Aerospace Sciences Meeting Including the New Horizons Forum and Aerospace Exposition, Orlando FL 4.-7.1.2010. 2010, AIAA. pp. 1-18.

[50] Dunne, F., Jonkman, B., Kelley, N., Pao, L.Y., Simley, E. & Wright A.D. Adding Feedforward Blade Pitch Control for Load Mitigation in Wind Turbines: Non-Casual Series Expansion, Preview Control and Optimized FIR Filter Methods. Mechatronics 21(2011)4, pp. 682-690.

[51] Johnson, K.E., Wang, N. & Wright, A.D. FX-RLS-Based Feedforward Control for LIDAR-Enabled Wind Turbine Load Mitigation. American Control Conference (ACC), San Francisco California 29.06-1.07.2011. 2011, AACC. pp. 1910 - 1915.

[52] Boyd, S., Brath, P., Soltani, M & Wisniewski, R. Load reduction of wind turbines using receding horizon control. 2011 IEEE International Conference on Control Applications (CCA), Denver CO 28.-30.9.2011. 2011, IEEE. pp. 852 - 857.

APPENDIX A: Further Figures

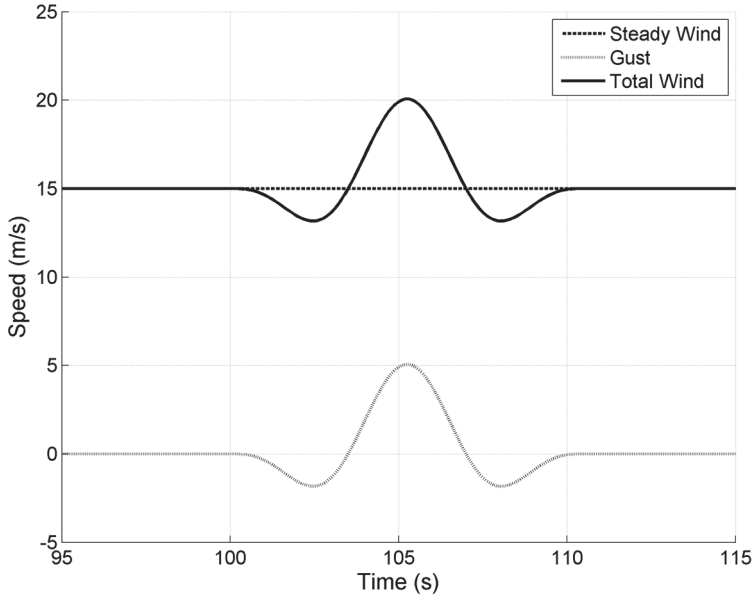

Figure A.1. *Wind profile for the extreme operating gust (EOG)*

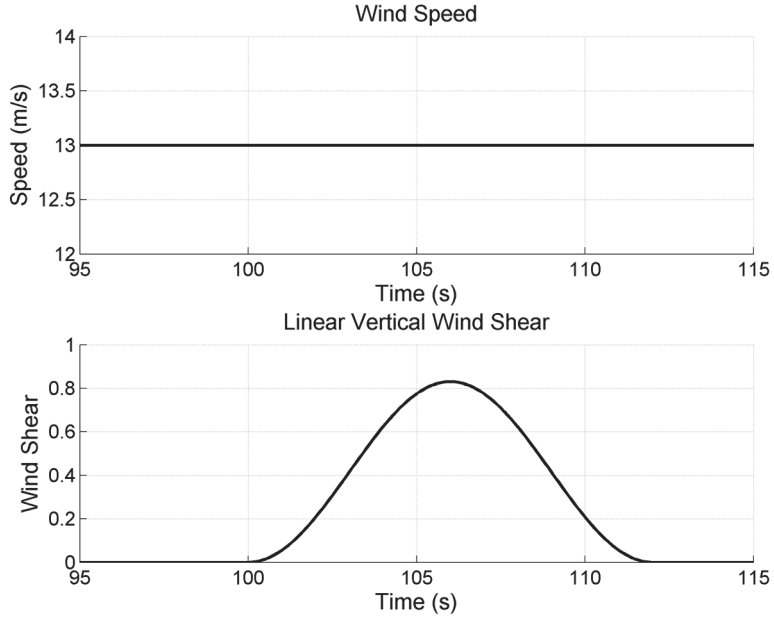

Figure A.2. *Wind profile for the extreme vertical wind shear (EWSV)*

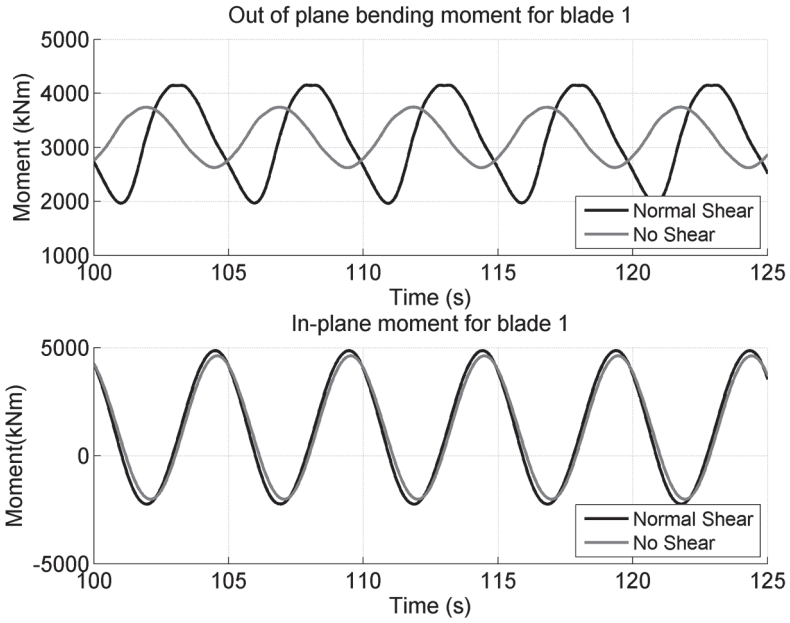

Figure A.3 *Effect of wind shear on the blade moments at the wind speed of 23.7 m/s*

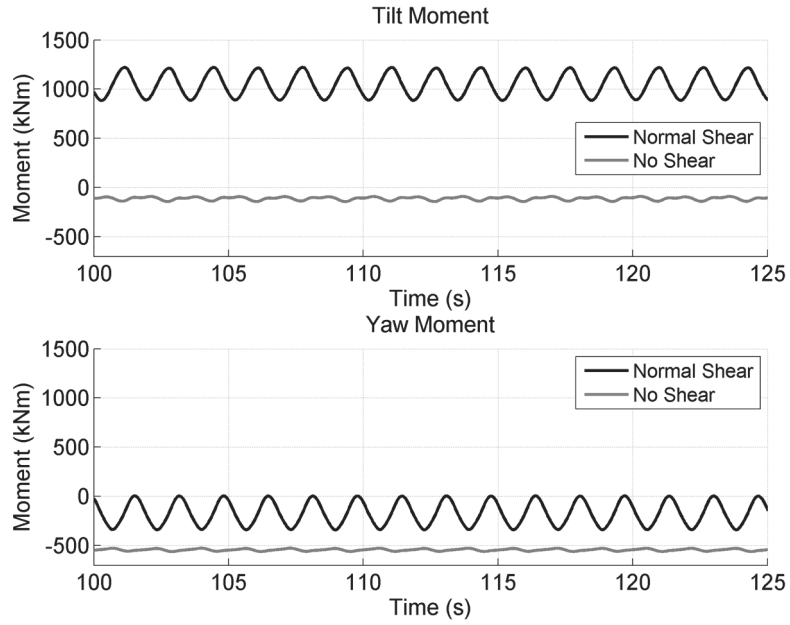

Figure A.4 *Effect of the wind shear on the tilt and yaw moments affecting on the top of the tower at the wind speed of 23.7 m/s*

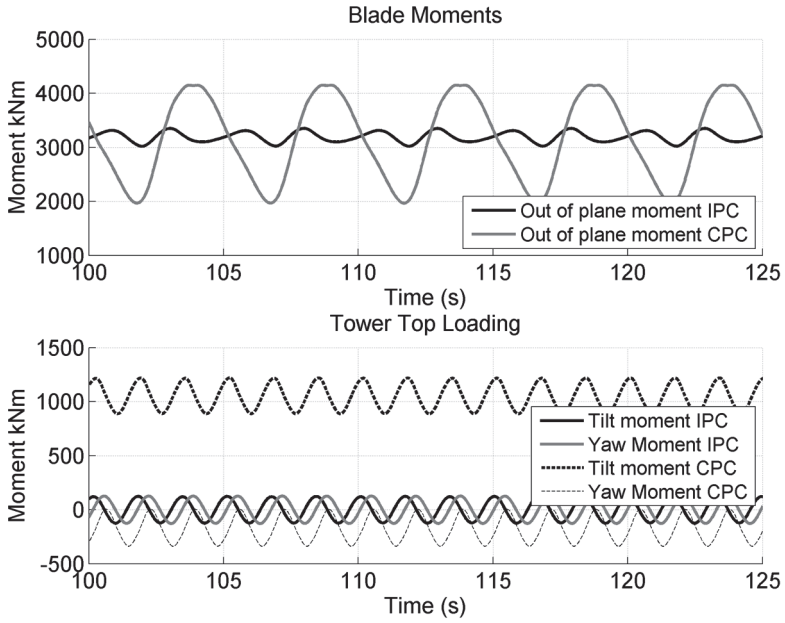

Figure A.5 *Comparison of the CPC and IPC at the wind speed of 23.7 m/s in the terms of the loads*

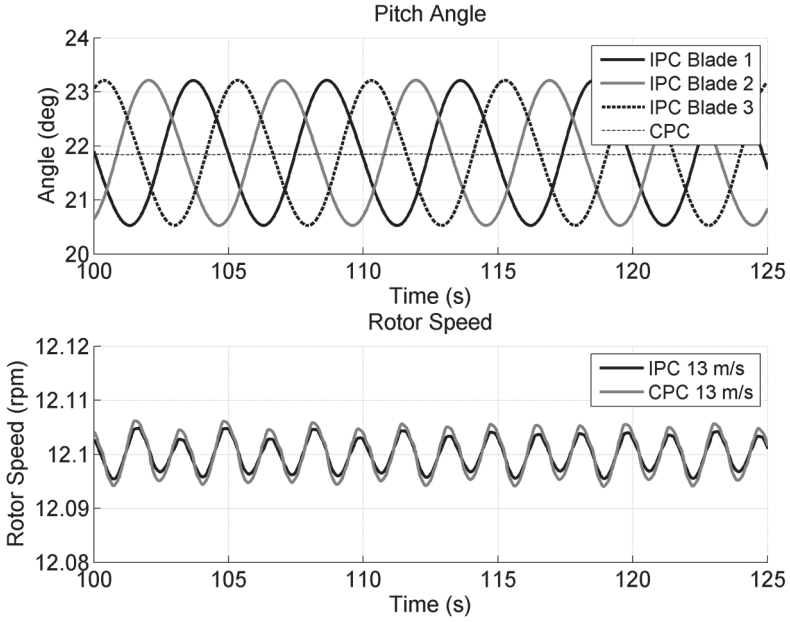

Figure A.6 *Comparison of the pitch angles and the rotor speed between IPC and CPC at the wind speed of 23.7 m/s*

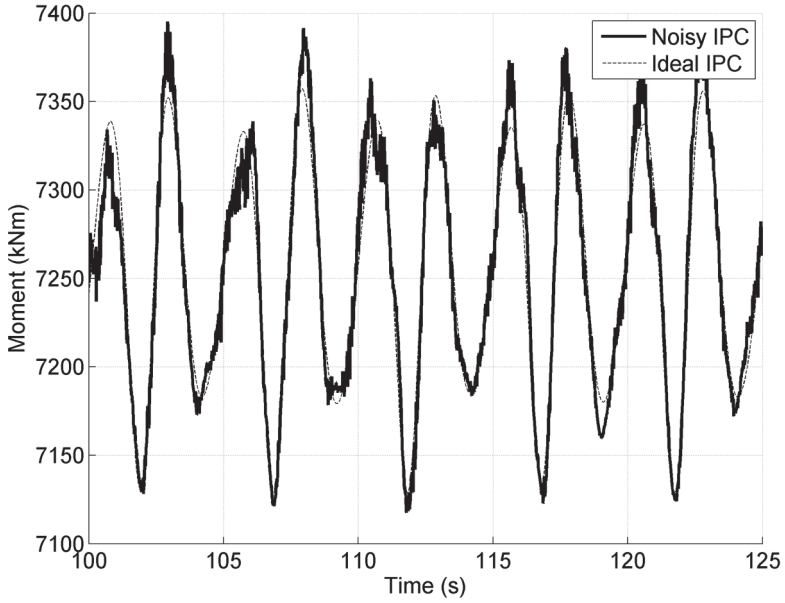

Figure A.7 *Out of plane blade bending moment in the presence of noisy azimuth angle*

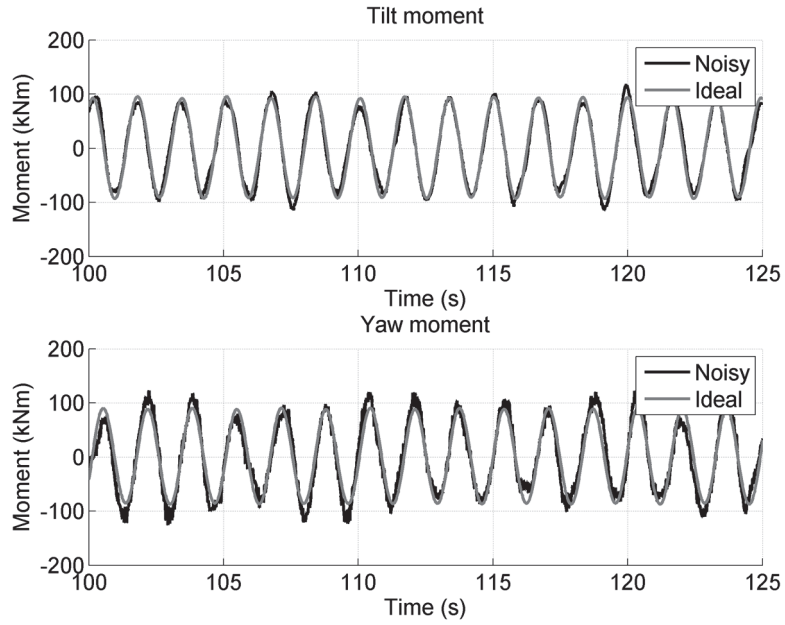

Figure A.8 *Tilt and yaw moments in the presence of noise in the azimuth angle*

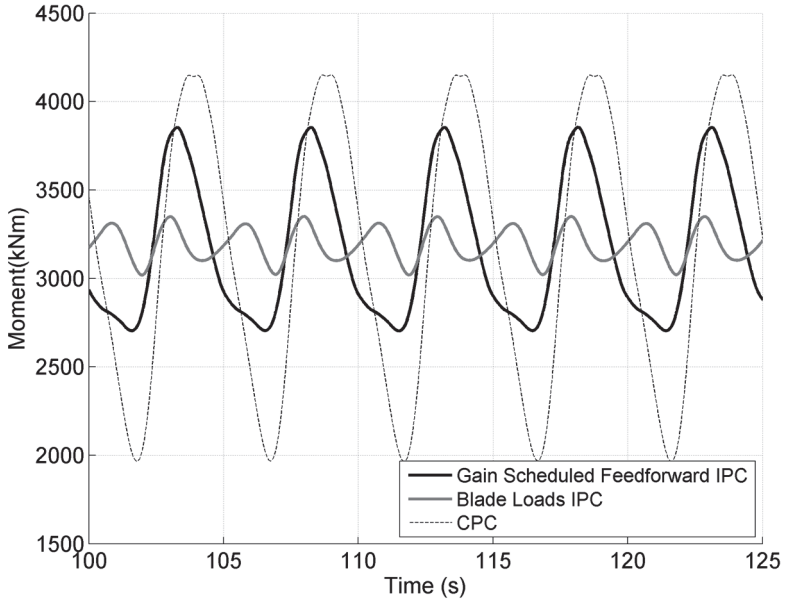

Figure A.9 *Out of plane blade bending moment for the different controllers at the wind speed of 23.7 m/s*

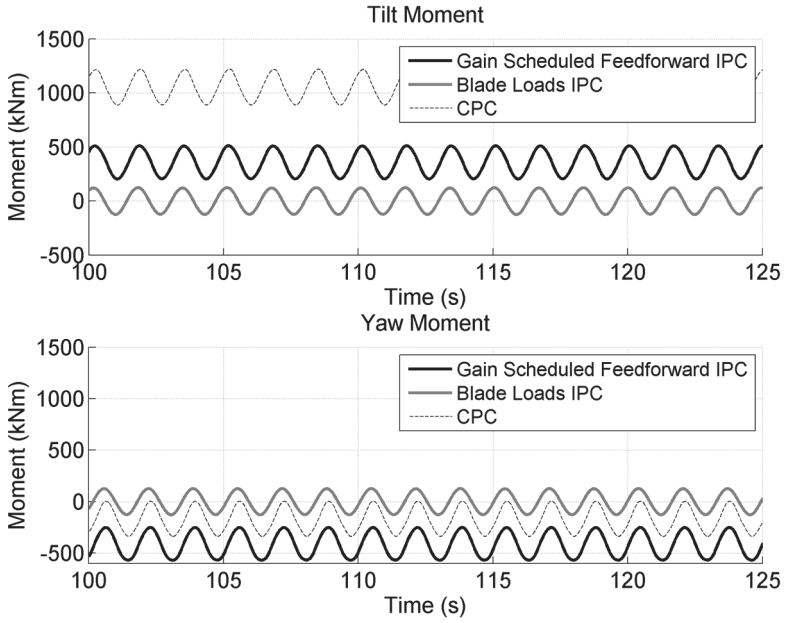

Figure A.10 *Tilt and yaw moments for the different controllers at the wind speed of 23.7 m/s*

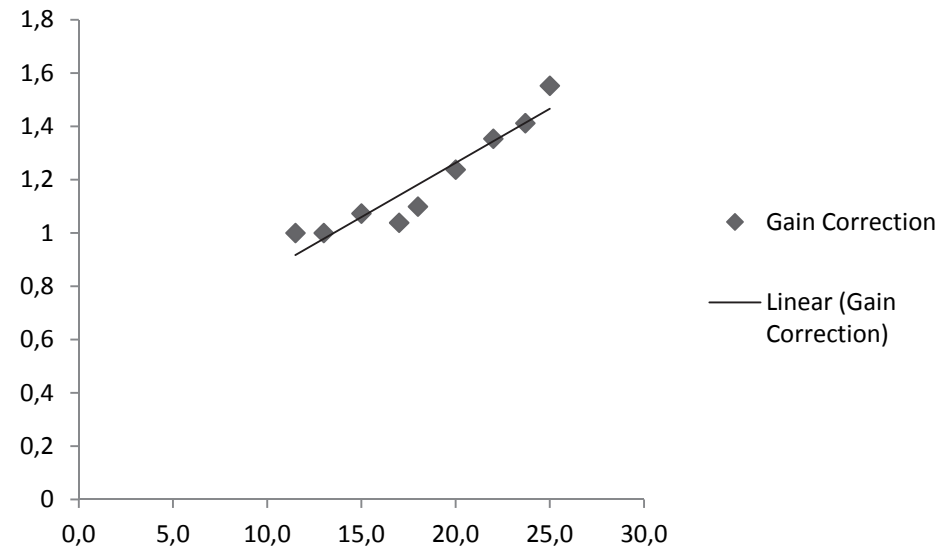

Figure A.11 *Gain correction factor for the gain scheduled feedforward IPC as a function of wind speed*

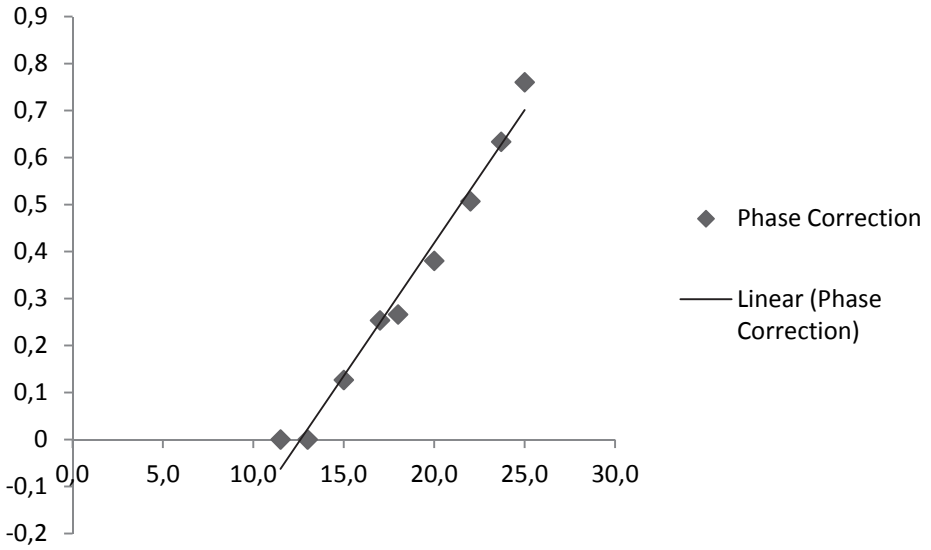

Figure A.12 *Phase correction factor for the gain scheduled feedforward IPC as a function of wind speed*

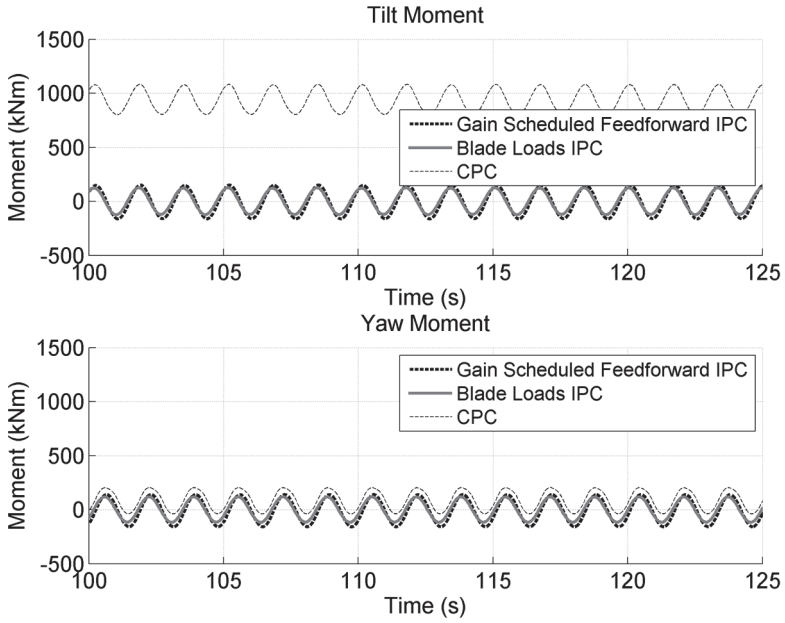

Figure A.13 *Performance of the gain scheduled feedforward IPC with interpolated control parameters in the terms tilt and yaw moments at the wind speed of 19 m/s*

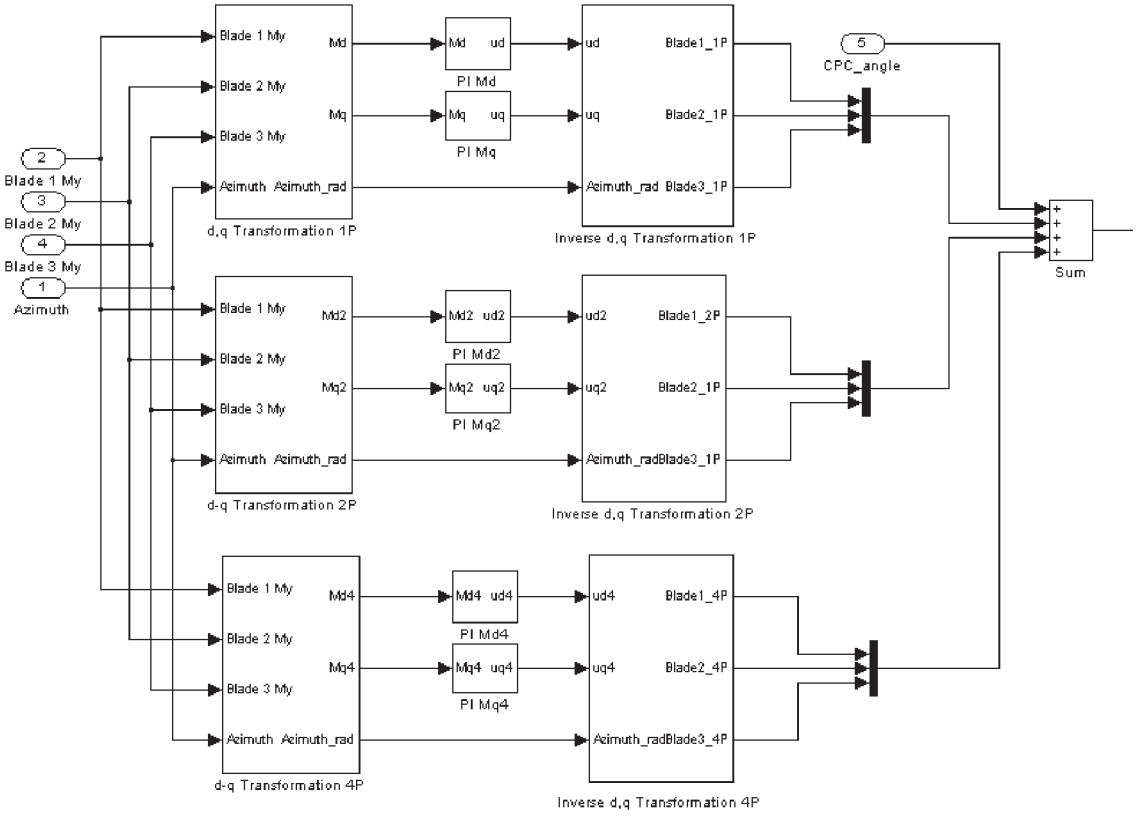

Figure A.14 *Simulink model of the extended IPC*

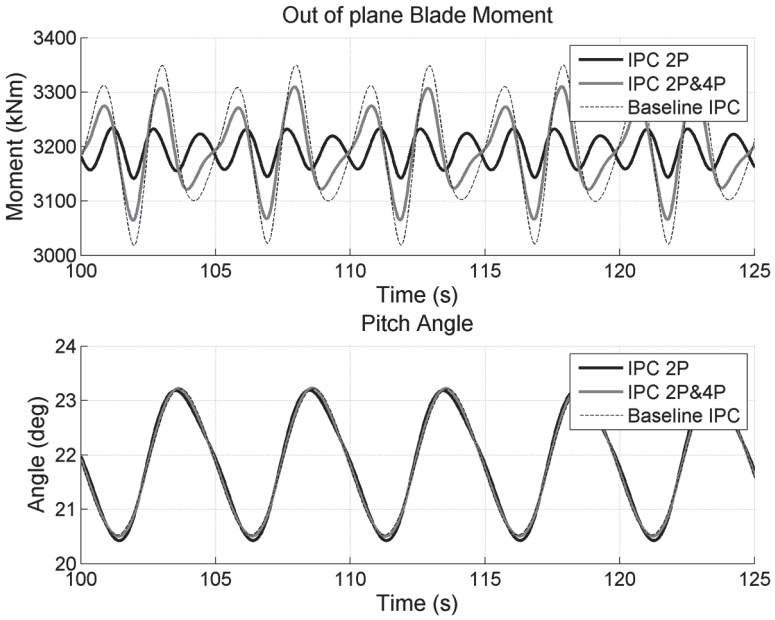

Figure A.15 *Comparison of the different IPCs in the terms of blade bending moment and the pitch angle for the blade one at the wind speed of 23.7 m/s*

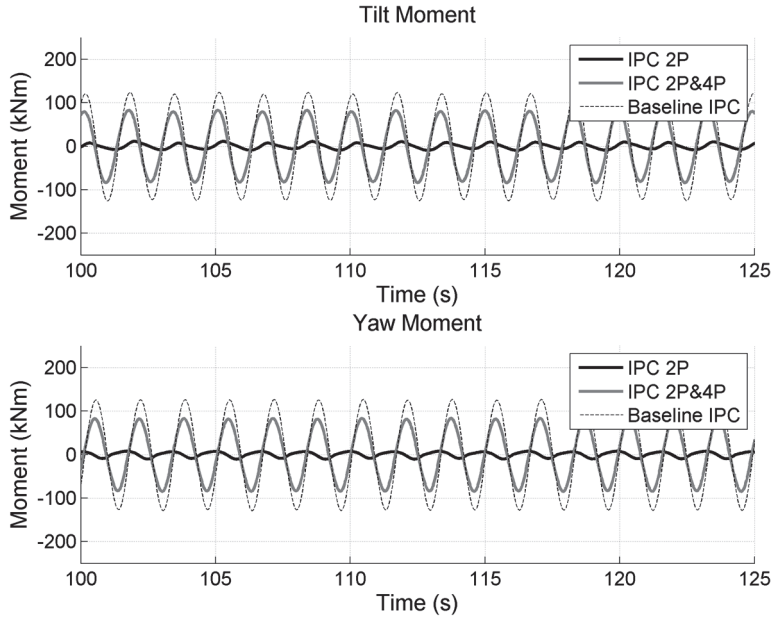

Figure A.16 *Comparison of the different IPCs in the terms of tilt and yaw moments at the wind speed of 23.7 m/s*

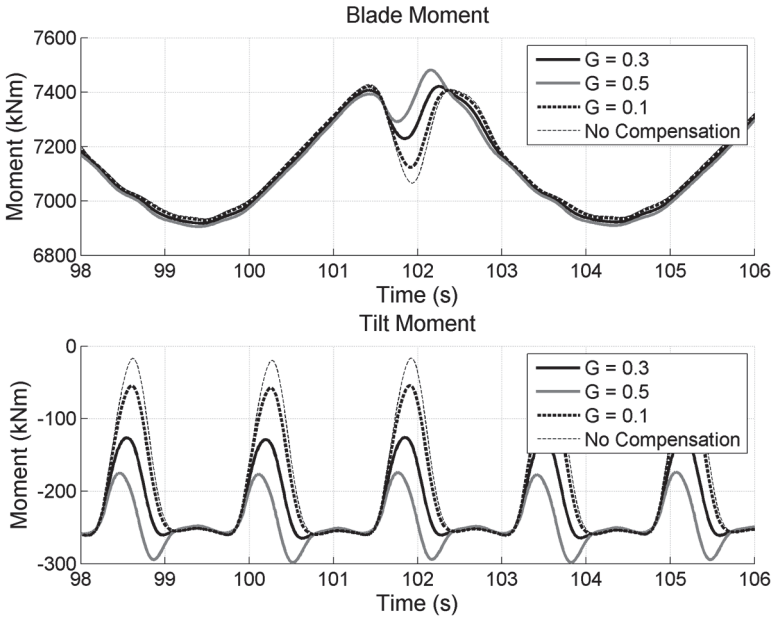

Figure A.17 *Effect of different values of G on the performance of feedforward tower shadow compensation*

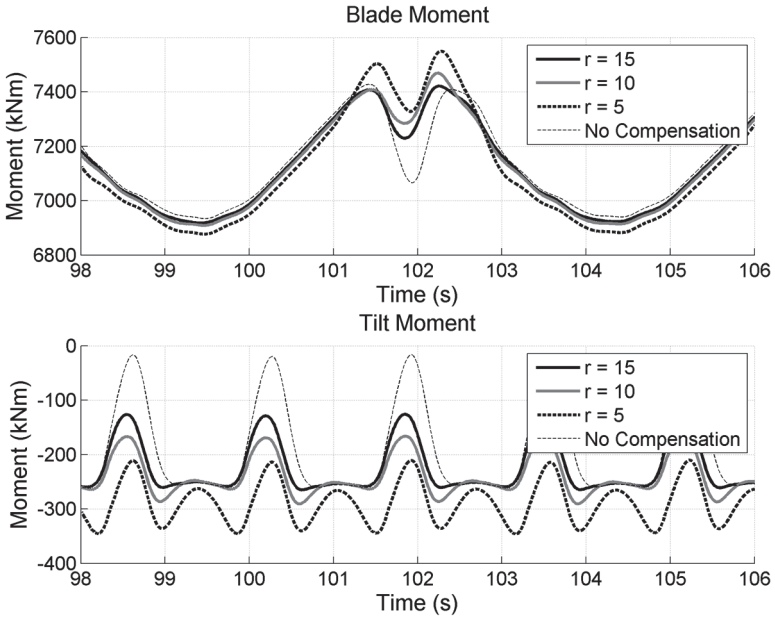

Figure A.18 *Effect of different values of r on the performance of feedforward tower shadow compensation*

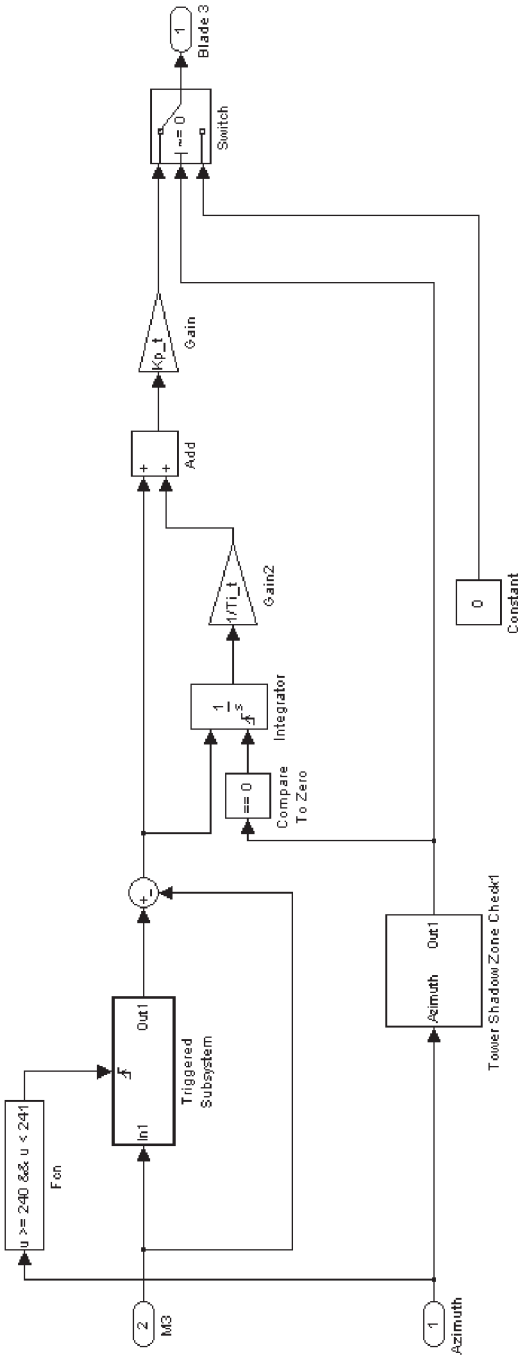

Figure A.19 *Feedback tower shadow compensation controller*